Interaction of Silver Nanoparticles (AgNP) with Rainbow Trout Gill Cell Lines

THÈSE No 6698 (2015)

PRÉSENTÉE LE 8 juin 2015

À LA FACULTÉ DE L'ENVIRONNEMENT NATUREL, ARCHITECTURAL ET CONSTRUIT
LABORATOIRE DE TOXICOLOGIE DE L'ENVIRONNEMENT
PROGRAMME DOCTORAL EN GÉNIE CIVIL ET ENVIRONNEMENT

ÉCOLE POLYTECHNIQUE FÉDÉRALE DE LAUSANNE

POUR L'OBTENTION DU GRADE DE DOCTEUR ÈS SCIENCES

PAR

Yang YUE

acceptée sur proposition du jury :

Prof. Urs von Gunten président du jury
Prof. Kristin Schirmer, directeur de thèse
Dr. Renata Behra, co-directeur de thèse
Prof. Patricia A. Holden, rapporteur
Prof. Vera I. Slaveykova, rapporteur
Prof. Rizlan Bernier-Latmani, rapporteur

EPFL

ÉCOLE POLYTECHNIQUE
FÉDÉRALE DE LAUSANNE

Suisse
2015

Aim high or you may fall below the average!

取法乎上，得乎其中。

Chinese proverb

Acknowledgements

Acknowledgements

Thanks to all the office mates in BU-F20, Muris, Linn, Alex, Niksa and the jungle! You are so nice! Thanks Franziska and Adducia for your kind help! I would also like to thank all the members in UTOX and Eawag. It is such an honor to work with all of you!

I would like to thanks Chris, Maja and Alla of the Scientific Center for Optical and Electron Microscopy (ScopeM, ETH-Zürich) for the help in electron microscopy work. Thanks to Romain and Diego in the Proteomics Core Facility (PCF, EPFL) for the work in protein identification.

I would like to thank all the Chinese friends I met in here. In the past four years, people were coming and going. Li Xiaomei, Wen Gang, He Xiaoqing, Yan Yigang, Shu longfei, Shi Yijing, Prof. Bai Yaohui, Prof. Yang Hong, Prof. Wang Jing, Men Yujie, Liu Wenfeng, Liu Zhengqian, that is really precious memory to have met all of you.

At the end, I would like to express the deepest appreciation to my girlfriend, Lu, and my family. Lu, without you, I would never have had the idea to study outside of China and may just have become a very common staff in some company in China. Thanks again for your great idea! Thanks to my parents and my sister' support!

Dübendorf, 17.06.2015

Abstract

Owing to their unique antimicrobial properties, silver nanoparticles (AgNP) are among the most widely used engineered nanoparticles in a variety of consumer products and medical applications. Their resulting release into the aquatic environment raises concern about potential adverse effects in aquatic organisms. While a number of studies measured AgNP toxicity on integrative toxicological outcomes in aquatic organisms, such as development or mortality, very little knowledge exists on the mechanisms of AgNP interactions with cells of such organisms. This thesis therefore focused on the interaction of AgNP with cells derived from fish gill, specifically a fish gill cell line from rainbow trout (*Oncorhynchus mykiss*), in an integrative way, starting from AgNP behavior in exposure media and upon contact with cells, following the formation of a protein corona around the AgNP during trafficking in intact cells and quantifying short- and long-term impact on cell viability.

The composition of cell exposure media was found to have a major effect on the AgNP behaviour and toxicity to the rainbow trout gill cell line, RTgill-W1. Three different exposure media (L15/ex, L15/ex w/o Cl and d-L15/ex) were used with varying ionic strength and chloride content, which had a dominant effect on the AgNP agglomeration, deposition and dissolved silver species in exposure media. Comparing the behaviour and toxicity of AgNP in the different media, stronger agglomeration of AgNP correlated with higher toxicity. Deposition of AgNP on cells might explain the higher toxicity of agglomerated AgNP compared to that of suspended AgNP. The newly developed low ionic strength medium, d-L15/ex, which can stabilize AgNP and better mimic the freshwater environment, offers an excellent exposure solution to study cellular and molecular effects of nanoparticles to gill cells.

Short-term exposures of the RTgill-W1 cells to AgNP allowed construction of concentration-response relationships for three parameters of cell viability, namely metabolic activity, cell- and lysosomal- membrane integrity, as a function of total or dissolved silver ions. These relationships, together with the limited prevention of cellular toxicity by silver ligands, indicated that AgNP elicited a particle-specific effect on the cells. Furthermore, the lysosomal membrane integrity was significantly more sensitive to AgNP exposure than cellular metabolic activity or cell membrane integrity

and showed the weakest protection by silver ligands. This revealed that AgNP seem to particularly affect RTgill-W1 cell lysosomes.

To shed light on the path of AgNP in cells leading to toxicity, AgNP uptake by the cells was explored on exposure in d-L15/ex medium. Quantification of silver associated with cells indicated that RTgill-W1 cells took up AgNP in a more efficient way than $AgNO_3$. Electron microscope imaging not only suggested that RTgill-W1 cells take up AgNP via an energy depend pathway but also that particles are stored in endocytic compartments, which include lysosomes and endosomes.

Knowing the general pathway of AgNP in the fish cells, the binding of proteins to AgNP to form a protein corona was addressed in order to identify protein targets of AgNP trafficking and potential toxicity. With subcellular fractionation, the AgNP-protein corona was recovered from intact subcellular compartments with high acid phosphatase activity (a marker for endocytic compartments) and/or high silver content. Proteins acquired from the AgNP-protein corona were identified by mass spectrometry and analyzed with Protein Ontology. 383 proteins were identified in this way and broadly classified as belonging to cell membrane functions as well as endocytosis and vesicle-mediated transport pathways. Of particular interest was the identification of "Na^+/K^+ ATPase" and "Rab Family Small GTPases" as these were previously implied to bind to nanoparticles. This is the first study that focuses on the interaction of industrial nanoparticles with proteins in living cells and an initial mechanism of AgNP uptake and toxicity was derived from it.

Long-term exposures of cells in culture is thus far restricted to media containing a non-defined serum component. However, especially cells of aquatic organisms that comprise a barrier to the environment, such as the gill epithelium, would not be expected to be exposed in such a way. Therefore, in order to allow long-term studies on the impact of nanoparticles with fish gill cells, a new *in vitro* cell model, based on the RTgill-W1 cell line, was developed and named as RTgill-W1-pf (protein free). This cell line was obtained by means of selection in a commercial, protein-free culture medium. Initial results with this new cell line demonstrated that AgNP inhibited RTgill-W1-pf cell proliferation in a twelve day exposure test.

To conclude, this thesis offers insights into the mechanisms of interaction of AgNP with fish gill cells. It provides fundamental information about AgNP uptake and interaction with proteins in these cells, which is useful for understanding AgNP toxicity and sustainable nanoparticle development.

Keywords

x

Résumé

Les nanoparticules d'argent (AgNP) font partie des nanoparticules synthétiques les plus utilisées dans divers produits de consommation et applications médicales, en raison de leurs propriétés an-timicrobiennes uniques. En conséquence, les apports de ces nanoparticules dans l'environnement aquatique donnent lieu à des questions concernant leurs possibles effets nocifs sur les organismes aquatiques. Tandis que de nombreuses études ont mesuré la toxicité des AgNP par rapport à des paramètres toxicologiques comme le développement ou la mortalité des organismes aquatiques, les mécanismes d'interactions des AgNP dans les cellules sont encore très peu connus. Cette thèse est donc focalisée sur les interactions des AgNP avec des cellules dérivées de branchies de poisson, en particulier une ligne de cellules des branchies de la truite arc-en-ciel (*Oncorhynchus mykiss*), avec une approche intégrative, qui comprend le comportement des AgNP dans les milieux d'exposition et au contact des cellules, puis l'étude de la formation d'une couronne de protéines autour des AgNP par interactions avec des cellules intactes et la quantification des effets à court et long terme sur la viabilité des cellules.

La composition des milieux d'exposition des cellules a un effet majeur sur le comportement des AgNP et leur toxicité sur la ligne de cellules des branchies de la truite arc-en-ciel, RTgill-W1. Trois milieux d'exposition différents (L15/ex, L15/ex w/o Cl et d-L15/ex) ont été utilisés, dont les diffé-rentes forces ioniques et teneurs en chlorure ont des effets dominants sur l'agglomération des AgNP, leur dépôt et les espèces dissoutes d'argent. En comparant le comportement et la toxicité des AgNP dans ces différents milieux, il a été observé qu'une plus forte agglomération des AgNP était corrélée avec une toxicité plus élevée. Le dépôt des AgNP sur les cellules peut expliquer la toxicité plus élevée des AgNP agglomérées en comparaison des AgNP en suspension. Le nouveau milieu d'exposition avec une plus faible force ionique, d-L15/ex qui stabilise les AgNP et simule un environnement d'eau douce, représente une excellente solution d'exposition pour étudier les effets cellulaires et moléculaires des nanoparticules sur les cellules de branchies.

Les expositions à court terme des cellules RTgill-W1 aux AgNP ont permis d'établir des relations entre concentration et réponse pour trois paramètres, l'activité métabolique, l'intégrité des mem-branes cellulaires et l'intégrité des membranes lysosomales, en fonction de l'argent total ou des

ions d'argent dissous. Ces relations indiquent que les AgNP exercent des effets spécifiques sur les cellules, qui sont aussi montrés par le manque d'effet protecteur des ligands complexant les ions d'argent. De plus, l'intégrité des membranes lysosomales est beaucoup plus sensible à l'exposition aux AgNP que l'activité métabolique et l'intégrité des membranes cellulaires et n'est que faiblement protégée par les ligands. Ces effets montrent que les AgNP affectent en particulier les lysosomes des cellules RTgill-W1.

Pour élucider le devenir des AgNP causant la toxicité dans les cellules, la prise en charge des AgNP par les cellules a été examinée dans le milieu d-L15/ex. Les teneurs en argent associées avec les cellules indiquent que les cellules RTgill-W1 prennent en charge les AgNP plus efficacement que les ions dissous. Les images par microscopie électronique suggèrent que non seulement les cellules RTgill-W1 prennent en charge les AgNP par transport dépendant de l'énergie, mais aussi que les nanoparticules sont stockées dans des compartiments endocytotiques, comprenant les lysosomes et endosomes.

Sur la base du devenir des AgNP dans les cellules, les interactions des protéines avec les AgNP pour former une couronne de protéines ont été étudiées pour identifier les protéines affectées par les AgNP et la possible toxicité. Les protéines associées avec les AgNP ont été enrichies par fractionnement subcellulaire à partir des compartiments subcellulaires intacts avec une forte activité de phosphatase acide (comme marqueur pour les compartiments endocytotiques) et ou une teneur élevée en argent. Les protéines isolées à partir des couronnes de protéines avec les AgNP ont été identifiées par spectrométrie de masse et analysées par Protein Ontology. Le nombre de protéines identifiées de cette manière est de 383 protéines qui ont été classifiées comme liées à des fonctions des membranes cellulaires, ainsi qu'aux voies de transport par endocytose et par les vésicules. Il est particulièrement intéressant que les protéines "Na$^+$/K$^+$ATPase" et "Rab Family Small GTPases" aient été identifiées pour lesquelles un rôle pour lier les nanoparticules a déjà été observé. Il s'agit ici de la première étude examinant les interactions de nanoparticules industrielles avec des protéines dans les cellules vivantes, dans laquelle un mécanisme de prise en charge des AgNP et de toxicité est proposé.

Les expositions de cellules en culture à long terme sont jusqu'ici limitées aux milieux contenant un composant de sérum mal défini. Toutefois, les cellules des organismes aquatiques qui constituent une barrière à l'environnement, comme les cellules des épithéliums des branchies, ne sont pas exposées de cette manière. Un nouveau modèle in vitro de cellules basé sur la ligne de cellules RTgill-W1 a donc été développé pour permettre des études à long terme des effets des nanoparticules sur

les cellules de branchies de poisson. Cette nouvelle ligne de cellules, nommée RTgill-W1-pf (protein free), a été obtenue par sélection dans un milieu sans protéines disponible commercialement. Les premiers résultats obtenus avec cette nouvelle ligne de cellules démontrent que les AgNP inhibent la prolifération des cellules RTgill-W1-pf pour une exposition pendant douze jours.

En conclusion, cette thèse permet de mieux concevoir les mécanismes d'interactions des AgNP avec des cellules de branchies de poisson et livre des informations fondamentales sur la prise en charge des AgNP et leurs interactions avec les protéines dans ces cellules, qui sont utiles pour comprendre la toxicité des AgNP et le développement durable des nanoparticules.

Mots-clés

Contents

Contents

Contents

List of Figures

List of Tables

Chapter 1 Introduction

The growing application of engineered nanoparticles in consumer and other products bears the risk of increased nanoparticles release into the environment. This raises concerns about the impact of these particles on organisms, such as those living in aquatic environments. One nanoparticle group of particular concern are engineered metal nanoparticles. Among them, silver nanoparticles have a clear path of release from its applications in textiles, filters, paints and other products into aquatic system. This thesis focuses on the impact of silver nanoparticles to fish gill cells *in vitro*. This introductory chapter aims to provide an overview of properties of engineered nanoparticles, their behaviour in the aquatic environment, and interactions with aquatic organisms, with an emphasis placed on silver nanoparticles specifically.

1.1 Nanotechnology and nanoparticles

1.1.1 Nanotechnology and nanoparticle applications

Nanotechnology is receiving increasing attention as a rapid growing field in the twenty-first century. Nanotechnology refers to the manipulation of matter on an atomic, molecular, and supramolecular scale. Engineered nanoparticles are an indispensable basis for the development of nanotechnology. The use of engineered nanoparticles is becoming increasingly common in medicine, cosmetics, textiles, electronics and other areas (Aitken et al. 2006; Masciangioli and Zhang 2003; Salata 2004). Nanoparticles (NP) are three-dimensional structures in which at least one of the dimensions does not exceed 100 nm (Bystrzejewska-Piotrowska et al. 2009). These nanoparticles can be produced in many different chemical forms, the main types including nano metals, metal oxides, quantum dots and carbon-based materials, such as carbon nanotubes and fullerenes.

The interest in nanoparticles stems from their unique properties. The small size range of engineered nanoparticles provides them with several special properties, such as large surface area and high reactivity. Large surface area means that there are more atoms or molecules present at the surface, being able to join in chemical reaction at the same mass. Theoretical calculation shows that the ratio of surface to total atoms or molecules increases exponentially with decreasing particle

size. Thus, particles in the nanometer size range exhibit high chemical activity, which has been confirmed by many studies (Bystrzejewska-Piotrowska et al. 2009; Oberdorster et al. 2005).

Among these engineered nanoparticles, different kinds of metal nanoparticles (MeNP) and metal oxide nanoparticles (MOx NP) have received increasing interest and rapid widespread uses. For example, gold nanoparticles (AuNP), silver nanoparticles (AgNP), titanium dioxide nanoparticles (TiO$_2$ NP), and zinc oxide nanoparticles (ZnO NP) are used in biomedicine, cosmetics, filters and other areas or products (Schrand et al. 2010). With their antimicrobial properties, AgNP are used in domestic appliances such as refrigerators, vacuum cleaners, air conditioning, textiles and plastics (Fabrega et al. 2011). The applications of TiO$_2$ NP include paint, toothpaste, UV protection, photocatalysis, photovoltaics, sensing, and electrochromics as well as photochromics, and the new generation of solar cells (Chen and Mao 2007). ZnO NP are the starting material for electronic applications, chemical sensors and UV-filters in sunscreens (Aruoja et al. 2009). Utilization of magnetite NP (Fe$_3$O$_4$ NP) is increasing in medicine, especially in biochemical assays and drug delivery (Verma et al. 2008). It is estimated that there are already more than 800 products from nanotechnologies in our daily lives and many new products are expected to appear on the market in the next few years (Maynard et al. 2006).

This variety of nanoparticles is further expended due to various surface modifications, which are used to stabilize particles in suspensions, conjugate with matrices, and improve intracellular uptake and the ability to target specific cells. For example, nanoparticles are often coated with citrate, carbonate, or polyvinylpyrrolidone (PVP) to maintain their stability (Klaine et al. 2008). Polyethylene glycol and folic acid modification of superparamagnetic magnetite nanoparticles is used to facilitate nanoparticle uptake in specific cancer cells for cancer therapy and diagnosis (Zhang et al. 2002).

Surface modified nanoparticles can be added in a variety of materials by deposition, covalent binding and embedding (Sperling and Parak 2010). For instance, AgNP can be deposited into or conjugated with fibers to produce clothes and filters which have antibacterial properties. AgNP can also be embedded in plastic and food containers to increase the shelf life of food. Paint with AgNP can be used as an efficient antimicrobial agent to coat surfaces such as wood, glass façade and walls. (Rai et al. 2009).

With washing, including by rain, nanoparticles can be significantly released from exterior surfaces into aquatic environments. several studies concerning AgNP release from different materials such

as textiles and paints and found significant leaching of AgNP release (Hedberg et al. 2014; Kaegi et al. 2010; Reidy et al. 2013).

1.1.2   Nanoparticles in the aquatic environment

In aquatic environments, the main processes affecting nanoparticle fate are agglomeration and aggregation, dissolution and transformation. Agglomeration and aggregation are two different phenomena. International Union of Pure and Applied Chemistry (IUPAC) defined agglomeration as "a process of contact and adhesion whereby dispersed particles are held together by weak physical interactions ultimately leading to phase separation by the formation of precipitates of larger than colloidal size". Agglomeration is a reversible process. In contrast, aggregation is the process in which dispersed molecules or particles assemble rather than remain as isolated single molecules or particles. In MeNP suspensions, agglomeration can lead to large complexes by loosely binding; agglomerated MeNPs can be easily dispersed again. On the contrary, covalent bonds are formed in aggregation and nanoparticles cannot be dispersed again (Aleman et al. 2007).

Surface charge is the most important factor influencing nanoparticle agglomeration and aggregation. Generally, nanoparticles with high negative or positive charges are much more stable in suspension than nanoparticles with low surface charges. Surface charge ensures repulsive forces between nanoparticles in suspension from Coulomb forces (Werth et al. 2003). Counter ions in solution form an electric double layer around nanoparticles, thereby creating a barrier between nanoparticles that repress interparticle interactions. The pH and ionic strength of the surrounding medium have a strong effect on nanoparticle surface charge and the electric double layer (Christian et al. 2008). For example, when the pH of a suspension is far away from the nanoparticle zero-point of charge, in which the nanoparticle has a net-zero surface charge, the surface charge will change to negative or positive. Also, increases in ionic strength compress the electric double layer and decrease the energy barrier between two particles, leading to agglomeration or aggregation.

Another process playing a key role in the fate and effects of nanoparticles is dissolution. Nanoparticle dissolution is highly dynamic and dependent on the nanoparticle properties (size, material, surface morphology) and environmental conditions (pH, ionic strength and absorbing species). Several types of nanoparticles are chemically unstable, and can release metal ions into suspension, e.g. Ag^+ from AgNP, Cu^{2+} from CuO NP and Zn^{2+} from ZnO NP.

Depending on the nanoparticle behaviour, organisms can have various interactions with nanoparticles in aquatic environments. Well dispersed nanoparticles are more bioavailable to organisms liv-

ing in the water column than nanoparticles that agglomerate or aggregate and as a consequence sink and sediment. However, sedimented nanoparticles can interact with benthic organisms, such as certain forage fish, crustaceans, aquatic molluscs, and biofilms (Ward and Kach 2009).

Upon contact with organisms, nanoparticles can elicit toxic effects. Reports measured the toxicity of MeNP on algae, aquatic invertebrates, fish, plants, bacteria, and fungi (Baun et al. 2008; Holden et al. 2013; Navarro et al. 2008a; Schirmer et al. 2013; Schultz et al. 2014; Sigg et al. 2014; Moos and Slaveykova 2013). *In vitro* and *in vivo* studies indicate that nanoparticles can affect biological behavior at the organ, tissue, cellular, subcellular, and protein levels (Schrand et al. 2010). ZnO was found to be toxic toward algae (*Pseudokirchneriella subcapitata*) and acute toxicity was observed upon CuNP exposure to zebra fish (*Danio rerio*) (Aruoja et al. 2009; Griffitt et al. 2007). Moreover, AgNP were found to have adverse effects on several organisms such as bacteria, algae, plants, fungi, fish organs and cell lines (Farkas et al. 2011; George et al. 2012; Ivask et al. 2014; Navarro et al. 2008b). A number of studies focus on acute toxicity and report the concentrations of nanoparticles that produce toxicity. Yet, there is a remarkable lack of information on the biological interactions of nanoparticles under environmentally relevant conditions.

This thesis focuses specifically on AgNP effects in the aquatic environment. As stated above, with its great antibacterial properties, AgNP are used in textiles, filters, food containers and paints. By washing and other routes, AgNP are released into aquatic environments and exposed to fish (Figure 1.1). With fish being the most diverse vertebrate group and with its importance in food chains and ecotoxicology, the goal of this study is the interaction of AgNP with cells of fish in fresh water.

Figure 1.1 AgNP are released into aquatic environments and may contact with fish.

1.2   Silver nanoparticles

1.2.1   Silver nanoparticle behaviour in aquatic media

The behaviour of AgNP in suspension is one important property to evaluate because it impacts the transport, bioavailability and toxicity of AgNP. Another property is the dissolution of AgNP. In aqueous solutions, Ag(0) can be partially oxidized to Ag^+ and sulfide containing compounds in the aquatic environment or in the cellular environment of an organism can react with Ag^+ and sulfidize AgNP to Ag_2S-NP.

Suspended nanoparticles are likely transported within the water phase and there is a high chance that they may interact with pelagic organisms. Large AgNP tend to be deposited onto sediments and decrease the bioavailability, at least for pelagic organisms. Various AgNP surface coatings are applied to stabilize AgNP, such as citrate, polyvinyl pyrrolidone (PVP), carbonate. These coatings can provide additional surface charge on AgNP and reduce AgNP agglomeration and aggregation. The surface charge of coated AgNP can be influenced by pH because the organic compounds have different charge depending on pH. For example, carbonate-coated and citrate-coated AgNP show agglomeration at low pH due to neutral charge (Piccapietra et al. 2012; Tejamaya et al. 2012). On the contrary, polymer-coating, like PVP coated AgNP, is quite stable as a function of pH and of media composition, owing to steric stabilization (Badawy et al. 2010).

Another important factor affecting AgNP stability is ionic strength (*I*). In AgNP suspensions, high concentration of ions can break the electrical double layers and decrease the surface charge, which leads to AgNP agglomeration. Among common ions, calcium ions (Ca^{2+}) can induce the strongest AgNP agglomeration, even with Ca^{2+} in the low millimolar range, compared to Na^+ and K^+. Piccapietra reported enhanced AgNP agglomeration in a simple medium with Ca^{2+} or Na^+ above 2 mM or 100 mM, respectively (Piccapietra et al. 2012). Leibovitz's L-15 medium, a commonly used fish cell culture medium, includes 1.26 mM Ca^{2+} and 0.14 M NaCl. In such high ionic strength media, AgNP become large as a result of strong agglomeration (Behra et al. 2013).

Other media components, like organic molecules or chloride, also play a role in AgNP stability in suspension. Organic molecules, such as humic acid, bovine serum albumin or fetal bovine serum (FBS), can bind to AgNP surfaces and form a new coating. This kind of coating can help to stabilize AgNP in medium. Humic acid or bovine serum albumin (BSA) stabilized AgNP in cell culture medium or buffer (Huynh and Chen 2011; MacCuspie et al. 2010). Low concentrations of chloride can stabi-

lize AgNP in suspension, which maybe due to chloride ions adsorbing on the AgNP surface, thereby adding more negative charge.

Dissolution of AgNP is another process of concern. In order for AgNP to dissolve, an additional step is needed: oxidation. This oxidation reaction takes place on the nanoparticles' surface. The oxidant can be oxygen, a reactive oxygen species, or another strong oxidant (Behra et al. 2013). The dissolution ability of AgNP is variable, depending on AgNP coating and the aqueous environment. In general, coated AgNP show less dissolution than bare AgNP. AgNP dissolution is also influenced by suspension pH. In natural water samples, dissolved Ag increased by about a factor 4 in the case of lake water with pH 6.4 and low ionic strength, in comparison with lake water at pH 8 and higher ionic strength (Odzak et al. 2015). The pH is extremely low in some biological compartments. For example, the pH of human gastric fluid is approximately 1.6 (Finholt and Solvang 1968) and pH in some cell organelles can be as low as 4.8, specifically in lysosomes (Ohkuma and Poole 1978). Extensive and rapid Ag NP dissolution would be expected at this low pH.

Dissolved silver can be complexed with several ions and molecules and form new silver species, which could shift the equilibrium of AgNP dissolution. An important ion influencing silver speciation is chloride. In different chloride concentrations, the reaction between Ag^+ and Cl^- can lead to numerous types of complexes, such as $AgCl^0(aq)$, $AgCl_2^-(aq)$, $AgCl_3^{2-}(aq)$, and the precipitate $AgCl(s)$. In contact with organisms, these silver species have different bioavailability and toxicity (Hogstrand et al. 1996; Wood 2011).

The second ion that should be considered is sulfide, which can react with silver ions forming Ag_2S as well as sulfidize AgNP. The affinity of Ag^+ to S^{2-} is extremely high ($K_{sp} \approx 10^{-51}$), and the dissolved silver at equilibrium with Ag_2S is lower than $10^{-10}M$. Thus, dissolved Ag^+ in the presence of sulfide is only present as Ag–HS complexes (Levard et al. 2011). Other compounds, like fulvic and humic acids in natural water, cysteine, and other organic ligands with thiol groups, can also react with dissolved silver and form new complexes. Due to the high affinity of Ag_2S, sulfidation of AgNP could significantly decrease the dissolved silver in suspension and reduce the dissolved silver bioavailability and toxicity. As for AgNP, sulfidation alters the pristine AgNP composition, coating, stability and effects to organisms. Due to the sulfidation time, sulfide concentration and oxidation state, pristine AgNP can be partially or totally transformed to Ag_2S-NP. In incomplete sulfidation, hybrid nanoparticles will form with a Ag(0) core and Ag_2S coating (Reinsch et al. 2012).

1.2.2   Silver nanoparticle toxicity

As discussed above, AgNP can be oxidized and released as silver ions in suspension. Silver ions can induce toxic effect to fish. Thus, when studying potential toxicity of AgNP, one should consider both the dissolved silver species as well as particle specific effects. AgNP can induce indirect toxicity by dissolved silver or a direct toxicity from the AgNP particle (Figure 1.2). The toxicity of silver ions to fish has been extensively studied in the past. However, knowledge on the AgNP nanoparticle specific toxicity is still scare.
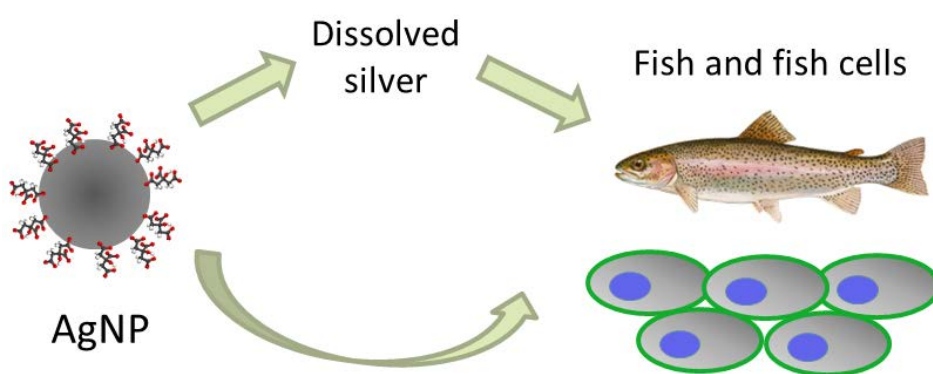
Figure 1.2 AgNP may elicit toxicity to fish and cells.

AgNP may induce toxicity to fish and cells via dissolved silver ions and/or particle-specific effects.

Silver ion toxicity has been extensively studied and several mechanisms have been proposed. The main mechanism of silver ion toxicity is the disruption of ion regulation. Due to fish plasma osmolality being much higher than external fresh water, fish need to actively take up ions such as Na^+, Cl^-, and Ca^{2+} across the gill surface into their body against a large electrochemical gradient in order to maintain proper ion concentrations for physiological processes. Na^+/K^+-ATPase in the gill is the main protein being responsible for this process. Research suggests that Ag^+ acts as a noncompetitive inhibitor of active gill Na^+ and Cl^- transport by blocking the Na^+/K^+-ATPase (Wood et al. 1996; Wood et al. 1999). Another potential mechanism of Ag^+ toxicity is the partial inhibition of the carbonic anhydrase enzyme. *In vitro* experiments indicated that Ag^+ may displace the Zn^{2+} from the interior of the carbonic anhydrase molecule in fish and thereby partially inhibit enzyme activity (Christensen and Tucker 1976; Mason and Jenkins 1995).

As for AgNP toxicity, much less mechanistic information exists. However, over the past years some mechanisms have been reported. When understanding the interaction of nanoparticles with cells, one must recognize that the nanometer size of the particles is very similar to the dimension of cel-

lular organelles, big complexes of protein molecules, and large DNA molecules. In biological systems, nanoparticles, therefore, may easily interact with biological macromolecules and cell organelles. Electron capture by nanoparticles can induce superoxide radical ($O_2^{-\bullet}$) production, which is the main source of oxidative stress in organisms (Oberdorster et al. 2005). Some studies have linked toxic effects to oxidative stress induced by nanoparticles (Moos and Slaveykova 2013; Schrand et al. 2010). For AgNP, it has been reported that they can cause to a reduction of mitochondrial membrane potential, disruption of mitochondrial respiratory chain, interruption of ATP synthesis, and increased reactive oxidative species (ROS) production (Kruszewski et al. 2011). Some studies reported that the cytotoxicity of AgNP was related to the change of antioxidant enzyme activities and membrane lipid peroxidation (Choi et al. 2010; Farkas et al. 2010; Foldbjerg et al. 2009; Piao et al. 2011).

AgNP also can affect Na^+/K^+-ATPase in fish gills. Schultz et al, focusing on juvenile rainbow trout gill, found that sodium regulation is disrupted by the nano specific effects of AgNP to Na^+/K^+-ATPase (Schultz et al. 2012). Morphological abnormalities in early stages of Japanese medaka (*Oryzias latipes*) development showed the potential developmental toxicities of AgNP (Wu et al. 2010). It seems that by means of interaction of AgNP with cells, AgNP may influence proteins, enzymes and membranes in cells, which can eventually impact the whole organism and induce toxicity.

In summary, depending on the AgNP behaviour in the aquatic environment, AgNP can induce toxicity by dissolved silver and AgNP via different mechanisms. To better understand the mechanism of AgNP toxic effects to fish, both the uptake of dissolved silver and AgNP need to be considered.

1.3   Uptake of nanoparticles in fish

Fish have several barriers, such as gill, skin and gut epithelium, to separate the fish organism from the water environment and keep a steady physiology state. Nanoparticles can overcome some barriers and be taken up into fish. Tissue distribution of AgNP in fish reveal that most AgNP are accumulated in fish gill, gastrointestinal tract and liver. After exposure of common carp to AgNP for seven days, significantly higher silver was detected in liver (5.61 mg/kg), gill (3.32 mg/kg), gastrointestinal tract (2.93 mg/kg) than in skeletal muscle (0.48 mg/kg), brain (0.14 mg/kg) and blood (0.02 mg/kg) (Jang et al. 2014). When internalized, nanoparticles will interact with different kinds of biomolecules. They can be digested or accumulated and induce toxic effect to fish.

1.3.1   Uptake routes

The fish skin with mucus secretions is often considered as a robust barrier to the external environment. Both nanoparticles and metal ions are trapped in skin mucus. Moreover, fish gut and gill have large surface areas which can interact with nanoparticles in the water. Therefore, the main routes for nanoparticles and metal ions are via gill and gut.

As the respiratory organ, the fish gill can be considered a primary target when nanoparticles are suspended in the water column. With its large surface area, the fish gill affords gas exchange between the external water environment and the organism internal environment. In this exchange process, other substances, like MeNP and organic compounds, can interact with fish gill cells. A previous study showed that AgNP were found to be most highly concentrated within gill tissues and liver of rainbow trout (*Oncorhynchus mykiss*) after a 10-day exposure (Scown et al. 2010). In a 21-day feeding exposure with up to 300 mg/g TiO_2 NP in the food of zebrafish (*Danio renio*) and rainbow trout, uptake was found directly from the water column and across the epithelial membrane in the gill (Johnston et al. 2010). Moreover, in zebrafish exposed to 1.5 mg/L CuNP, biochemical analyses revealed that the gill was the primary target organ for CuNP. Histological analyses confirmed that CuNP damaged the gill lamellae, characterized by proliferation of epithelial cells as well as edema of primary and secondary gill filaments (Griffitt et al. 2007). Respiratory toxicity of nanoparticles in fish was reported by some publications. Bilberg found that exposure of Eurasian perch to AgNP resulted in impairment of tolerance to hypoxia and considered AgNP affecting the gills externally (Bilberg et al. 2010). Exposure of rainbow trout to TiO_2 NP caused gill pathologies including edema and thickening of the lamellae (Federici et al. 2007).

Uptake of nanoparticles by fish gill cells has also been demonstrated by *in vitro* fish gill cell culture studies. In rainbow trout primary gill cell exposures, Farkas observed that AgNP can be taken up by these cells (Farkas et al. 2011). Using the rainbow trout gill cell line, RTgill-W1, uptake of tungsten carbide nanoparticles in different exposure media was also shown (Kühnel et al. 2009).

Except for the fish gill system, nanoparticles can enter through the fish intestine with water fluid during the dietary and drinking processes. Ramsden observed significant TiO_2 NP uptake in the intestine of juvenile rainbow trout, which were treated with a sublethal concentration of TiO_2 NP in their diet (Ramsden et al. 2009). AgNP was detected in intestinal tissues in Japanese medaka after 14 d exposure (Wu and Zhou 2013). Waterborne exposure of CuO-NP and ZnO-NP suspensions to Gold fish (*Carassius auratus*) resulted in copper and zinc accumulation in the intestine as well (Ates et al. 2015).

1.3.2 Uptake mechanisms

As discussed above, nanoparticle uptake by fish gill and gut takes place by incorporation into cells. Understanding of the mechanism of uptake at cellular level is necessary to understand nanoparticle toxicity. Due to the distinct properties, dissolved metal ions and nanoparticles enter cells via different pathways.

In the aquatic environment, dissolved silver can form different species: free Ag^+, $AgCl^0$, $AgCl_2^-$, $AgCl_3^{2-}$ and so on. Due to their different charges, cells take up these dissolved silver species via ion channels, passive diffusion or other pathways. Recent work suggests that Ag^+ enters fish by two pathways: Na^+ channels and the high-affinity Cu transporter Ctr1 (Grosell and Wood 2002; Lee et al. 2002), whereas $AgCl^0$ uptake occurs via simple diffusion due to its neutral charge (Hogstrand et al. 2003; Wood et al. 2002). For the negatively charged silver species, the precise uptake mechanisms are still unclear. But some evidence suggests that these negatively charged silver species still contribute to toxicity (Groh et al. 2014; Wood 2011).

In most studies, it was concluded that nanoparticles enter cells via energy-dependent, endocytic pathways (Stern et al. 2012). However, due to specific nanoparticle properties, some nanoparticles may enter cells by passive routes (Van Lehn et al. 2013). In general, vertebrate cells, such as from mammals or fish, take up nanoparticles by different kinds of endocytic pathways. Endocytosis is a fundamental process in cellular activities; it controls the exchange of particles or droplets between the external and the internal side of cells, signal transport, cell mortality and mitosis. Several kinds of endocytic pathways were identified for nanoparticle incorporation into animal cells: clathrin-

mediated endocytosis, caveolae-mediated endocytosis, macropinocytosis and phagocytosis (Figure 1.3) (Stern et al. 2012).
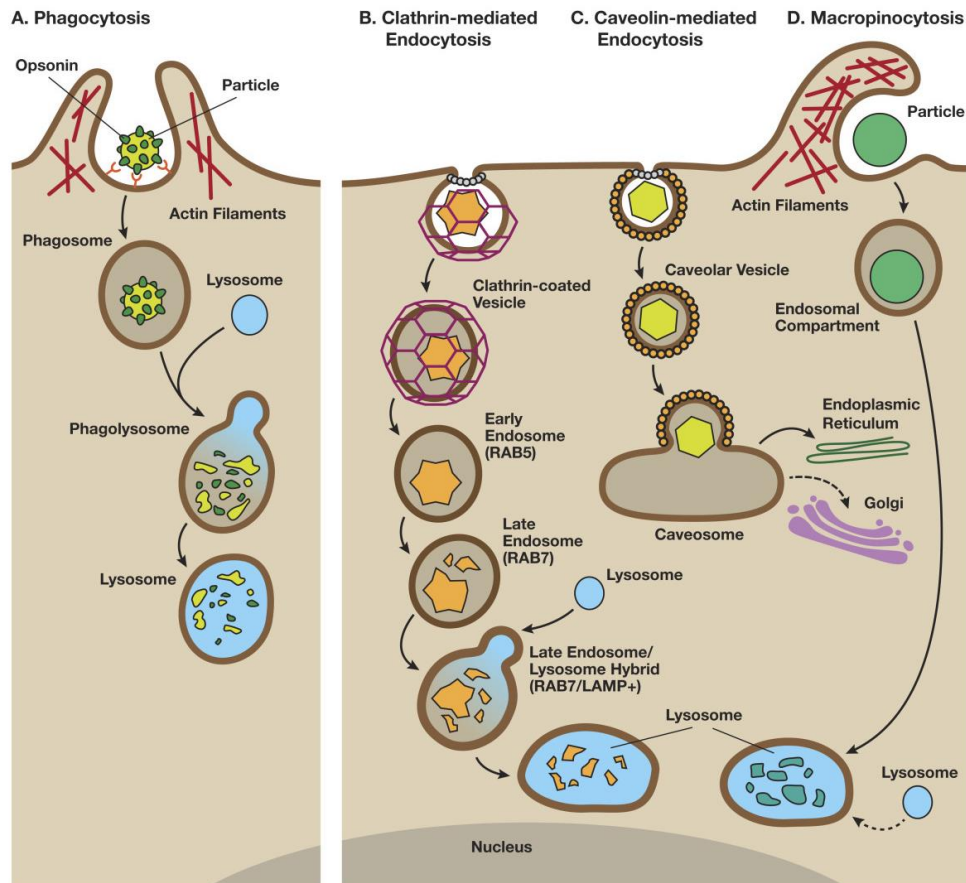
Figure 1.3 An overview of endocytic pathways.

(A) Phagocytosis. (B) Clathrin-mediated endocytosis. (C) Caveolin-mediated endocytosis. (D) Macropinocytosis. RAB: Rab Family Small GTPases. LAMP: Lysosome-associated membrane proteins. (Figure from Stern et al. 2012)

Clathrin-mediated endocytosis is by far the most studied endocytosis pathway. It contributes to nutrient uptake, efficient receptor signaling, as well as virus internalization. In the first stage of this pathway, clathrin, adaptor proteins (APs), receptors and other cytosolic proteins assemble clathrin-coated vesicles at the cytosolic side. Assembled clathrin-coated vesicles can detach from the cell membrane and undergo intracellular trafficking into the endo-lysosomal degradation system. Receptors in the clathrin-coated vesicle are recycled to the plasma membrane. The normal size of clathrin-coated vesicles are 50-300 nm. Using microcopy and endocytosis inhibitors, Greulich found

that AgNP enter human mesenchymal stem cells through clathrin-mediated endocytosis (Greulich et al. 2011).

Caveolae-mediated endocytosis is the most studied clathrin-independent carrier pathway. Caveolae-mediated endocytosis is identified in many biological processes, such as signaling transport, lipid regulation, and vesicular transport. Caveolae are small flask-shaped pits in the plasma membrane, consisting of caveolins. Caveolin-1 and caveolin-2 are the main biomarkers in this pathway, which form a striated coat on the surface of the caveolae membrane. After transport into the cytoplasm, caveolar vesicles fuse with early endosomes and form a caveosome. The caveosome is an endosomal compartment with neutral pH and transported to the endoplasmic reticulum and the Golgi. Nanoparticles in the caveosome avoid degradation in lysosomes. The size of caveolae are 200-500 nm. Xian found that caveolae-mediated endocytosis was the dominant pathway for the intracellular delivery of 4.5 nm AuNP in Hela cells (Xian et al. 2012).

Macropinocytosis is a cell drinking process, in which cells engulf a large quantity of external fluid by forming large organelles called macropinosomes. Unlike the other endocytosis mechanisms, macropinocytosis is an actin-regulated endocytic process and not directly driven by the cargo or the receptors, which means that macropinocytosis is a non-specific uptake pathway. Compared with other endocytic vesicles, macropinosomes have a larger (0.5-5 μm) size, lack a cytosolic coat and have an irregular shape. Macropinosomes also undergo the endo-lysosomal degradation pathway. HeLa and A549 cancer cell lines were shown to take up to 110 nm mesoporous silica nanoparticles by micropinocytosis (Meng et al. 2011).

Phagocytosis is a kind of endocytosis that occurs only in a few specialized cells, focusing on large extracellular particles such as pathogens, dead cells, and cell debris. Phagocytosis is triggered by a specific cell membrane recognition of the particle through the recruitment of receptors and is an actin-filament dependent process. The phagosome is fused with a lysosome, taking the typical lysosome degradation pathway.

1.3.3   Fate of nanoparticles in cells

Once the vesicles carrying nanoparticles detach from the plasma membrane, the vesicles are sorted and transported to different endocytic compartments. In most cases, the vesicle transport in the cytoplasma is an energy dependent process. Following sorting and transporting, trafficking vesicles deliver cargo to other subcellular compartments in endocytic pathways, from early endosome and a multivesicular bodies to late endosomes and lysosomes (Figure 1.4) (Canton and Battaglia 2012). In-

teracting with various biomolecules, nanoparticles can be degraded or accumulated in these endocytic compartments.
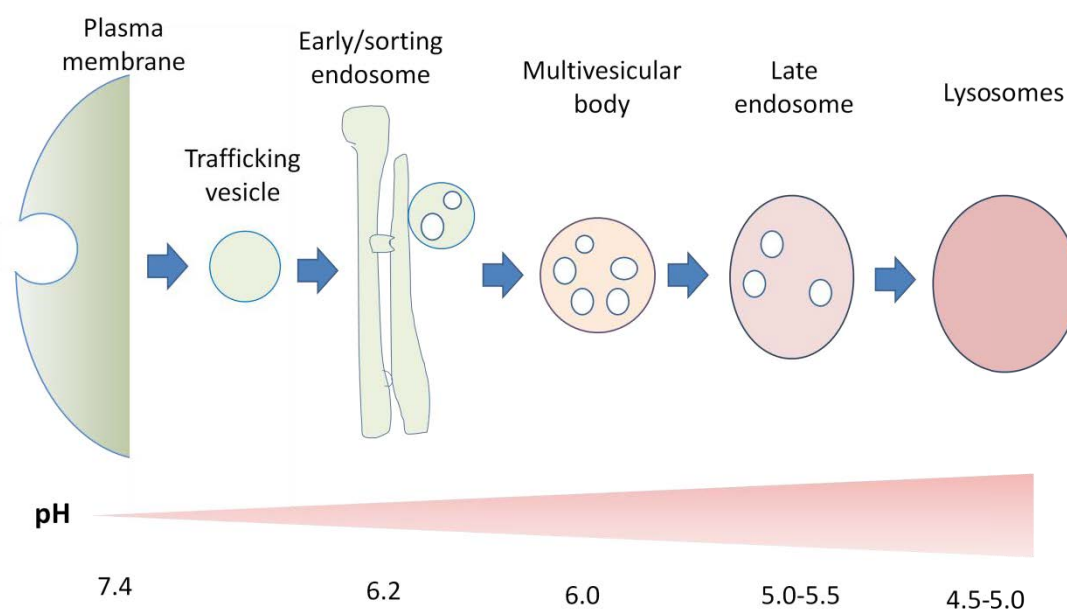
Figure 1.4 Schematics of the different endocytic compartments transported in cells.

The endocytic pathway is a dynamic process with spatiotemporal succession of different compartments, which continuously interchange their content. (Figure modified from Canton and Battaglia 2012).

Endocytic compartments are serial dynamic organelles in the cytoplasm which continuously interchange their content and are difficult to distinguish one from another. The nanoparticles can be transported from the plasma membrane to endosomes or lysosomes (Canton and Battaglia 2012).

Regarding nanoparticle toxicity, pH in the endocytic compartments is likely the most important parameter. As discussed above, nanoparticles can release metal ions in aqueous suspension. The dissolution of nanoparticles is mainly dependent on the pH. Often, nanoparticles have a significantly higher dissolution in acidic rather than neutral environments. In the endocytic compartments, the pH decreases from the early endosome to lysosome. The internal environment of a lysosome is harsh with a pH below 5.0. In this environment, nanoparticles, especially AgNP, CuNP, and ZnO-NP, are expected to release much more metal ions and can even be totally degraded. Setyawati tested the stability of AgNP under neutral physiological conditions, representing the cytosol and under conditions mimicking the lysosome. They found a 2-3 fold higher dissolution in the lysosome-

mimicking environment (pH 4.8) compared to the cytosol-mimicking solution (pH 6.9) (Setyawati et al. 2014).

Except for pH, biomolecules and inorganic ions in the endocytic pathways also affect the nanoparticles' stability. Functional groups, like sulfhydryl (R-SH) groups, have an extremely high association constant and strongly react with dissolved metal ions. As a result, the equilibrium of dissolving nanoparticles shifts further enhancing dissolution. For some specific nanoparticles, such as AgNP, dissolution is altered with the chloride concentration leading to $AgCl_n$ complex formation.

1.4   Interactions of nanoparticles with proteins

1.4.1   NP-protein corona

Nanoparticles, with very high surface to volume ratios, have a great active surface than large sized particles. In biological systems, nanoparticles tend to have a reduced surface active energy from being covered with various biomolecules (Klein 2007; Monopoli et al. 2011). Upon interact with cells, the surfaces of nanoparticles are immediately covered by biomolecules and sorption processes may change the fate of nanoparticles and the effects of nanoparticles to cells (Cedervall et al. 2007; Engel et al. 2004; Lynch and Dawson 2008; Nel et al. 2009). This sorption results in a biological "corona" on the surface of nanoparticles and builds a new "bio-nano interface" between nanoparticles and the biological system (Ge et al. 2015; Lai et al. 2012; Shemetov et al. 2012).

It has previously been proposed that the function and fate of nanoparticles in biological environments is related to the nature and composition of their surface protein corona (Lynch et al. 2006; Monopoli et al. 2012). Thus, the NP-protein complex interacts with the biological system rather than with the bare nanoparticles surface. This, is a key phenomenon that needs to be understood in order to develop smart nanomaterials and to ensure the safe implementation of nanotechnology.

The formation of the corona is a complex dynamic process. There are different kinds of interactions in this process, such as hydrodynamic interactions, electro-dynamic interactions, electrostatic interactions, steric interactions and polymer bridging interactions (Lynch and Dawson 2008; Nel et al. 2009). Initially, low-affinity, high-abundance proteins bind quickly to the surface of nanoparticles. Subsequently, proteins on the surface are exchanged by other lower abundance but higher affinity proteins. Adsorption reaches equilibrium, where exchanges continue between NP-absorbed proteins and free proteins in the surrounding environment. Research suggested that the protein corona is composed of an outer layer of weakly bound proteins with a quick exchange rate with free proteins (soft corona) and an inner layer of selected proteins with a high affinity and low exchange rate (hard corona) (Figure 1.5) (Mahmoudi et al. 2011a; Walczyk et al. 2010).
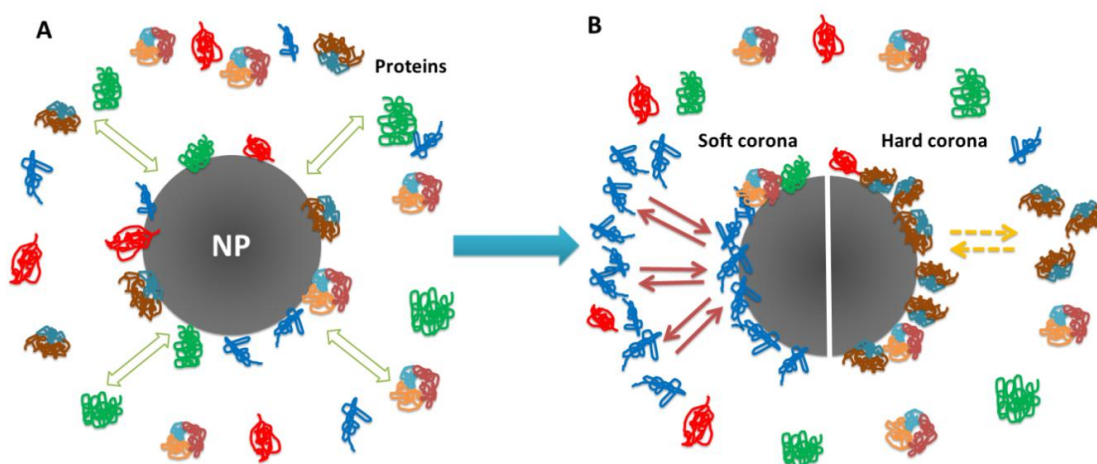
Figure 1.5 Interaction of nanoparticles and proteins.

(A) Figure shows the possible exchange/interaction at the bio-nano-interface initially. (B) Nanoparticle is surrounded by the protein corona composed of an outer weakly interacting layer of protein (left, full red arrows) rapidly exchanging with a collection of free proteins (soft corona) and a slowly exchanging corona of proteins (right, dashed yellow arrows, hard corona).

1.4.2   Impact of NP-protein interaction on proteins

With the formation of the NP-protein corona, the properties and functions of nanoparticles change compared to bare nanoparticles. It is the NP-protein corona that plays a role in the uptake, intracellular distribution and fate of nanoparticles. However, it is also important to understand to what extent NP-protein corona complexes impact the properties of proteins.

One type of effect may be conformational changes of proteins after interaction with nanoparticles. Since protein function is explicitly linked with protein conformation, understanding the type of conformational changes influenced by the proteins upon interaction with nanoparticles is important. For proteins, there are two kinds of changes: reversible and irreversible conformational changes. From a toxicity perspective, irreversible changes of protein conformation are more important because they may result in cell damage, organ pathogeny and injury.

The conformational changes of bovine serum albumin (BSA) at the BSA-AuNP interface were considered as an example of reversible conformational changes (Shang et al. 2007). In this work, BSA was found to undergo conformational changes at both secondary and tertiary structure levels, which were investigated by ultraviolet–visible spectroscopy (UV/Vis) absorption, fluorescence, cir-

cular dichroism (CD), and Fourier transform infrared spectroscopy (FTIR). Another group studied the interaction of AgNP with different concentrations of BSA and found the absorption of UV/Vis in NP-protein to shift as a function of BSA concentration and pH (Ravindran et al. 2010).

Irreversible conformational changes were also observed in the interaction of iron-saturated human transferrin and super paramagnetic iron oxide nanoparticles (SPIONs) (Mahmoudi et al. 2011b). The authors confirmed that the exposure of iron-saturated human transferrin to the SPIONs resulted in the release of iron, which caused irreversible changes to the main function of this protein, the transport of iron between cells. Furthermore, conformation of transferrin changed from a compact to an open state. After removal of the magnetic nanoparticles by magnetic-activated cell sorting (MACS), the original protein conformation was not recovered, indicating irreversible changes in the transferrin conformation after interaction with the SPIONs.

The interaction with nanoparticles can also lead to protein dysfunction, such as altered enzyme activity and structure. Linse showed that nanoparticles (copolymer particles, cerium oxide particles, quantum dots, and carbon nanotubes) enhanced the probability of appearance of a critical nucleus for nucleation of protein fibrils from human β2-microglobulin (Linse et al. 2007). Another study found that AgNP undergo a size dependent interaction with HIV-1virus via preferential binding to the gp120 glycoprotein knobs and inhibit the virus from binding to host cells *in vitro* (Elechiguerra et al. 2005). Wu et al. observed that TiO_2 NP can promote Aβ fibrillation by shortening the nucleation process, which is the key rate determining step of fibrillation. They concluded that the interaction between Aβ and nanoparticles may contribute to Alzheimer's disease (AD) etiology (Wu et al. 2008).

1.4.3 NP-protein corona in biological environments

Studies on the NP-protein corona initially focused on single proteins, but there is increasing interest in more complex interactions. Such complex biological systems are blood plasma, extracellular proteins secreted from cells, cell extracts or even within living cells.

Several groups studied the interaction of various nanoparticles with blood proteins. Some reported that the interaction between nanoparticles and common blood proteins may lead to protein fibrillation (Shemetov et al. 2012). Tenzer developed a label-free snapshot proteomics approach that can be used to obtain quantitative time-resolved profiles of human plasma coronas formed on silica and polystyrene nanoparticles of various size and surface functionalization. It was found that the corona forms rapidly (< 0.5 minutes) and changes significantly in terms of the amount of protein

bound. Rapid corona formation was found to affect haemolysis, thrombocyte activation, nanoparticle uptake and endothelial cell death at an early exposure time (Tenzer et al. 2013).

Others have reported nanoparticle interactions with proteins extracted from cells. Comparing the AgNP-protein corona composition with different size and coatings of AgNP in cell culture medium, researchers found that the difference in corona formation was based on surface curvature as well as on electrostatic and hydrophobic interactions (Shannahan et al. 2013). Wigginton incubated AgNP with proteins sourced from *E. coli* and analyzed the AgNP-protein corona composition. They found that tryptophanase (TNase) has an especially high affinity for AgNP, despite its low abundance in *E. coli*. Further experiments showed that AgNP preferentially bind to a protein fragment containing a residue (Arg103) in the TNase active site and induce an TNase enzymatic activity loss (Wigginton et al. 2010). Eigenheer investigated AgNP interacting with proteins from yeast extracts across six samples with varied AgNP properties and solution conditions. Their results revealed that engineered surface coatings strongly mediate protein corona formation and that the protein affinities are similar for different biological and environmental systems (Eigenheer et al. 2014).

Exploiting the specific properties of magnetic nanoparticles, two studies investigated the NP-protein interaction in living cells. Bertoli isolated the silica coated magnetite nanoparticles enriched in organelles from A549 cells in a time resolved manner. The NP-protein corona was isolated by lysis of these organelles. Corona composition analysis suggested that a significant portion of the original corona (derived from the serum in which particles were presented to the cells) was preserved as nanoparticles trafficked through the cells (Bertoli et al. 2014). Using a similar technique, Hofmann isolated intracellular vesicles containing superparamagnetic iron oxide-polystyrene nanoparticles from HeLa cells and analyzed the protein composition by mass spectrometry (Hofmann et al. 2014). Results showed that the entry mechanism is controlled by actin reorganization and ADP-ribosylation factor 1. Their proteomics data demonstrated a central role for multivesicular bodies and multilamellar lysosomes in trafficking and final nanoparticle storage.

1.5   Research objectives

Summarizing the state of the art on AgNP and the impact on aquatic organisms, it can be stated that both uptake and toxicity have been demonstrated for various species. However, the exact mechanisms by which AgNP interact with aquatic organism at the cellular level are not yet understood. In light of this, the overall aim of this thesis research was to explore the interaction of citrate-coated AgNP with cells of an aquatic organism, specifically rainbow trout (*Oncorhynchus mykiss*). Citrate is a commonly used reducing agent and stabilizer in the synthesis of metal colloids and has long been applied to controllably synthesize AgNP (Panáček et al. 2006). As a common molecule in organisms, citrate also has a good biocompatibility. Rainbow trout belongs to the salmon family, which is ecologically and economically important and also widely applied in environmental toxicology research and in risk assessment of chemicals. In order to advance mechanistic knowledge of AgNP-fish cell interactions, a permanent rainbow trout cell line was chosen as an experimental model. A permanent cell line is a homogeneous batch of cells that can be cultured indefinitely. Such models are ideal for mechanistic studies because the experimental environment can be completely controlled and because cellular behaviors can be studied under defined conditions. As well, dosing of cell cultures is easier and more reproducible than of intact animals and, can potentially avoid the use of animals (Bols et al. 2005). Inasmuch as nanoparticles in the water column are likely to get in contact with the respiratory organ of fish, i.e. the gills, I selected the rainbow trout gill cell line, RTgill-W1 (Bols et al. 1994), for my research. The RTgill-W1 cell line is a well-established *in vitro* model (Bols et al. 2005; Lee et al. 2009). Importantly, it is known for its ability to withstand exposure to very simple culture media (Dayeh et al. 2002; Schirmer et al. 1997) and to take up nanoparticles even if they are present in an agglomerated state in the exposure medium (Kühnel et al. 2009).

Focusing on AgNP and the RTgill-W1 cell line, I addressed the following questions in my research:

- How do AgNP behave in different cell exposure environments, and what are the concentrations causing toxic effects to cells?

- How, and to what extents are AgNP taken up by the cells and what is their intracellular distribution and fate over both short (few hours) and long (several days) exposure durations?

- Which intracellular proteins interact with the AgNP and can they provide clues to shed light on the mechanisms of AgNP toxicity?

To address these questions, I carried out this research in four steps (Figure 1.6). In the first step, AgNP behaviour was investigated in cell exposure media by determining the size, surface charge and dissolution rate. In the second step, short term and long term toxicity of AgNP to RTgill-W1 cells were tested and quantified by different measurements. To be able to expose the RTgill-W1 cells in a protein-free exposure environment for long-term toxicity studies, a new RTgill-W1 strain was established by a selection procedure. The cellular uptake of AgNP was studied in a third step. Finally, a new method was developed to isolate the AgNP-protein corona from intact RTgill-W1 cells and the proteins were identified by mass spectrometry. With this work, my thesis contributes to a mechanistic understanding of AgNP interactions with cells by linking and quantifying exposures to effects.
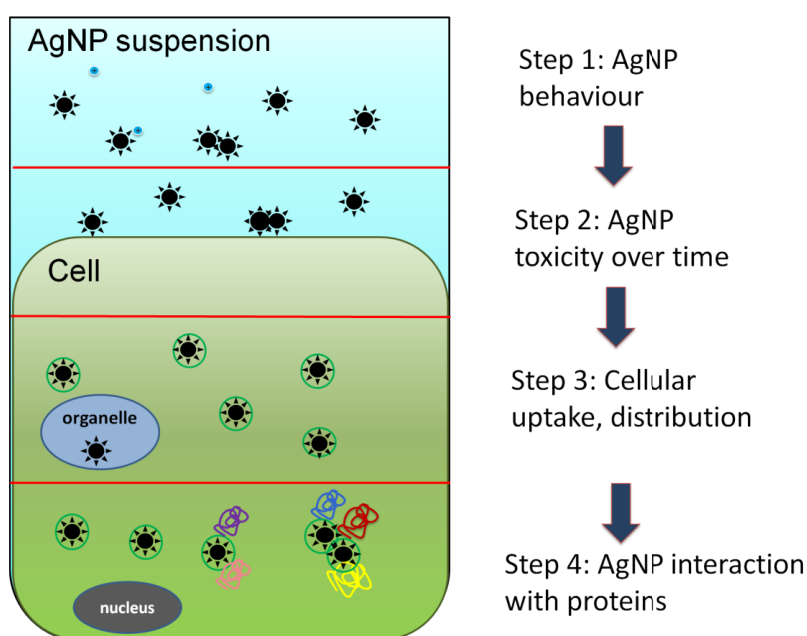
Figure 1.6 Scheme of this project.

In order to achieve my research aim, I designed a four-step procedure to systematically link nanoparticles exposure and effects to RTgill-W1 cells.

The results of my research are presented in three chapters, with a brief introduction to each chapter given below. In the final chapter 5, I summarize the major outcomes of this research and conclude with an outlook to suggest the next research steps.

Chapter 2 (Step 1 and 2): **Toxicity of silver nanoparticles to a fish gill cell line: role of medium composition.**

In aqueous solutions, AgNP behaviour is affected by a variety of factors which lead to altered AgNP size and toxicity. This chapter explores the effect of media composition on AgNP behaviour and toxicity to the RTgill-W1 cells. Three different exposure media (L15/ex, L15/ex w/o Cl and d-L15/ex) were used. It was found that ionic strength and chloride content had a dominant effect on the behaviour of AgNP. Stronger agglomeration of AgNP led to higher toxicity, likely due to increased exposure by deposition of AgNP onto the cells. Considering the effect of dissolved silver and silver ligands to AgNP toxicity, a particle-specific effect was confirmed in RTgill-W1 cells. This effect was specifically seen as an impairment of lysosome integrity.

Chapter 3 (Step 3 and 4): **Silver nanoparticle-protein interactions in intact rainbow trout gill cells.**

This chapter focuses on the AgNP uptake and accumulation in the RTgill-W1 cells and on the resulting interaction of the AgNP with cellular proteins. It was shown that RTgill-W1 cells accumulated total silver more efficiently upon exposure to AgNP compared to $AgNO_3$. Electron microscopy and dependence of uptake on temperature suggests that RTgill-W1 cells take up AgNP via an energy depend pathway and store it in endocytic compartments, such as endosomes and lysosomes. With subcellular fractionation, the AgNP-protein corona was recovered from intact endocytic and other compartments and analyzed by mass spectrometry. Based on the sub-cellular location and function of proteins identified from the AgNP-protein corona, an initial mechanism of AgNP toxicity is described involving cell membrane and adhesion functions, uptake and vesicular trafficking, cell cycle, and stress response.

Chapter 4 (Step 2 and 3): **Silver nanoparticles inhibit fish gill cell proliferation in protein free culture medium.**

In this chapter, a long term exposure of RTgill-W1 cells to AgNP in a protein-free medium and ensuing toxicity is discussed. Vertebrate cells normally require an undefined serum component to be able to remain viable and proliferate over extended times. Major components of the serum are proteins, such as serum albumin, which are known to alter the behavior of nanoparticles. Thus, in order to conduct AgNP exposure without interference by proteins, a new strain of RTgill-W1 cells was isolated after adaptation to a commercially available protein-free medium. This new strain was

RTgill-W1-pf. Twelve days exposure of these cells to AgNP in this medium demonstrated that AgNP can inhibit RTgill-W1-pf proliferation.

References

Aitken RJ, Chaudhry MQ, Boxall ABA, Hull M. 2006. Manufacture and use of nanomaterials: current status in the UK and global trends. Occupational Medicine-Oxford 56(5):300-306.

Aleman J, Chadwick AV, He J, Hess M, Horie K, Jones RG, Kratochvil P, Meisel I, Mita I, Moad G and others. 2007. Definitions of terms relating to the structure and processing of sols, gels, networks, and inorganic-organic hybrid materials (IUPAC Recommendations 2007). Pure and Applied Chemistry 79(10):1801-1827.

Aruoja V, Dubourguier H-C, Kasemets K, Kahru A. 2009. Toxicity of nanoparticles of CuO, ZnO and TiO2 to microalgae Pseudokirchneriella subcapitata. Science of The Total Environment 407(4):1461-1468.

Ates M, Arslan Z, Demir V, Daniels J, Farah IO. 2015. Accumulation and toxicity of CuO and ZnO nanoparticles through waterborne and dietary exposure of goldfish (Carassiusauratus). Environmental Toxicology 30(1):119-128.

Badawy AME, Luxton TP, Silva RG, Scheckel KG, Suidan MT, Tolaymat TM. 2010. Impact of Environmental Conditions (pH, Ionic Strength, and Electrolyte Type) on the Surface Charge and Aggregation of Silver Nanoparticles Suspensions. Environmental Science & Technology 44(4):1260-1266.

Baun A, Hartmann N, Grieger K, Kusk K. 2008. Ecotoxicity of engineered nanoparticles to aquatic invertebrates: a brief review and recommendations for future toxicity testing. Ecotoxicology 17(5):387-395.

Behra R, Sigg L, Clift MJD, Herzog F, Minghetti M, Johnston B, Petri-Fink A, Rothen-Rutishauser B. 2013. Bioavailability of silver nanoparticles and ions: from a chemical and biochemical perspective. Journal of The Royal Society Interface 10(87).

Bertoli F, Davies G-L, Monopoli MP, Moloney M, Gun'ko YK, Salvati A, Dawson KA. 2014. Magnetic Nanoparticles to Recover Cellular Organelles and Study the Time Resolved Nanoparticle-Cell Interactome throughout Uptake. Small 10(16):3307-3315.

Bilberg K, Malte H, Wang T, Baatrup E. 2010. Silver nanoparticles and silver nitrate cause respiratory stress in Eurasian perch (Perca fluviatilis). Aquatic Toxicology 96(2):159-165.

Bols NC, Barlian A, Chirinotrejo M, Caldwell SJ, Goegan P, Lee LEJ. 1994. Development of a Cell-Line from Primary Cultures of Rainbow-Trout, Oncorhyrzchus Mykiss (Walbaum), Gills. Journal of Fish Diseases 17(6):601-611.

Bols NC, Dayeh VR, Lee LEJ, Schirmer K. 2005. Chapter 2 Use of fish cell lines in the toxicology and ecotoxicology of fish. Piscine cell lines in environmental toxicology. In: Mommsen TP, Moon TW, editors. Biochemistry and Molecular Biology of Fishes: Elsevier. p 43-84.

Bystrzejewska-Piotrowska G, Golimowski J, Urban PL. 2009. Nanoparticles: Their potential toxicity, waste and environmental management. Waste Management 29(9):2587-2595.

Canton I, Battaglia G. 2012. Endocytosis at the nanoscale. Chemical Society Reviews 41(7):2718-2739.

Cedervall T, Lynch I, Lindman S, Berggård T, Thulin E, Nilsson H, Dawson KA, Linse S. 2007. Understanding the nanoparticle–protein corona using methods to quantify exchange rates and affinities of proteins for nanoparticles. Proceedings of the National Academy of Sciences 104(7):2050-2055.

Chen X, Mao SS. 2007. Titanium dioxide nanomaterials: Synthesis, properties, modifications, and applications. Chemical Reviews 107(7):2891-2959.

Choi JE, Kim S, Ahn JH, Youn P, Kang JS, Park K, Yi J, Ryu D-Y. 2010. Induction of oxidative stress and apoptosis by silver nanoparticles in the liver of adult zebrafish. Aquatic Toxicology 100(2):151-159.

Christensen GM, Tucker JH. 1976. Effects of selected water toxicants on the in vitro activity of fish carbonic anhydrase. Chemico-Biological Interactions 13(2):181-192.

Christian P, Von der Kammer F, Baalousha M, Hofmann T. 2008. Nanoparticles: structure, properties, preparation and behaviour in environmental media. Ecotoxicology 17(5):326-343.

Dayeh VR, Schirmer K, Bols NC. 2002. Applying whole-water samples directly to fish cell cultures in order to evaluate the toxicity of industrial effluent. Water Research 36(15):3727-3738.

Eigenheer R, Castellanos ER, Nakamoto MY, Gerner KT, Lampe AM, Wheeler KE. 2014. Silver nanoparticle protein corona composition compared across engineered particle properties and environmentally relevant reaction conditions. Environmental Science: Nano.

Elechiguerra J, Burt J, Morones J, Camacho-Bragado A, Gao X, Lara H, Yacaman M. 2005. Interaction of silver nanoparticles with HIV-1. Journal of Nanobiotechnology 3(1):6.

Engel MFM, Visser AJWG, van Mierlo CPM. 2004. Conformation and orientation of a protein folding intermediate trapped by adsorption. Proceedings of the National Academy of Sciences of the United States of America 101(31):11316-11321.

Fabrega J, Luoma SN, Tyler CR, Galloway TS, Lead JR. 2011. Silver nanoparticles: Behaviour and effects in the aquatic environment. Environment International 37(2):517-531.

Farkas J, Christian P, Gallego-Urrea JA, Roos N, Hassellöv M, Tollefsen KE, Thomas KV. 2011. Uptake and effects of manufactured silver nanoparticles in rainbow trout (Oncorhynchus mykiss) gill cells. Aquatic Toxicology 101(1):117-125.

Farkas J, Christian P, Urrea JAG, Roos N, Hassellöv M, Tollefsen KE, Thomas KV. 2010. Effects of silver and gold nanoparticles on rainbow trout (Oncorhynchus mykiss) hepatocytes. Aquatic Toxicology 96(1):44-52.

Federici G, Shaw BJ, Handy RD. 2007. Toxicity of titanium dioxide nanoparticles to rainbow trout (Oncorhynchus mykiss): Gill injury, oxidative stress, and other physiological effects. Aquatic Toxicology 84(4):415-430.

Finholt P, Solvang S. 1968. Dissolution kinetics of drugs in human gastric juice—the role of surface tension. Journal of Pharmaceutical Sciences 57(8):1322-1326.

Foldbjerg R, Olesen P, Hougaard M, Dang DA, Hoffmann HJ, Autrup H. 2009. PVP-coated silver nanoparticles and silver ions induce reactive oxygen species, apoptosis and necrosis in THP-1 monocytes. Toxicology Letters 190(2):156-162.

Ge C, Tian J, Zhao Y, Chen C, Zhou R, Chai Z. 2015. Towards understanding of nanoparticle–protein corona. Archives of Toxicology:1-21.

George S, Lin S, Ji Z, Thomas CR, Li L, Mecklenburg M, Meng H, Wang X, Zhang H, Xia T and others. 2012. Surface Defects on Plate-Shaped Silver Nanoparticles Contribute to Its Hazard Potential in a Fish Gill Cell Line and Zebrafish Embryos. Acs Nano 6(5):3745-3759.

Greulich C, Diendorf J, Simon T, Eggeler G, Epple M, Köller M. 2011. Uptake and intracellular distribution of silver nanoparticles in human mesenchymal stem cells. Acta Biomaterialia 7(1):347-354.

Griffitt RJ, Weil R, Hyndman KA, Denslow ND, Powers K, Taylor D, Barber DS. 2007. Exposure to Copper Nanoparticles Causes Gill Injury and Acute Lethality in Zebrafish (Danio rerio). Environmental Science & Technology 41(23):8178-8186.

Groh KJ, Dalkvist T, Piccapietra F, Behra R, Suter MJF, Schirmer K. 2014. Critical influence of chloride ions on silver ion-mediated acute toxicity of silver nanoparticles to zebrafish embryos. Nanotoxicology:1-11.

Grosell M, Wood CM. 2002. Copper uptake across rainbow trout gills: mechanisms of apical entry. Journal of Experimental Biology 205(8):1179-1188.

Hedberg J, Skoglund S, Karlsson M-E, Wold S, Odnevall Wallinder I, Hedberg Y. 2014. Sequential Studies of Silver Released from Silver Nanoparticles in Aqueous Media Simulating Sweat, Laundry Detergent Solutions and Surface Water. Environmental Science & Technology 48(13):7314-7322.

Hofmann D, Tenzer S, Bannwarth MB, Messerschmidt C, Glaser S-F, Schild H, Landfester K, Mailänder V. 2014. Mass Spectrometry and Imaging Analysis of Nanoparticle-Containing Vesicles Provide a Mechanistic Insight into Cellular Trafficking. ACS Nano 8(10):10077-10088.

Hogstrand C, Galvez F, Wood CM. 1996. Toxicity, silver accumulation and metallothionein induction in freshwater rainbow trout during exposure to different silver salts. Environmental Toxicology and Chemistry 15(7):1102-1108.

Hogstrand C, Grosell M, Wood CM, Hansen H. 2003. Internal redistribution of radiolabelled silver among tissues of rainbow trout (*Oncorhynchus mykiss*) and European eel (*Anguilla anguilla*): the influence of silver speciation. Aquatic Toxicology 63(2):139-157.

Holden PA, Nisbet RM, Lenihan HS, Miller RJ, Cherr GN, Schimel JP, Gardea-Torresdey JL. 2013. Ecological Nanotoxicology: Integrating Nanomaterial Hazard Considerations Across the Subcellular, Population, Community, and Ecosystems Levels. Accounts of Chemical Research 46(3):813-822.

Huynh KA, Chen KL. 2011. Aggregation Kinetics of Citrate and Polyvinylpyrrolidone Coated Silver Nanoparticles in Monovalent and Divalent Electrolyte Solutions. Environmental Science & Technology 45(13):5564-5571.

Ivask A, ElBadawy A, Kaweeteerawat C, Boren D, Fischer H, Ji Z, Chang CH, Liu R, Tolaymat T, Telesca D and others. 2014. Toxicity Mechanisms in *Escherichia coli* Vary for Silver Nanoparticles and Differ from Ionic Silver. ACS Nano 8(1):374-386.

Jang M-H, Kim W-K, Lee S-K, Henry TB, Park J-W. 2014. Uptake, Tissue Distribution, and Depuration of Total Silver in Common Carp (Cyprinus carpio) after Aqueous Exposure to Silver Nanoparticles. Environmental Science & Technology 48(19):11568-11574.

Johnston BD, Scown TM, Moger J, Cumberland SA, Baalousha M, Linge K, van Aerle R, Jarvis K, Lead JR, Tyler CR. 2010. Bioavailability of Nanoscale Metal Oxides TiO2, CeO2, and ZnO to Fish. Environmental Science & Technology 44(3):1144-1151.

Kaegi R, Sinnet B, Zuleeg S, Hagendorfer H, Mueller E, Vonbank R, Boller M, Burkhardt M. 2010. Release of silver nanoparticles from outdoor facades. Environmental Pollution 158(9):2900-2905.

Klaine SJ, Alvarez PJJ, Batley GE, Fernandes TF, Handy RD, Lyon DY, Mahendra S, McLaughlin MJ, Lead JR. 2008. Nanomaterials in the environment: Behavior, fate, bioavailability, and effects. Environmental Toxicology and Chemistry 27(9):1825-1851.

Klein J. 2007. Probing the interactions of proteins and nanoparticles. Proceedings of the National Academy of Sciences 104(7):2029-2030.

Kruszewski M, Brzoska K, Brunborg G, Asare N, Dobrzyńska M, Dušinská M, Fjellsbø LM, Georgantzopoulou A, Gromadzka-Ostrowska J, Gutleb AC and others. 2011. Chapter Five - Toxicity of Silver Nanomaterials in Higher Eukaryotes. In: James CF, editor. Advances in Molecular Toxicology: Elsevier. p 179-218.

Kühnel D, Busch W, Meißner T, Springer A, Potthoff A, Richter V, Gelinsky M, Scholz S, Schirmer K. 2009. Agglomeration of tungsten carbide nanoparticles in exposure medium does not prevent uptake and toxicity toward a rainbow trout gill cell line. Aquatic Toxicology 93(2-3):91-99.

Lai ZW, Yan Y, Caruso F, Nice EC. 2012. Emerging Techniques in Proteomics for Probing Nano–Bio Interactions. Acs Nano 6(12):10438-10448.

Lee J, Peña MMO, Nose Y, Thiele DJ. 2002. Biochemical Characterization of the Human Copper Transporter Ctr1. Journal of Biological Chemistry 277(6):4380-4387.

Lee L, Dayeh V, Schirmer K, Bols N. 2009. Applications and potential uses of fish gill cell lines: examples with RTgill-W1. In Vitro Cellular & Developmental Biology - Animal 45(3):127-134.

Levard C, Reinsch BC, Michel FM, Oumahi C, Lowry GV, Brown GE, Jr. 2011. Sulfidation Processes of PVP-Coated Silver Nanoparticles in Aqueous Solution: Impact on Dissolution Rate. Environmental Science & Technology 45(12):5260-5266.

Linse S, Cabaleiro-Lago C, Xue W-F, Lynch I, Lindman S, Thulin E, Radford SE, Dawson KA. 2007. Nucleation of protein fibrillation by nanoparticles. Proceedings of the National Academy of Sciences 104(21):8691-8696.

Lynch I, Dawson KA. 2008. Protein-nanoparticle interactions. Nano Today 3(1-2):40-47.

Lynch I, Dawson KA, Linse S. 2006. Detecting Cryptic Epitopes Created by Nanoparticles. Science Signaling 2006(327):pe14.

MacCuspie RI, Allen AJ, Hackley VA. 2010. Dispersion stabilization of silver nanoparticles in synthetic lung fluid studied under in situ conditions. Nanotoxicology 5(2):140-156.

Mahmoudi M, Lynch I, Ejtehadi MR, Monopoli MP, Bombelli FB, Laurent S. 2011a. Protein–Nanoparticle Interactions: Opportunities and Challenges. Chemical Reviews 111(9):5610-5637.

Mahmoudi M, Shokrgozar MA, Sardari S, Moghadam MK, Vali H, Laurent S, Stroeve P. 2011b. Irreversible changes in protein conformation due to interaction with superparamagnetic iron oxide nanoparticles. Nanoscale 3(3):1127-1138.

Masciangioli T, Zhang W-X. 2003. Peer Reviewed: Environmental Technologies at the Nanoscale. Environmental Science & Technology 37(5):102A-108A.

Mason A, Jenkins K. 1995. Metal detoxification in aquatic organisms. Metal speciation and bioavailability in aquatic systems 3:479-608.

Maynard AD, Aitken RJ, Butz T, Colvin V, Donaldson K, Oberdorster G, Philbert MA, Ryan J, Seaton A, Stone V and others. 2006. Safe handling of nanotechnology. Nature 444(7117):267-269.

Meng H, Yang S, Li Z, Xia T, Chen J, Ji Z, Zhang H, Wang X, Lin S, Huang C and others. 2011. Aspect Ratio Determines the Quantity of Mesoporous Silica Nanoparticle Uptake by a Small GTPase-Dependent Macropinocytosis Mechanism. ACS Nano 5(6):4434-4447.

Monopoli MP, Aberg C, Salvati A, Dawson KA. 2012. Biomolecular coronas provide the biological identity of nanosized materials. Nature Nanotechnology 7(12):779-786.

Monopoli MP, Walczyk D, Campbell A, Elia G, Lynch I, Baldelli Bombelli F, Dawson KA. 2011. Physical−Chemical Aspects of Protein Corona: Relevance to in Vitro and in Vivo Biological Impacts of Nanoparticles. Journal of the American Chemical Society 133(8):2525-2534.

Moos N, Slaveykova VI. 2013. Oxidative stress induced by inorganic nanoparticles in bacteria and aquatic microalgae – state of the art and knowledge gaps. Nanotoxicology 8(6):605-630.

Navarro E, Baun A, Behra R, Hartmann N, Filser J, Miao A-J, Quigg A, Santschi P, Sigg L. 2008a. Environmental behavior and ecotoxicity of engineered nanoparticles to algae, plants, and fungi. Ecotoxicology 17(5):372-386.

Navarro E, Piccapietra F, Wagner B, Marconi F, Kaegi R, Odzak N, Sigg L, Behra R. 2008b. Toxicity of Silver Nanoparticles to Chlamydomonas reinhardtii. Environmental Science & Technology 42(23):8959-8964.

Nel AE, Madler L, Velegol D, Xia T, Hoek EMV, Somasundaran P, Klaessig F, Castranova V, Thompson M. 2009. Understanding biophysicochemical interactions at the nano-bio interface. Nat Mater 8(7):543-557.

Oberdorster G, Oberdorster E, Oberdorster J. 2005. Nanotoxicology: An emerging discipline evolving from studies of ultrafine particles. Environmental Health Perspectives 113(7):823-839.

Odzak N, Kistler D, Behra R, Sigg L. 2015. Dissolution of metal and metal oxide nanoparticles under natural freshwater conditions. Environmental Chemistry 12(2):138-148.

Ohkuma S, Poole B. 1978. Fluorescence probe measurement of the intralysosomal pH in living cells and the perturbation of pH by various agents. Proceedings of the National Academy of Sciences 75(7):3327-3331.

Panáček A, Kvítek L, Prucek R, Kolář M, Večeřová R, Pizúrová N, Sharma VK, Nevěčná Tj, Zbořil R. 2006. Silver Colloid Nanoparticles: Synthesis, Characterization, and Their Antibacterial Activity. The Journal of Physical Chemistry B 110(33):16248-16253.

Piao MJ, Kang KA, Lee IK, Kim HS, Kim S, Choi JY, Choi J, Hyun JW. 2011. Silver nanoparticles induce oxidative cell damage in human liver cells through inhibition of reduced glutathione and induction of mitochondria-involved apoptosis. Toxicology Letters 201(1):92-100.

Piccapietra F, Sigg L, Behra R. 2012. Colloidal Stability of Carbonate-Coated Silver Nanoparticles in Synthetic and Natural Freshwater. Environmental Science & Technology 46(2):818-825.

Rai M, Yadav A, Gade A. 2009. Silver nanoparticles as a new generation of antimicrobials. Biotechnology Advances 27(1):76-83.

Ramsden C, Smith T, Shaw B, Handy R. 2009. Dietary exposure to titanium dioxide nanoparticles in rainbow trout, (<i>Oncorhynchus mykiss</i>): no effect on growth, but subtle biochemical disturbances in the brain. Ecotoxicology 18(7):939-951.

Ravindran A, Singh A, Raichur AM, Chandrasekaran N, Mukherjee A. 2010. Studies on interaction of colloidal Ag nanoparticles with Bovine Serum Albumin (BSA). Colloids and Surfaces B: Biointerfaces 76(1):32-37.

Reidy B, Haase A, Luch A, Dawson KA, Lynch I. 2013. Mechanisms of silver nanoparticle release, transformation and toxicity: a critical review of current knowledge and recommendations for future studies and applications. Materials 6(6):2295-2350.

Reinsch BC, Levard C, Li Z, Ma R, Wise A, Gregory KB, Brown GE, Lowry GV. 2012. Sulfidation of Silver Nanoparticles Decreases Escherichia coli Growth Inhibition. Environmental Science & Technology 46(13):6992-7000.

Salata OV. 2004. Applications of nanoparticles in biology and medicine. Journal of Nanobiotechnology 2(1):3.

Schirmer K, Behra R, Sigg L, Sutera MJ-F. 2013. Ecotoxicological Aspects of Nanomaterials in the Aquatic Environment. Safety Aspects of Engineered Nanomaterials:135.

Schirmer K, Chan AGJ, Greenberg BM, Dixon DG, Bols NC. 1997. Methodology for demonstrating and measuring the photocytotoxicity of fluoranthene to fish cells in culture. Toxicology in Vitro 11(1-2):107-119.

Schrand AM, Rahman MF, Hussain SM, Schlager JJ, Smith DA, Syed AF. 2010. Metal-based nanoparticles and their toxicity assessment. Wiley Interdisciplinary Reviews-Nanomedicine and Nanobiotechnology 2(5):544-568.

Schultz AG, Boyle D, Chamot D, Ong KJ, Wilkinson KJ, McGeer JC, Sunahara G, Goss GG. 2014. Aquatic toxicity of manufactured nanomaterials: challenges and recommendations for future toxicity testing. Environmental Chemistry 11(3):207-226.

Schultz AG, Ong KJ, MacCormack T, Ma G, Veinot JGC, Goss GG. 2012. Silver Nanoparticles Inhibit Sodium Uptake in Juvenile Rainbow Trout (Oncorhynchus mykiss). Environmental Science & Technology 46(18):10295-10301.

Scown TM, Goodhead RM, Johnston BD, Moger J, Baalousha M, Lead JR, van Aerle R, Iguchi T, Tyler CR. 2010. Assessment of cultured fish hepatocytes for studying cellular uptake and (eco)toxicity of nanoparticles. Environmental Chemistry 7(1):36-49.

Setyawati MI, Yuan X, Xie J, Leong DT. 2014. The influence of lysosomal stability of silver nanomaterials on their toxicity to human cells. Biomaterials 35(25):6707-6715.

Shang L, Wang Y, Jiang J, Dong S. 2007. pH-Dependent Protein Conformational Changes in Albumin:Gold Nanoparticle Bioconjugates: A Spectroscopic Study. Langmuir 23(5):2714-2721.

Shannahan JH, Lai X, Ke PC, Podila R, Brown JM, Witzmann FA. 2013. Silver Nanoparticle Protein Corona Composition in Cell Culture Media. PLoS ONE 8(9):e74001.

Shemetov AA, Nabiev I, Sukhanova A. 2012. Molecular Interaction of Proteins and Peptides with Nanoparticles. ACS Nano 6(6):4585-4602.

Sigg L, Behra R, Groh K, Isaacson C, Odzak N, Piccapietra F, Röhder L, Schug H, Yue Y, Schirmer K. 2014. Chemical Aspects of Nanoparticle Ecotoxicology. CHIMIA International Journal for Chemistry 68(11):806-811.

Sperling RA, Parak WJ. 2010. Surface modification, functionalization and bioconjugation of colloidal inorganic nanoparticles. Philosophical Transactions of the Royal Society of London A: Mathematical, Physical and Engineering Sciences 368(1915):1333-1383.

Stern S, Adiseshaiah P, Crist R. 2012. Autophagy and lysosomal dysfunction as emerging mechanisms of nanomaterial toxicity. Particle and Fibre Toxicology 9(1):20.

Tejamaya M, Römer I, Merrifield RC, Lead JR. 2012. Stability of Citrate, PVP, and PEG Coated Silver Nanoparticles in Ecotoxicology Media. Environmental Science & Technology.

Tenzer S, Docter D, Kuharev J, Musyanovych A, Fetz V, Hecht R, Schlenk F, Fischer D, Kiouptsi K, Reinhardt C and others. 2013. Rapid formation of plasma protein corona critically affects nanoparticle pathophysiology. Nat Nano 8(10):772-781.

Van Lehn RC, Atukorale PU, Carney RP, Yang Y-S, Stellacci F, Irvine DJ, Alexander-Katz A. 2013. Effect of Particle Diameter and Surface Composition on the Spontaneous Fusion of Monolayer-Protected Gold Nanoparticles with Lipid Bilayers. Nano Letters 13(9):4060-4067.

Verma A, Uzun O, Hu Y, Hu Y, Han H-S, Watson N, Chen S, Irvine DJ, Stellacci F. 2008. Surface-structure-regulated cell-membrane penetration by monolayer-protected nanoparticles. Nat Mater 7(7):588-595.

Walczyk D, Bombelli FB, Monopoli MP, Lynch I, Dawson KA. 2010. What the Cell "Sees" in Bionanoscience. Journal of the American Chemical Society 132(16):5761-5768.

Ward JE, Kach DJ. 2009. Marine aggregates facilitate ingestion of nanoparticles by suspension-feeding bivalves. Marine Environmental Research 68(3):137-142.

Werth JH, Linsenbühler M, Dammer SM, Farkas Z, Hinrichsen H, Wirth KE, Wolf DE. 2003. Agglomeration of charged nanopowders in suspensions. Powder Technology 133(1–3):106-112.

Wigginton NS, Titta Ad, Piccapietra F, Dobias J, Nesatyy VJ, Suter MJF, Bernier-Latmani R. 2010. Binding of Silver Nanoparticles to Bacterial Proteins Depends on Surface Modifications and Inhibits Enzymatic Activity. Environmental Science & Technology 44(6):2163-2168.

Wood CM. 2011. 1 - Silver. In: Chris M. Wood APF, Colin J. Brauner, editor. Homeostasis and Toxicology of Non-Essential Metals: Academic Press. p 1-65.

Wood CM, Grosell M, Hogstrand C, Hansen H. 2002. Kinetics of radiolabelled silver uptake and depuration in the gills of rainbow trout (Oncorhynchus mykiss) and European eel (Anguilla anguilla): the influence of silver speciation. Aquatic Toxicology 56(3):197-213.

Wood CM, Hogstrand C, Galvez F, Munger RS. 1996. The physiology of waterborne silver toxicity in freshwater rainbow trout (Oncorhynchus mykiss) 1. The effects of ionic Ag+. Aquatic Toxicology 35(2):93-109.

Wood CM, Playle RC, Hogstrand C. 1999. Physiology and modeling of mechanisms of silver uptake and toxicity in fish. Environmental Toxicology and Chemistry 18(1):71-83.

Wu W-h, Sun X, Yu Y-p, Hu J, Zhao L, Liu Q, Zhao Y-f, Li Y-m. 2008. TiO2 nanoparticles promote β-amyloid fibrillation in vitro. Biochemical and Biophysical Research Communications 373(2):315-318.

Wu Y, Zhou Q. 2013. Silver nanoparticles cause oxidative damage and histological changes in medaka (Oryzias latipes) after 14 days of exposure. Environmental Toxicology and Chemistry 32(1):165-173.

Wu Y, Zhou Q, Li H, Liu W, Wang T, Jiang G. 2010. Effects of silver nanoparticles on the development and histopathology biomarkers of Japanese medaka (Oryzias latipes) using the partial-life test. Aquatic Toxicology 100(2):160-167.

Xian H, Jiazhen W, Yuping S, Mingjun C, Xin S, Junguang J, Hongda W. 2012. Caveolae-mediated endocytosis of biocompatible gold nanoparticles in living Hela cells. Journal of Physics: Condensed Matter 24(16):164207.

Zhang Y, Kohler N, Zhang M. 2002. Surface modification of superparamagnetic magnetite nanoparticles and their intracellular uptake. Biomaterials 23(7):1553-1561.

Chapter 2 Toxicity of silver nanoparticles to a fish gill cell line: role of medium composition

In aqueous solutions, silver nanoparticles (AgNP) behaviour is affected by a variety of factors which lead to altered AgNP size and toxicity. Our research aims to explore the effect of media composition on citrate-coated AgNP (AgNP) behaviour and toxicity to the cell line from rainbow trout (*Oncorhynchus mykiss*) gill, RTgill-W1. Three different exposure media (L15/ex, L15/ex w/o Cl and d-L15/ex) were used. These were characterized by varying ionic strength and chloride content, both of which had a dominant effect on the behaviour of AgNP. Comparing the behaviour and toxicity of AgNP in the different media, stronger agglomeration of AgNP correlated with higher toxicity. Deposition of AgNP on cells might explain the higher toxicity of agglomerated AgNP compared to that of suspended AgNP. The AgNP concentration-response curves as a function of dissolved silver ions, and the limited prevention of toxicity by silver ligands, indicated that AgNP elicited a particle-specific effect on the cells. Furthermore, the lysosomal membrane integrity was significantly more sensitive to AgNP exposure than cellular metabolic activity or cell membrane integrity and showed the weakest protection by silver ligands. This revealed that AgNP toxicity seems to particularly act on RTgill-W1 cell lysosomes. The newly developed low ionic strength medium, d-L15/ex, which can stabilize AgNP and better mimic the freshwater environment, offers an excellent exposure solution to study cellular and molecular effects of nanoparticles to gill cells.

2.1 Introduction

Due to their physicochemical and antibacterial properties, silver nanoparticles (AgNP) are currently among the most widely used nanomaterials (Woodrow Wilson International Center for Scholars 2013). The application of AgNP in cosmetics, textiles and disinfection products, to name a few, will lead to their release into the aquatic environment, raising concern about potential adverse effects in organisms living in the aquatic environment (Fabrega et al. 2011; Navarro et al. 2008a; Wijnhoven et al. 2009).

Toxicity of AgNP to aquatic organisms has been investigated in different species but the causes for toxicity are still unclear (Fabrega et al. 2011; Wijnhoven et al. 2009). In aqueous solutions, AgNP can release silver ions, which are known to be toxic not only to prokaryotes but also to invertebrates and fish (Bianchini and Wood 2003; Wood et al. 1999). There is still an ongoing debate, however, as to whether AgNP toxicity is only due to dissolved silver ions (Ag^+) and other dissolved silver species (including all the silver species in oxidized state ($Ag(I)$) in aqueous solution, such as $AgCl_n$ (aq), AgOH (aq) or whether AgNP also have particle specific effects. As for the direct toxicity of AgNP, published research showed different results with varied experimental models and exposure conditions: some suggested that the toxicity of AgNP is mainly due to dissolved silver ions to daphnia, algae and nematodes (Kennedy et al. 2010; Navarro et al. 2008b; Yang et al. 2011), while others reported that silver ions could not fully explain the observed AgNP toxicity and that both silver ions and AgNP contribute to the toxicity to lung and hepatoma cells (Beer et al. 2012; Kawata et al. 2009).

Several investigations indicated that the toxicity of AgNP is dependent on the behavior and fate of the nanoparticles in the exposure environment (Behra et al. 2013; Fabrega et al. 2011; Liu et al. 2010). To date, most AgNP toxicity studies were performed in fresh water or complex culture media, but the influence of the exposure medium on the toxicity has rarely been considered (Ahamed et al. 2010). It has been clearly demonstrated that the composition and properties of the exposure solutions largely affect AgNP behaviour. For instance, Piccapietra reported enhanced AgNP agglomeration in a simple medium with Ca^{2+} or Na^+ above 2 mM or 100 mM, respectively (Piccapietra et al. 2011). By contrast, humic acid or bovine serum albumin (BSA) stabilized AgNP in cell culture medium or buffer (Huynh and Chen 2011; MacCuspie et al. 2010). Aside from AgNP, studies with other nanoparticles demonstrated that the ionic strength or fetal bovine serum (FBS) influence nanoparticles behavior and toxicity. Zebrafish (*Danio rerio*) embryo morbidity and mortality were induced after exposure to gold nanoparticles in a low ionic strength medium in which the nanoparticles were well dispersed whereas no toxicity was seen in ion rich medium in which the nanoparticles

were agglomerated (Truong et al. 2011). On the other hand, Kühnel *et al* found that agglomeration of tungsten carbide nanoparticles in a simple medium did not prevent the uptake and toxicity to a fish gill cell line. They also demonstrated that FBS or BSA stabilized tungsten carbide nanoparticles in the exposure medium (Kühnel et al. 2009; Meißner et al. 2010).

Based on these considerations, it is important to investigate the role of the composition of exposure medium in AgNP behavior because it is otherwise difficult to link the characteristics and behavior of nanoparticles to their toxicity in the respective model system. Therefore, the aim of this study was to explore the effect of media composition on AgNP behaviour and toxicity to fish gill cells. Since citrate is frequently used to stabilize AgNP suspensions, citrate coated AgNP (AgNP) were used in this work. Gill-derived cells were selected because, as the respiratory organ, the gill is likely a primary route of uptake for fish exposed to nanoparticles in the water phase. Recent work indeed demonstrated that AgNP, titanium dioxide nanoparticles and copper nanoparticles accumulated in fish gill or induced fish gill injury (Farkas et al. 2010; Federici et al. 2007; Griffitt et al. 2007). The RTgill-W1 cell line (Bols et al. 1994), which was derived from rainbow trout (*Oncorhynchus mykiss*) gill, was selected as model to test the AgNP toxicity. The RTgill-W1 cell line has been demonstrated to survive in a very simple exposure medium and even tolerate low ionic strength buffer, which allows to more closely mimic the natural environment (Dayeh et al. 2002; Lee et al. 2009; Schirmer et al. 1997; Tanneberger et al. 2012). Accordingly, the AgNP behaviour and toxicity were studied in three different exposure media varying in ionic strength and chloride content.

2.2 Results

2.2.1 Design of exposure media

Exposure experiments were carried out in three different media: L15/ex (Schirmer et al. 1997), L15/ex without chloride (L15/ex w/o Cl) and d-L15/ex (Table 2.1). L15/ex is a modification of the original Leibovitz' 15 (L15) culture medium (Leibovitz 1963), specifically developed for short term chemical exposure of RTgill-W1 cells. It contains only salts, sodium pyruvate and galactose in concentrations as present in L15. L15/ex w/o Cl is a chloride free L15/ex medium in which chloride is replaced by nitrate to avoid the formation of AgCl. To maintain AgNP stable and more closely mimic the natural environment with regard to ionic strength and medium composition, a new medium, d-L15/ex, was developed. This medium was obtained by diluting L15/ex w/o Cl medium with nanopure water (L15/ex w/o Cl: nanopure water = 40: 60) and then adding NaCl to a final concentration of 0.5 mM, the optimized NaCl concentration allowing to stabilize AgNP while keeping as much of free silver ion in solution as possible as verified by Visual MINTEQ (see below). The pH in the exposure media was 7.1-7.4.

Table 2.1 Formulation of L15/ex, L15/ex w/o Cl and d-L15/ex exposure media.

Ion species/compound (mM)	L15/ex[§]	L15/ex w/o Cl	d-L15/ex
Cl^-	168.9	---	0.5
Ca^{2+}	1.5	1.5	0.6
Mg^{2+}	4.3	3.8	1.5
Na^+	158.2	158.2	63.3
K^+	6.1	6.1	2.4
PO_4^{3-}	2.0	2.0	0.8
SO_4^{2-}	1.9	3.8	1.5
NO_3^-	---	164.5	65.8
Galactose	5.7	5.7	2.3
Sodium Pyruvate	5.7	5.7	2.3
Ionic strength[#]	**173.0**	**177.1**	**72.0**

[#] Ionic strength was calculated by Visual MINTEQ, ver. 3.0.

[§] see also Schirmer *et al.*, 1997.

2.2.2 Cell viability in exposure media

Viability of RTgill-W1 cells in the two newly developed media (L15/ex w/o Cl and d-L15/ex) was tested before AgNP exposure experiments. Cell viability was maintained above 80% in all media compared to L15 medium over 24 h (Figure 2.1). Cell viability was the lowest in L15/ex w/o Cl medium probably due to the absence of chloride and high concentrations of nitrate. In d-L15/ex medium, after adding only low concentrations of chloride and decreasing the nitrate content by dilution, cell viability was similar to L15/ex despite the lower ionic strength environment (Table 2.1). Over

all, all three kinds of media were considered suitable for toxicity studies with AgNP in our experimental system.
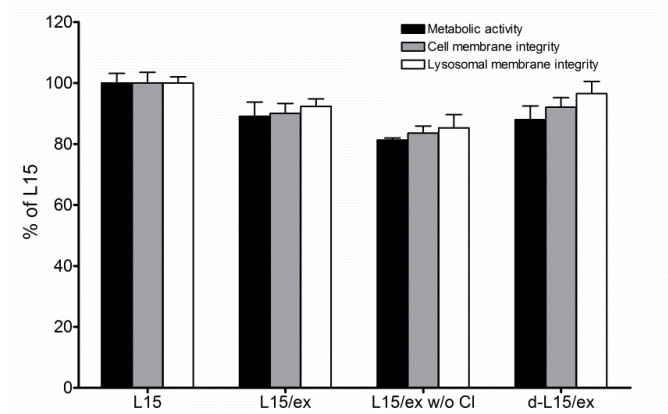
Figure 2.1 Cell viability of RTgill-W1 in different media.

Cell viability for the different variants of L15/ex media was expressed as % of fluorescent units measured for the different viability indicator dyes for cells cultured in L15. The composition of L15 was according to Leibovitz (1963) and contained 1% penicillin/streptomycin. Time of culture in the media was for 24 h.

2.2.3   Silver ion species in the three exposure media

Figure 2.2 shows the distribution of silver ion species in the different media as calculated by Visual MINTEQ with 1 µM total silver. The free silver ion percentage of total silver varied little for the presumed total silver concentration range of 0.01-5 µM. In L15/ex medium, most of silver species can be expected in the form of $AgCl_2^-$ and $AgCl_3^{2-}$, and only 0.03% of total silver in the free Ag^+ form. In contrast, free Ag^+ in L15/ex w/o Cl medium and d-L15/ex medium were approximately 92% and 59% of total silver, respectively.
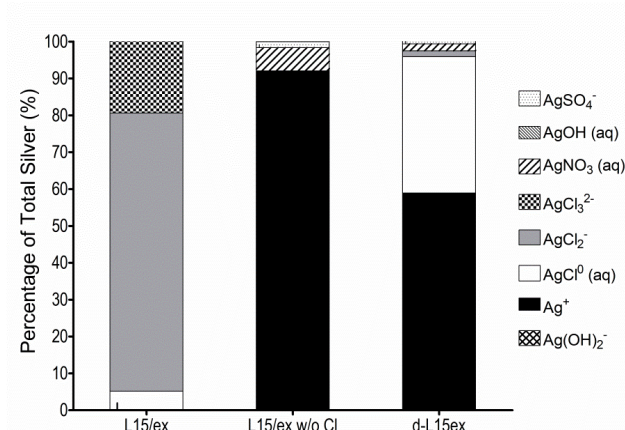
Figure 2.2 Silver ion species distribution in the three exposure media.

Silver ion species distributions were calculated by Visual MINTEQ ver.3.0; it showed very little change with the initial silver ion concentration ranging from 0.01-10 µM. Here only the calculation for 1 µM total silver is shown.

2.2.4   AgNP behaviour in exposure media

The Z-average of the size AgNP (distribution by intensity) in the original stock suspension is 19.4±0.4 nm and the zeta potential -30±0.9 mV (Figure 2.3A, Figure 2.4A & B). The size distribution ranges from 7 nm to 65 nm and the polydispersity index (PDI) is 0.163±0.004. The AgNP suspension in nanopure water has a maximal UV-VIS absorbance at 410-420 nm.

The AgNP showed different behavior in the exposure media (Figure 2.3-5, Figure S2.1, Figure S2.2 and Table S2.1). In L15/ex medium, TEM images showed that AgNP agglomerated moderately (Figure 2.3B); Z-average size was 200-500 nm (PDI: 0.35-1.00) and zeta potential was around -15 mV depending on the particle concentration (Figure 2.4C). In L15/ex w/o Cl medium, AgNP strongly agglomerated (Figure 2.3C) with sizes of 1000-1750 nm (PDI: 0.21-0.77) and a zeta potential of around -10 mV (Figure 2.4 D). In d-L15/ex medium, TEM results displayed that AgNP dispersed very well (Figure 2.3D); Z-average size was 40-100 nm (PDI: 0.46-0.85) and zeta potential was around -20 mV (Figure 2.4E). Colour changes of AgNP suspensions were evident in the test tubes, and sedimentation was observed in the L15/ex w/o Cl medium (Figure 2.5A). UV-VIS spectrum confirmed a change in size for the AgNP (Figure 2.5B).
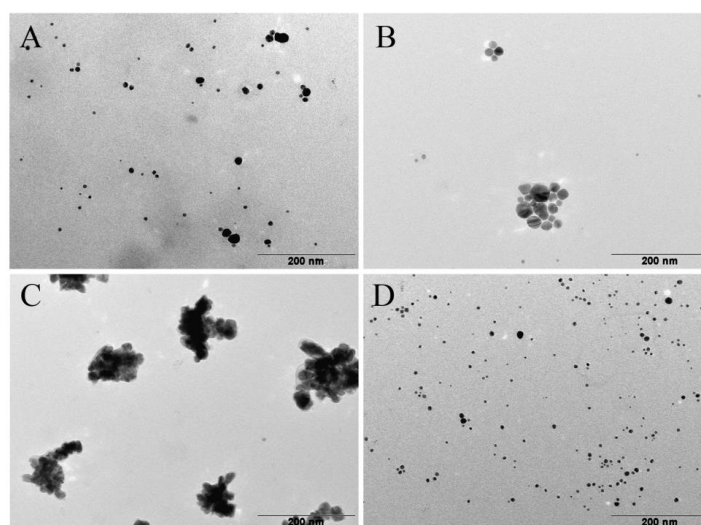
Figure 2.3 Representative TEM images showing AgNP in nanopure water and exposure media.

(A) AgNP in nanopure water; (B) AgNP in L15/ex medium; (C) AgNP in L15/ex w/o Cl medium; (D) AgNP in d-L15/ex medium.
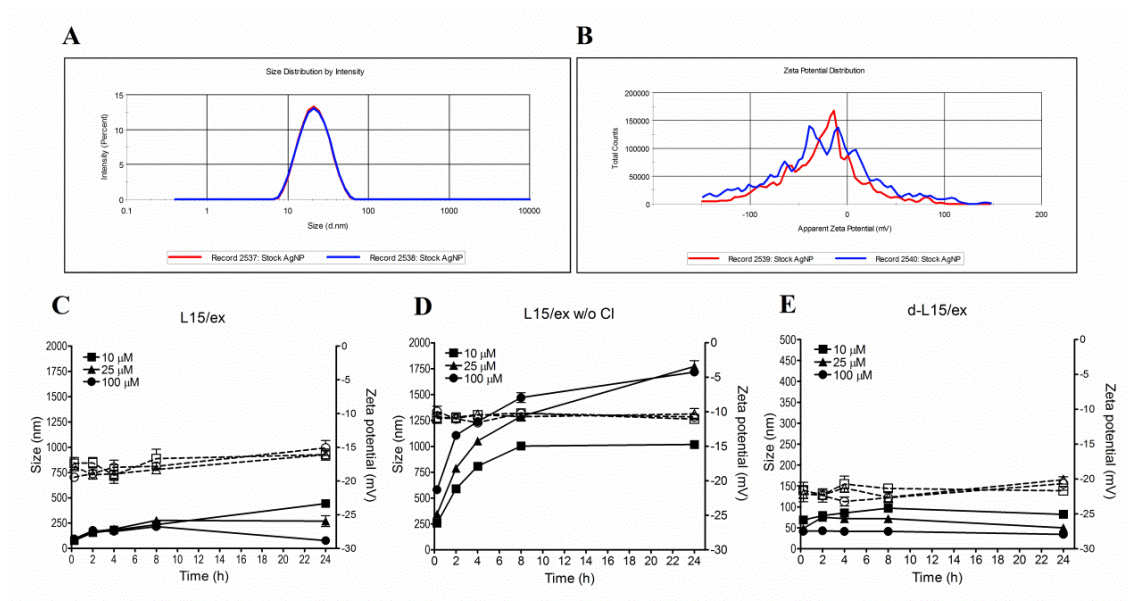
Figure 2.4 Behaviour of AgNP in stock solution and exposure media.

(A, B) Z-average size and Zeta potential distribution of AgNP in the nanopure water. (C-E) Z-average size and Zeta potential in L15/ex (C), L15/ex w/o Cl (D) and d-L15/ex (E) media. Z-average size (solid line, left Y axis) and zeta potential (dashed line, right Y axis) of 10 μM (■), 25 μM (▲), 100 μM (●) AgNP suspensions were measured by DLS.
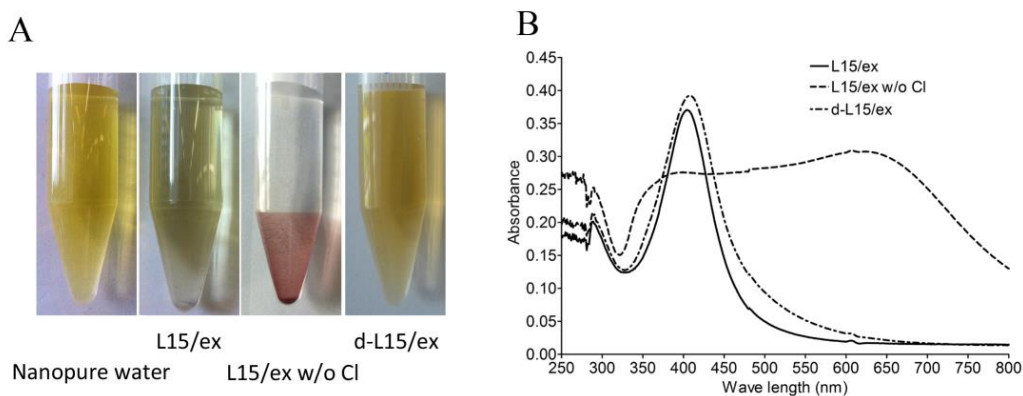
Figure 2.5 100 μM AgNP in exposure media for 24 h.

(A) Colour changes in AgNP suspensions; (B) UV-VIS absorbance of AgNP suspensions. The AgNP have the maximal absorbance at 410-420 nm. The lack of this absorbance peak in L15/ex w/o Cl indicates a lack of particles in suspension.

2.2.5   Dissolved silver in exposure media

The ratio of total dissolved silver in AgNP suspensions varied in the different media and AgNP concentrations (Table 2.2). Generally, dissolved silver determined by ultra-filtration was lower than values determined by ultra-centrifugation. On one hand, underestimation by ultra-filtration maybe due to some silver adsorbing on the filter as indicated by the low recovery of $AgNO_3$ (about 70%). On the other hand, overestimation by ultra-centrifugation may occur due to small AgNP (diameter less than 2 nm) remaining in the supernatant under the applied centrifugation conditions. Thus, the average of the results obtained by ultra-filtration and ultra-centrifugation was used for recalculation of the concentration-response curves as a function of dissolved silver (see below). In the L15/ex medium, 1.89% of total silver were dissolved. Only 0.67% and 0.40% of total silver were dissolved in L15/ex w/o Cl and in d-L15/ex media, respectively.

Table 2.2 Percentage of dissolved silver in AgNP suspensions.

	Centrifugal Ultrafiltration		Ultra-centrifugation		Average
	25 µM	100 µM	25 µM	100 µM	
L15/ex	0.77	0.39	4.23	2.15	1.89
L15/ex w/o Cl	0.31	0.05	1.12	1.20	0.67
d-L15/ex	0.23	0.04	0.84	0.48	0.40

Total silver: 25 µM and 100 µM. Separation of dissolved Ag^+ from AgNP after 24 h by Amicon® Ultra-4 Centrifugal Filter Units and Ultra-centrifugation (145 000 × g for 3 h). Silver concentration was measured by ICP-MS. Values are given as % dissolved silver from AgNP.

2.2.6   Cell viability after exposure to AgNP and $AgNO_3$

Both AgNP and $AgNO_3$ caused significant toxicity to RTgill-W1 cells in all exposure media as indicated by the three measurements of cell viability (Figure 2.6, Table S2.2). Concentrations of AgNP or $AgNO_3$ causing 50% effect (EC50), based on total silver concentrations, are listed in Table 2.3. From the concentration-response curves and EC50 values, we conclude that AgNP and $AgNO_3$ toxicity to RTgill-W1 cells differed depending on the media and the endpoints of the cell viability measurements.
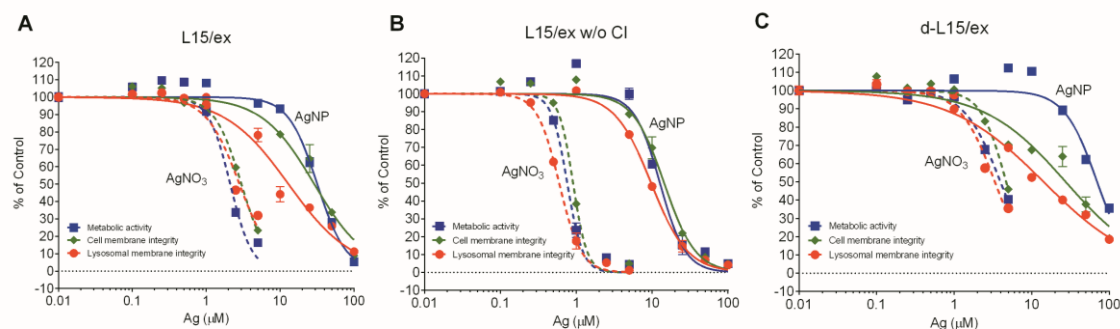
Figure 2.6 Toxicity of AgNP and AgNO$_3$ as function of total silver in the three media.

Effect of AgNP and AgNO$_3$ to RTgill-W1 cells was measured after 24 h of exposure in L15/ex (A), L15/ex w/o Cl. Average and standard deviation of three independent experiments is shown (n=3). The endpoints measured are metabolic activity (■), cell membrane integrity (♦) and lysosomal integrity (●). Solid lines represent AgNP effects and dashed lines represent AgNO$_3$ effects.

Table 2.3 EC50 values (in μM) determined on AgNP and AgNO3 exposure of RTgill-W1 cells for 24 h.

		Metabolic activity	Cell membrane integrity	Lysosomal membrane integrity
L15/ex	AgNP	31.7±2.6	29.0±3.6	13.2±2.6[#]
	AgNO$_3$	2.1±0.1	3.1±0.8	2.9±0.5
L15/ex w/o Cl	AgNP	12.7±2.5[*]	14.4±4.4[*]	9.8±4.5
	AgNO$_3$	0.8±0.1[*]	0.9±0.2[*]	0.6±0.2[*]
d-L15/ex	AgNP	70.3±4.7	27.8±4.2	15.5±5.5[#]
	AgNO$_3$	4.0±0.2	4.7±0.1	3.4±0.6

Standard deviation was calculated based on three independent experiments (n=3). * EC50s in L15/ex w/o Cl medium were significantly different from EC50s determined in the other two kinds of media P < 0.05, two-way ANOVA. # EC50s determined for the lysosomal membrane integrity were significantly different from EC50s determined for the other two measures of cell viability; P < 0.05, two-way ANOVA.

The first difference was that EC50 values of AgNO$_3$ appeared 5-15 fold lower (i.e. more toxic) to RTgill-W1 cells in all tested media than the values of AgNP. Second, AgNO$_3$ was most toxic to cells exposed in L15/ex w/o Cl but resulted in little difference in L15/ex and d-L15/ex. A similar pattern in sensitivity differences between the three media was observed for AgNP. Finally, a striking difference was observed among the endpoints for cell viability with AgNP treated cells exposed in L15/ex and d-L15/ex media. The lysosomal membrane integrity was significantly more affected than cellular metabolic activity or cell membrane integrity. Yet, when cells were treated with AgNO$_3$, all the three cell viability measurements gave similar results in each of the exposure media.

2.2.7 Recalculation of concentration-response curves as a function of dissolved silver and free Ag+

The effect of AgNP to RTgill-W1 cells as function of total silver was re-calculated based on the dissolved silver in the AgNP suspensions obtained by the average percentage from ultra-filtration and ultra-centrifugation. Figure 2.7A shows the recalculated curve for the lysosomal membrane integrity. The same pattern was observed for the other measurements of cell viability. Figure 2.7B shows the EC50 values derived for AgNP and $AgNO_3$ as a function of dissolved silver. In both AgNP and $AgNO_3$ exposures, dissolved silver in L15/ex w/o Cl medium had higher toxicity than in the other two media with chloride. Considering the toxicity as a function of dissolved silver in all three media, the AgNP exposures elicited a higher toxicity than $AgNO_3$.

EC50 values were also calculated as a function of free Ag^+ in AgNP and $AgNO_3$ exposures (Figure 2.7C). Assuming that the effects observed are related to the free Ag^+ ion concentration, the EC50 values were recalculated using the free Ag^+/total dissolved species ratio in the exposure media (derived from Visual MINTEQ calculations shown in Figure 2.2). By expressing the EC50 values in terms of estimated Ag^+ concentrations, the toxicity for exposure in L15/ex medium was significantly higher than for the two other media.
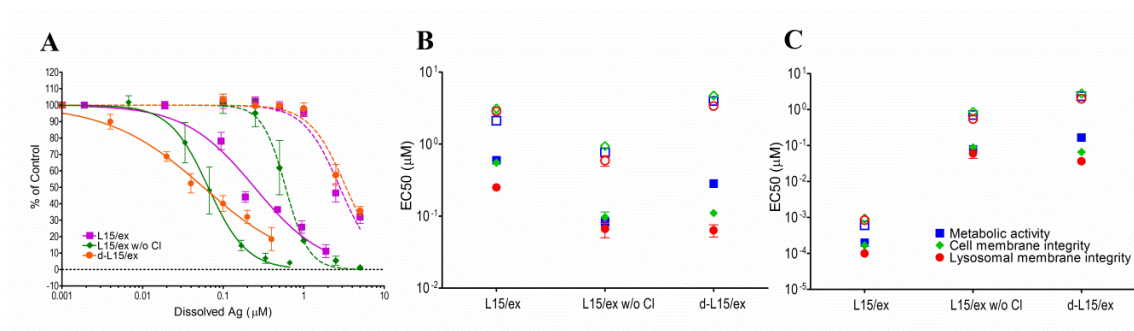
Figure 2.7 Toxicity of AgNP and $AgNO_3$ as a function of total dissolved silver and of free Ag^+ in the exposure media.

A: shows the lysosomal membrane integrity as a function of dissolved silver. The effects of dissolved silver from AgNP exposures are depicted with solid lines and the effects of $AgNO_3$ with dashed lines. Effect data are expressed as percent viability compared to cells not exposed to silver (control). B: EC50 of AgNP and $AgNO_3$ exposures as a function of dissolved silver. The concentration used for dissolved silver in AgNP suspensions in A and B was based on the average percentage from the centrifugal ultrafiltration and ultra-centrifugation methods. C: EC50 of AgNP and $AgNO_3$ exposures as a function of free Ag^+. Calculation based on the free silver ion ratio in the three media obtained by Visual MINTEQ. In B and C, solid symbols represent AgNP effects and open symbols represent $AgNO_3$ effects.

2.2.8   Cell viability in the presence of silver ion ligands

Both cysteine and DMPS prevented all (for AgNO$_3$) or some (for AgNP) of the toxic effects in a concentration–dependent manner (Figure 2.8). 12.5 µM cysteine (Figure 2.8A) or 100 µM DMPS (data not shown) completely prevented the impact of AgNO$_3$ on cell viability. However, when cysteine (Figure 2.8B) or DMPS (Figure 2.8C) were added to AgNP exposure media, protection of the cells by the ligands was not completed. Even with the highest ligand concentrations, which presumably yielded an excess compared to total dissolved silver of 17-67 fold, RTgill-W1 cell viability was still decreased by 20~60%.

Differences in protection were also observed for the different measurements of cell viability. Cell metabolic activity and cell membrane integrity were better protected than lysosomal membrane integrity after treatment with AgNP and ligands. In fact, lysosomal activity was protected to a very limited extent on AgNP exposure, whereas it was completely protected by ligands when cells were exposed to AgNO$_3$.
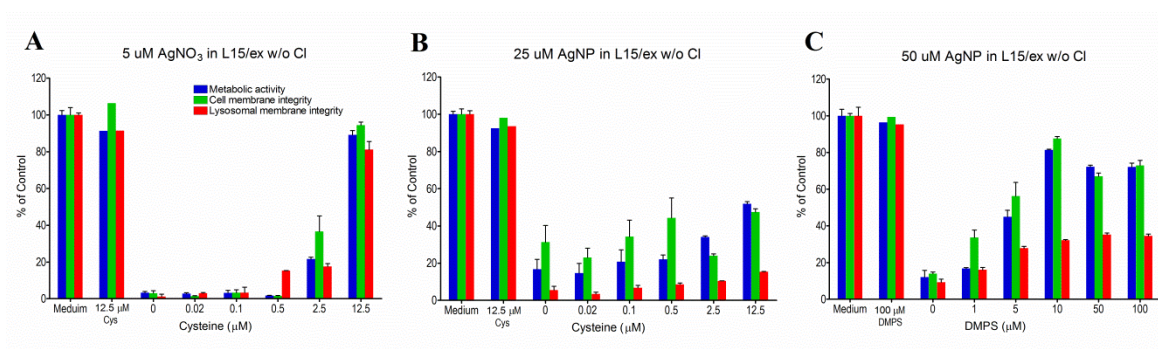
Figure 2.8 Effect of silver ligands on AgNP and AgNO$_3$ toxicity.

Effect of silver ligands on toxicity elicited by AgNO$_3$ (A) and AgNP (B, C) to RTgill-W1 cells, using the results for L15/ex w/o Cl as example. Silver ligands: Cysteine (A, B) and DMPS (C).

2.3 Discussion

In this study, we demonstrated the different toxicity of AgNP to fish gill cells in varied ionic strength and chloride concentration media. Many factors are expected to influence the AgNP toxicity: agglomeration state and behavior of AgNP, bioavailability of AgNP as well as the concentration of dissolved silver from AgNP available for uptake and effects.

Both ionic strength and chloride content indeed strongly influenced the agglomeration in the three exposure media. High agglomeration of AgNP occurred in the medium of higher ionic strength (I=177.1 mM) and absence of chloride (L15/ex w/o Cl). On the contrary, in the medium of d-L15/ex, with the decreased ionic strength (I=72 mM) and 0.5 mM Cl^-, AgNP showed only slight agglomeration. Previous studies highlighted the importance of ionic strength on particle behavior in suspension (MacCuspie 2011; Piccapietra et al. 2011). The zeta potential of AgNP in chloride-free medium was less negative than that observed for AgNP in chloride-containing media. As some silver ions are released from the AgNP, chloride ions in the chloride-containing media likely adsorbed on the surface of the AgNP and increased the surface negative charges, thereby maintaining AgNP stability. Cell viability tests showed that both L15/ex w/o Cl and d-L15/ex medium support RTgill-W1 cell survival for 24 h. Based on these results, we investigated the AgNP toxicity in all three kinds of media.

The degree of particle agglomeration in the exposure media positively correlated with the toxicity of AgNP on cell viability. The strongly agglomerated AgNP (1000 nm in L15/ex w/o Cl) showed an about 2 fold higher toxicity than moderately agglomerated AgNP (250 nm in L15/ex) and a 2-5 fold higher toxicity than weakly agglomerated AgNP (100 nm in d-L15/ex). This trend suggests that agglomeration and deposition could enhance the interaction of AgNP with RTgill-W1 cell and induce high toxicity. A modeling study showed that behavior of particles ranging from ~10 to 100 nm is controlled by both diffusion and deposition and that the transport is slower than for particles over 200 nm, whose behavior is controlled by deposition (Hinderliter et al. 2010; Teeguarden et al. 2007). With an upright/inverted configuration system, Cho also reported that sedimentation increases the cellular uptake of gold nanoparticles (Cho et al. 2011). In the present study, one explanation might be that agglomeration increases the interaction of AgNP with cells because of particle deposition on the cell monolayer. In the *in vitro* cell exposure system, RTgill-W1 cells are attached to the bottom of wells and the liquid exposure column height is about 0.5 cm. Only when the particles move to the bottom to reach the liquid-cell interface, could AgNP have direct interaction with cells and induce toxicity.

If AgNP-cell interaction is a determinant of toxicity by enhancing bioavailability, AgNP should yield a particle-specific contribution to toxicity. In the present work, the AgNP indeed had a particle-specific impact on RTgill-W1 cells. This conclusion can be drawn from the concentration-response curves and EC50 values accounting for dissolved silver, in which the AgNP exposures showed higher toxicity compared to $AgNO_3$ exposures. In contrast, if all the toxicity of AgNP suspensions was due to dissolved silver, the AgNP should have the same toxicity as $AgNO_3$ when calculated as a function of dissolved silver. Moreover, silver ligands only partly prevented toxicity to cells by AgNP but completely protected cells from the toxicity of $AgNO_3$, again supporting a AgNP specific effect to RTgill-W1 cells.

Another factor potentially affecting the toxicity of AgNP suspensions is the dissolved silver species. Re-calculation of AgNP EC50 values as a function of dissolved silver showed exposures in L15/ex w/o Cl medium to result in higher toxicity than the other two media. The toxicity of $AgNO_3$ in L15/ex w/o Cl medium was also 2-5 fold higher than that in L15/ex and d-L15/ex media. Thus, dissolved silver toxicity decreased with the chloride concentration rising in the exposure medium. This trend is reminiscent of what was reported in a previous *in vivo* silver toxicity study with juvenile rainbow trout exposed under various freshwater conditions (Wood et al 2011). In fact, the LC50 of dissolved silver (as $AgNO_3$) for juvenile rainbow trout in that study was 0.25-2.5 µM, which is similar to the EC50 values (0.6-4.7 µM) for RTgill-W1 cells in the present study. Calculations with Visual MINTEQ showed that in L15/ex, most of dissolved silver were the negatively charged species, $AgCl_2^-$ and $AgCl_3^{2-}$. In L15/ex w/o Cl, most of dissolved silver were free Ag^+. In d-L15/ex, aside from the approximately 60% Ag^+, most other dissolved silver was of the uncharged species, $AgCl^0$(aq). Earlier studies reported that silver ions form $AgCl_n$ complexes in solution with chloride, and in this way significantly affect silver uptake and toxicity in rainbow trout (Grosell et al. 2000; Hogstrand et al. 1996; McGeer and Wood 1998). Moreover, it was showed that free Ag^+ has a higher bioavailability than $AgCl_n$ complexes in rainbow trout and atlantic salmon (Bury and Hogstrand 2002). Free Ag^+ enter into gill via copper transporters and sodium channels, whereas $AgCl^0$(aq) may be taken up by simple diffusion (Wood et al 2011). Yet, the uptake of $AgCl_2^-$ and $AgCl_3^{2-}$ is still not clear.

To better observe the effects by $AgCl_n$ complexes and Ag^+, EC50 values based on dissolved silver were re-calculated as a function of free Ag^+ using the free Ag^+ ratio in the media. Both AgNP and $AgNO_3$ exposures had remarkable higher toxicity in L15/ex medium than exposures in L15/ex w/o Cl medium as a function of free Ag^+. This indicated that $AgCl_2^-$ and $AgCl_3^{2-}$ complexes still elicit toxic ef-

fects to cells. The toxicity in L15/ex was also higher than in d-L15/ex medium as a function of free Ag$^+$, which demonstrated that AgCl$_2^-$ and AgCl$_3^{2-}$ complexes had higher toxicity than AgCl^0 (aq).

The different cell viability measurements revealed that AgNP seem to particularly act on RTgill-W1 cell lysosomes. The lysosomal membrane integrity was significantly more sensitive to AgNP exposure than cellular metabolic activity or cell membrane integrity. As well, prevention by silver ligands of the AgNP effect was the least for lysosomal membrane integrity in all the three cell viability measurements. On the contrary, we did not observe these difference in cells treated with AgNO$_3$. Thus, our results indicate that AgNP act on RTgill-W1 cells mainly via lysosomes. It seems plausible that, unlike silver ions, AgNP could be taken up by cells via endocytotic processes, thereby accumulating in lysosomes (Greulich et al. 2011). NP accumulation in lysosome may lead to lysosome destabilization and dysfunction, which could subsequently impact metabolic function and plasma membrane integrity (Johansson et al. 2010; Kolter and Sandhoff 2010; Stern et al. 2012).

Our study demonstrates that the composition of cell exposure media has a dominant effect on the behaviour and toxicity of AgNP. Ionic strength and chloride concentrations influenced AgNP agglomeration, deposition and dissolved silver species in exposure media. Deposition and silver species had important effects on AgNP bioavailability and toxicity to RTgill-W1 cells. Therefore, when comparing the toxicity data from different studies, the exposure environment, AgNP behaviour and dissolved silver species should be considered. We derived a new exposure medium, d-L15/ex, which has low ionic strength and low chloride concentration. This protein-free medium supported cell survival and stabilized the AgNP for at least 24 h, thus allowing small-size particles to be studied with respect to uptake and effects in cells without sedimentation of particles onto cells due to particle agglomeration. Based on its ionic strength, d-L15/ex also better reflects the freshwater environment to which gill cells of freshwater fish, such as rainbow trout, would be exposed. Thus, we propose to use the newly developed medium to explore the cellular and molecular effects of nanoparticles to gill cells.

2.4   Materials and methods

2.4.1   Materials

The AgNP were purchased from NanoSys GmbH (Wolfhalden, Switzerland) as aqueous suspension with a concentration of 1g/L (9.27 mM, pH=6.46). The stock AgNP solution was stored in the dark and experimental solutions were prepared in relevant cell exposure media or nanopure water (16–18 MΩ cm^{-1}; Barnstead Nanopure Skan AG, Basel-Allschwil, Switzerland). A stock solution of AgNO$_3$ (Sigma-Aldrich, Buchs SG, Switzerland) was prepared at a concentration of 10 mM in nanopure water.

2.4.2   Nanoparticle characterization

The AgNP were characterized in nanopure water and under experimental conditions (i.e. in the three exposure media). The Z-average size and zeta potential of the AgNP were measured by dynamic light scattering (DLS) and electrophoretic mobility using a Zetasizer (Nano ZS, Malvern Instruments, UK). In addition, AgNP size and morphology in the three exposure media were verified by transmission electron microscopy (TEM, FEI Morgagni 268, 100 kV). In addition, the UV-VIS absorption spectrum of 100 µM AgNP suspensions was scanned from 250 nm to 800 nm using a spectrophotometer UVIKON 930 (Kontron Instruments).

2.4.3   Quantification of dissolved silver

To measure the concentration of dissolved silver in the AgNP suspensions, two different methods were used: centrifugal ultrafiltration and ultra-centrifugation. 4 mL 25 µM and 100 µM AgNP suspensions were added to Amicon ultra-4 centrifugal filter units (Millipore, Germany) with a nominal molecular weight limit of 3 kDa and centrifuged for 30 min at 3 000 × g (Megafuge 1.0R, Heraeus Instruments, Germany). The filtrates were diluted 10 times with nanopure water and the concentrations of silver measured by ICP-MS (Element 2 High Resolution Sector Field ICP-MS; Thermo Finnigan, Bremen, Germany) in 1% of HNO$_3$. The recovery of AgNO$_3$ in centrifugal ultrafiltration was around 70%. For ultracentrifugation, 10 mL of AgNP suspensions were centrifuged at 145 000 × g (CENTRIKON T-2000, KONTRON Instruments, Switzerland) for 3 h. A volume of 0.5 mL supernatant was digested with 4.5 mL of 65% HNO$_3$ in a high-performance microwave digestion unit (MLS-1200 MEGA, Oberwil, Switzerland) at a maximal temperature of 195 °C for 20 min. The digests were diluted 50-times and measured by ICP-MS. The recovery of AgNO$_3$ in ultracentrifugation was over

98%. The reliability of the measurements was determined using specific water references (M105A, IFA-Tull, Austria).

2.4.4   Silver species distribution in exposure media

As silver ions can react with different medium components and form different species in the aqueous environment, Visual MINTEQ (Visual MINTEQ, ver. 3.0, 2011) was used to calculate the distribution of silver species, based on dissolved Ag(I), in exposure media. The media pH was set to 7.1 and temperature to 19 ℃. Speciation was calculated based on a silver ion concentration of 0.01-10 μM.

2.4.5   RTgill-W1 culture and exposure

RTgill-W1 cells were routinely cultivated in L15 medium (Invitrogen, Basel, Switzerland), supplemented with 5% fetal bovine serum (FBS, Gold, PAA Laboratories GmbH, Austria) and 1% penicillin/streptomycin (Sigma-Aldrich, Buchs, Switzerland; 10 000 U/ml penicillin, 10 mg/ml streptomycin) in 75 cm^2 flasks (TPP, Trasadingen, Switzerland). Cells were maintained at 19℃ in normal atmosphere and split once (1 flask to 2 flasks) in 1-2 weeks. Confluent cells were washed twice with Versene (Invitrogen/Gibco, Germany) and cells detached by trypsin (0.25% in phosphate-buffered saline, Biowest, Germany).

For exposure to AgNP and AgNO$_3$, confluent cells were used to seed 24-well microtiter plates (Greiner Bio-One, Frickenhausen, Germany) at an initial cell density of 3*10^5 cells in each well in 1 mL of L15 culture medium. After 24 h, the seeded cells were fully confluent and used for toxicity assessment. The confluent cell monolayers were washed (1 mL/well) with either L15/ex, L15/ex w/o Cl or d-L15/ex. Then, 1 mL/well AgNP or AgNO$_3$ suspension in the respective media was added. Exposure was done at 19℃ in the dark and lasted 24 h. Each experiment was performed three times independently with cells from different passages.

To determine the contribution to toxicity of dissolved silver from AgNP, two strong silver ion ligands, L-cysteine and 2, 3-Dimercapto-1-propanesulfonic acid (DMPS), were used to decrease the free Ag$^+$ concentration in AgNP suspensions to a very low level (Hussain et al. 1994; Navarro et al. 2008b). Different concentrations of the ligands in media were added to a fixed AgNP concentration with the highest ligand concentrations being chosen such that they by themselves did not affect cell viability (12.5 μM and 100 μM in the case of L-cysteine and DMPS, respectively) but at the same time provide an excess of ligand compared to the maximal possible Ag$^+$ concentration. RTgill-W1

cells were exposed to these AgNP-ligand suspensions under the same conditions as described above in order to study if removal of Ag^+ altered impact on cell viability.

2.4.6   Cell viability assays

Toxicity was assessed by three measurements: cellular metabolic activity, cell membrane integrity and the lysosomal membrane integrity (Schirmer et al. 1997; Schirmer et al. 1998). Alamar Blue (AB, Invitrogen, Basel, Switzerland) was used to measure the cellular metabolic activity; 5-carboxyfluorescein diacetate acetoxymethyl ester (CFDA-AM, Invitrogen, Basel, Switzerland) to measure the cell membrane integrity; Neutral Red (NR, Sigma-Aldrich, Buchs, Switzerland) to measure the lysosomal membrane integrity.

After 24 h of AgNP or $AgNO_3$ exposure, the exposure medium was discarded, cells were gently washed with 1 mL PBS, followed by adding 400 μL of AB and CFDA-AM working solution, containing 5% v/v AB and 4 μM CFDA-AM in PBS. After incubation for 30 min, fluorescence of each well was quantified by the Infinite M200 plate reader (TECAN, Männedorf, Switzerland) at respective excitation/emission wavelengths of 530/595 nm for AB and 485/530 nm for CFDA-AM. Thereafter, the AB/CFDA-AM working solution was discarded and 400 μL of NR solution, containing 1.5% v/v NR in PBS, were added and incubated for 60 min. Then, cells were fixed with 400 μL fixative (0.5% v/v formaldehyde and 1% w/v $CaCl_2$). Finally, NR was extracted from the lysosomes using 400 μL of an extraction solution (1% v/v acetic acid and 50% v/v ethanol) and gently shaken on a horizontal shaker (TiMix 2, Johanna Otto GmbH, Hechingen, Germany) for 10 min. NR fluorescence was measured at excitation/emission wavelengths of 530/645 nm using the same plate reader.

2.4.7   Data treatment

Exposure experiments were performed in triplicate wells in three independent experiments. Fluorescent units obtained in the cell viability assays were converted to percent viability of control cells. Concentrations leading to 50% reduction in cell viability (EC50) were determined by the nonlinear regression sigmoidal dose–response curve fitting module using the Hill slope equation (GraphPad Prism version 4.00 for Windows, San Diego, USA) and were presented as mean±standard deviation (SD) of 3 independent experiments (each having 3 technical replicates) with cells of different passages (biological replicates). Two-way ANOVA was used to test the variation of EC50 values in different media and cell viability endpoints. Values of $p < 0.05$ were considered statistically significant. Graphs were created with GraphPad Prism as well.

2.5   Supplementary Material

A

B

C
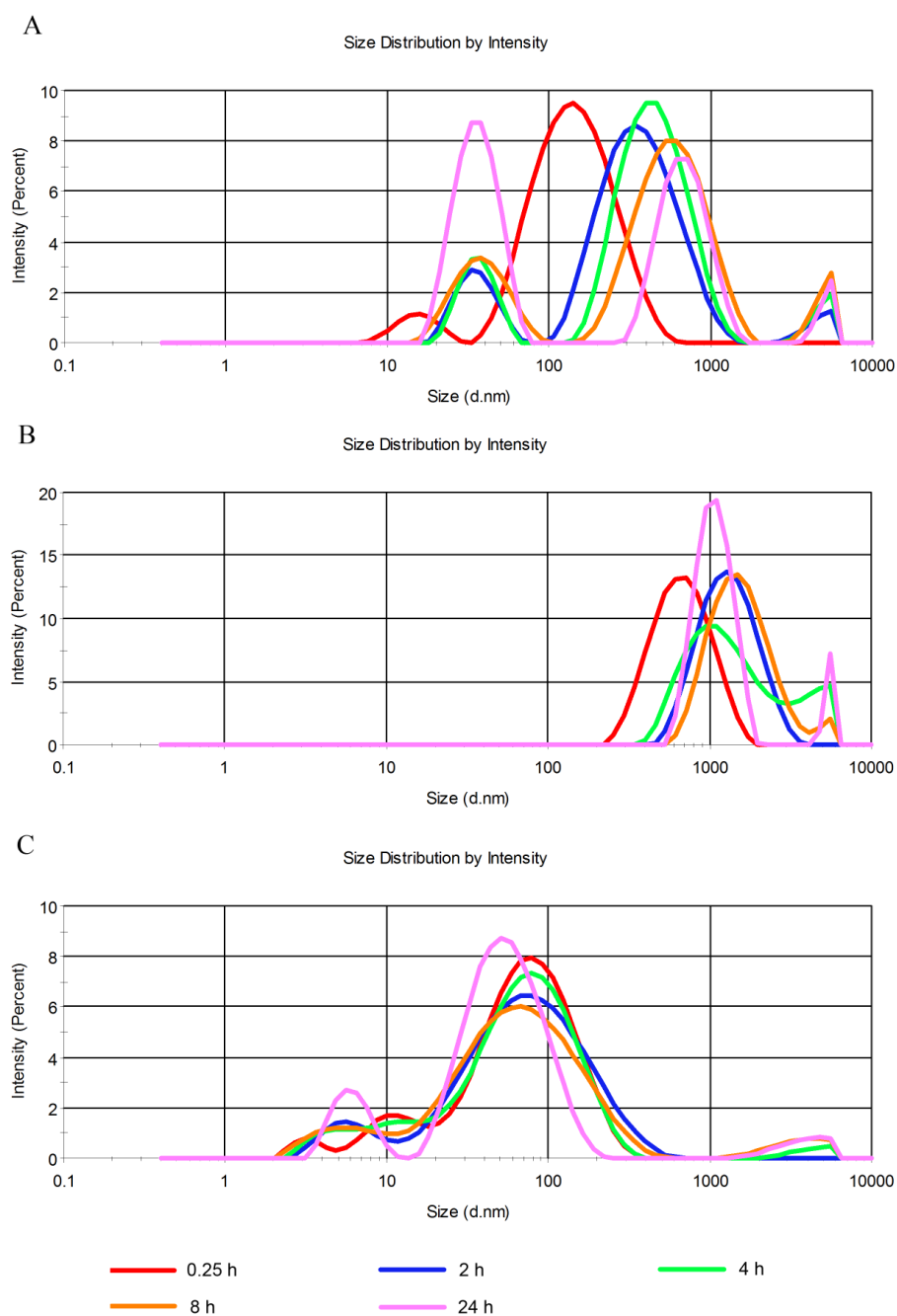
Figure S2.1 100 µM AgNP size distribution shift by intensity.

(A) AgNP in L15/ex, (B) AgNP in L15/ex w/o Cl, (C) AgNP in d-L15/ex.
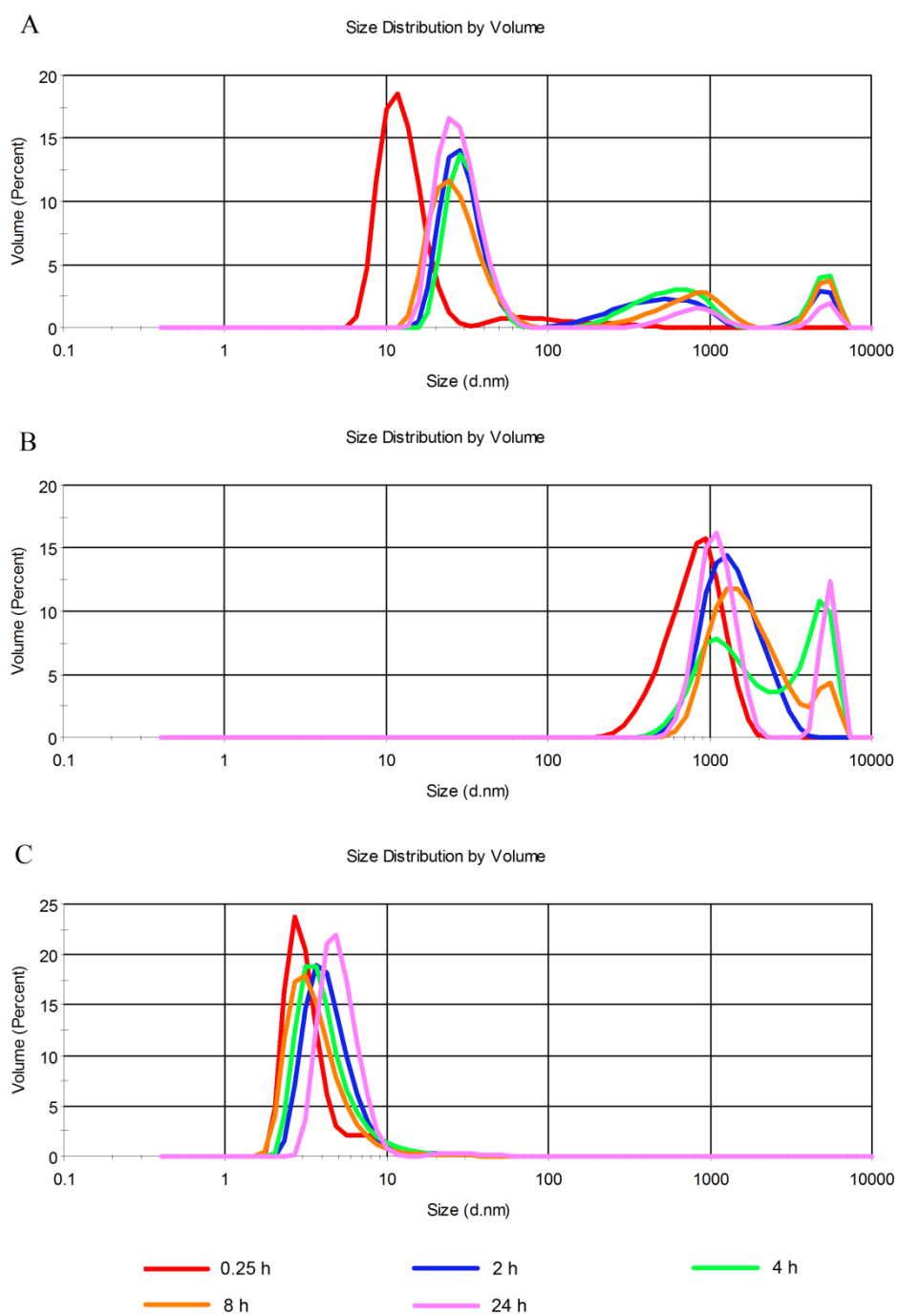
Figure S2.2 100 µM AgNP size distribution shift by volume.

(A) AgNP in L15/ex, (B) AgNP in L15/ex w/o Cl, (C) AgNP in d-L15/ex.

Table S2.1 PDI of DLS measurements for AgNP in different media in Figure 2.4.

	AgNP	0.25 h	2 h	4 h	8 h	24 h
L15/ex	10 µM	0.41 ± 0.03	0.38 ± 0.01	0.39 ± 0.04	0.50 ± 0.08	0.61 ± 0.03
	25 µM	0.35 ± 0.07	0.49 ± 0.02	0.56 ± 0.13	0.64 ± 0.13	0.84 ± 0.08
	100 µM	0.41 ± 0.07	0.61 ± 0.02	1.00 ± 0.00	0.80 ± 0.18	0.47 ± 0.10
L15/ex w/o Cl	10 µM	0.21 ± 0.01	0.27 ± 0.03	0.35 ± 0.03	0.42 ± 0.01	0.77 ± 0.14
	25 µM	0.21 ± 0.01	0.26 ± 0.02	0.37 ± 0.03	0.36 ± 0.04	0.42 ± 0.03
	100 µM	0.23 ± 0.01	0.27 ± 0.05	0.35 ± 0.06	0.35 ± 0.06	0.61 ± 0.12
d-L15/ex	10 µM	0.46 ± 0.03	0.53 ± 0.02	0.52 ± 0.02	0.85 ± 0.23	0.63 ± 0.06
	25 µM	0.51 ± 0.01	0.55 ± 0.03	0.69 ± 0.19	0.88 ± 0.00	0.70 ± 0.08
	100 µM	0.55 ± 0.01	0.52 ± 0.00	0.53 ± 0.01	0.50 ± 0.03	0.48 ± 0.02

Table S2.2 EC50 Values, Corresponding 95% Confidence Intervals, Hill slope and R^2 of concentration-response curves in Figure 2.6.

			EC50 (µM)	95% confidence interval	Hill Slope	R^2
L15/ex	AgNP	Metabolic activity	31.81	29.05-34.84	-2.225	0.9815
		Cell membrane integrity	28.98	23.87-35.18	-1.230	0.9389
		Lysosomal membrane integrity	12.96	10.36-16.22	-1.007	0.9476
	AgNO$_3$	Metabolic activity	2.110	1.835-2.426	-2.957	0.9497
		Cell membrane integrity	2.991	2.608-3.431	-2.394	0.9296
		Lysosomal membrane integrity	2.812	2.432-3.252	-1.935	0.9329
L15/ex w/o Cl	AgNP	Metabolic activity	12.68	10.41-15.45	-2.586	0.9427
		Cell membrane integrity	14.42	12.01-17.31	-2.102	0.9525
		Lysosomal membrane integrity	9.716	7.759-12.17	-1.811	0.9316
	AgNO$_3$	Metabolic activity	0.761	0.6936-0.8359	-4.259	0.9761
		Cell membrane integrity	0.908	0.8220-1.003	-4.713	0.9647
		Lysosomal membrane integrity	0.595	0.5076-0.6983	-2.999	0.9409
d-L15/ex	AgNP	Metabolic activity	69.94	59.24-82.57	-2.057	0.8982
		Cell membrane integrity	27.47	21.58-34.97	-0.827	0.9287
		Lysosomal membrane integrity	14.25	11.13-18.24	-0.727	0.9418
	AgNO$_3$	Metabolic activity	3.955	3.598-4.347	-1.869	0.9598
		Cell membrane integrity	4.687	4.219-5.207	-2.652	0.9175
		Lysosomal membrane integrity	3.351	2.958-3.796	-1.931	0.9408

References

Ahamed M, AlSalhi MS, Siddiqui MKJ. 2010. Silver nanoparticle applications and human health. Clinica Chimica Acta 411(23-24):1841-1848.

Beer C, Foldbjerg R, Hayashi Y, Sutherland DS, Autrup H. 2012. Toxicity of silver nanoparticles—Nanoparticle or silver ion? Toxicology Letters 208(3):286-292.

Bianchini A, Wood CM. 2003. Mechanism of acute silver toxicity in Daphnia magna. Environmental Toxicology and Chemistry 22(6):1361-1367.

Bols NC, Barlian A, Chirinotrejo M, Caldwell SJ, Goegan P, Lee LEJ. 1994. Development of a Cell-Line from Primary Cultures of Rainbow-Trout, Oncorhyrzchus Mykiss (Walbaum), Gills. Journal of Fish Diseases 17(6):601-611.

Cho EC, Zhang Q, Xia Y. 2011. The effect of sedimentation and diffusion on cellular uptake of gold nanoparticles. Nat Nano 6(6):385-391.

Dayeh VR, Schirmer K, Bols NC. 2002. Applying whole-water samples directly to fish cell cultures in order to evaluate the toxicity of industrial effluent. Water Research 36(15):3727-3738.

Fabrega J, Luoma SN, Tyler CR, Galloway TS, Lead JR. 2011. Silver nanoparticles: Behaviour and effects in the aquatic environment. Environment International 37(2):517-531.

Farkas J, Christian P, Urrea JAG, Roos N, Hassellöv M, Tollefsen KE, Thomas KV. 2010. Effects of silver and gold nanoparticles on rainbow trout (Oncorhynchus mykiss) hepatocytes. Aquatic Toxicology 96(1):44-52.

Federici G, Shaw BJ, Handy RD. 2007. Toxicity of titanium dioxide nanoparticles to rainbow trout (Oncorhynchus mykiss): Gill injury, oxidative stress, and other physiological effects. Aquatic Toxicology 84(4):415-430.

Greulich C, Diendorf J, Simon T, Eggeler G, Epple M, Köller M. 2011. Uptake and intracellular distribution of silver nanoparticles in human mesenchymal stem cells. Acta Biomaterialia 7(1):347-354.

Griffitt RJ, Weil R, Hyndman KA, Denslow ND, Powers K, Taylor D, Barber DS. 2007. Exposure to Copper Nanoparticles Causes Gill Injury and Acute Lethality in Zebrafish (Danio rerio). Environmental Science & Technology 41(23):8178-8186.

Grosell M, Hogstrand C, Wood CM, Hansen HJM. 2000. A nose-to-nose comparison of the physiological effects of exposure to ionic silver versus silver chloride in the European eel (Anguilla anguilla) and the rainbow trout (Oncorhynchus mykiss). Aquatic Toxicology 48(2–3):327-342.

Hamilton R, Wu N, Porter D, Buford M, Wolfarth M, Holian A. 2009. Particle length-dependent titanium dioxide nanomaterials toxicity and bioactivity. Particle and Fibre Toxicology 6(1):35.

Hinderliter P, Minard K, Orr G, Chrisler W, Thrall B, Pounds J, Teeguarden J. 2010. ISDD: A computational model of particle sedimentation, diffusion and target cell dosimetry for in vitro toxicity studies. Particle and Fibre Toxicology 7(1):36.

Hogstrand C, Galvez F, Wood CM. 1996. Toxicity, silver accumulation and metallothionein induction in freshwater rainbow trout during exposure to different silver salts. Environmental Toxicology and Chemistry 15(7):1102-1108.

Hussain S, Meneghini E, Moosmayer M, Lacotte D, Anner BM. 1994. Potent and reversible interaction of silver with pure Na,K-ATPase and Na,K-ATPase-liposomes. Biochimica et Biophysica Acta (BBA) - Biomembranes 1190(2):402-408.

Hussain S, Thomassen L, Ferecatu I, Borot M-C, Andreau K, Martens J, Fleury J, Baeza-Squiban A, Marano F, Boland S. 2010. Carbon black and titanium dioxide nanoparticles elicit distinct apoptotic pathways in bronchial epithelial cells. Particle and Fibre Toxicology 7(1):10.

Huynh KA, Chen KL. 2011. Aggregation Kinetics of Citrate and Polyvinylpyrrolidone Coated Silver Nanoparticles in Monovalent and Divalent Electrolyte Solutions. Environmental Science & Technology 45(13):5564-5571.

Kawata K, Osawa M, Okabe S. 2009. In Vitro Toxicity of Silver Nanoparticles at Noncytotoxic Doses to HepG2 Human Hepatoma Cells. Environmental Science & Technology 43(15):6046-6051.

Kim S, Choi JE, Choi J, Chung K-H, Park K, Yi J, Ryu D-Y. 2009. Oxidative stress-dependent toxicity of silver nanoparticles in human hepatoma cells. Toxicology in Vitro 23(6):1076-1084.

Kühnel D, Busch W, Meißner T, Springer A, Potthoff A, Richter V, Gelinsky M, Scholz S, Schirmer K. 2009. Agglomeration of tungsten carbide nanoparticles in exposure medium does not prevent uptake and toxicity toward a rainbow trout gill cell line. Aquatic Toxicology 93(2-3):91-99.

Lee L, Dayeh V, Schirmer K, Bols N. 2009. Applications and potential uses of fish gill cell lines: examples with RTgill-W1. In Vitro Cellular & Developmental Biology - Animal 45(3):127-134.

Ma X, Wu Y, Jin S, Tian Y, Zhang X, Zhao Y, Yu L, Liang X-J. 2011. Gold Nanoparticles Induce Autophagosome Accumulation through Size-Dependent Nanoparticle Uptake and Lysosome Impairment. Acs Nano 5(11):8629-8639.

MacCuspie R. 2011. Colloidal stability of silver nanoparticles in biologically relevant conditions. Journal of Nanoparticle Research 13(7):2893-2908.

MacCuspie RI, Allen AJ, Hackley VA. 2010. Dispersion stabilization of silver nanoparticles in synthetic lung fluid studied under in situ conditions. Nanotoxicology 5(2):140-156.

McGeer JC, Wood CM. 1998. Protective effects of water Cl- on physiological responses to waterborne silver in rainbow trout. Canadian Journal of Fisheries and Aquatic Sciences 55(11):2447-2454.

Meißner T, Kühnel D, Busch W, Oswald S, Richter V, Michaelis A, Schirmer K, Potthoff A. 2010. Physical-chemical characterization of tungsten carbide nanoparticles as a basis for toxicological investigations. Nanotoxicology 4(2):196-206.

Navarro E, Baun A, Behra R, Hartmann N, Filser J, Miao A-J, Quigg A, Santschi P, Sigg L. 2008a. Environmental behavior and ecotoxicity of engineered nanoparticles to algae, plants, and fungi. Ecotoxicology 17(5):372-386.

Navarro E, Piccapietra F, Wagner B, Marconi F, Kaegi R, Odzak N, Sigg L, Behra R. 2008b. Toxicity of Silver Nanoparticles to Chlamydomonas reinhardtii. Environmental Science & Technology 42(23):8959-8964.

Nel A, Xia T, Mädler L, Li N. 2006. Toxic Potential of Materials at the Nanolevel. Science 311(5761):622-627.

Oberdorster G, Oberdorster E, Oberdorster J. 2005. Nanotoxicology: An emerging discipline evolving from studies of ultrafine particles. Environmental Health Perspectives 113(7):823-839.

Piccapietra F, Sigg L, Behra R. 2011. Colloidal Stability of Carbonate-Coated Silver Nanoparticles in Synthetic and Natural Freshwater. Environmental Science & Technology 46(2):818-825.

Schirmer K, Chan AGJ, Greenberg BM, Dixon DG, Bols NC. 1997. Methodology for demonstrating and measuring the photocytotoxicity of fluoranthene to fish cells in culture. Toxicology in Vitro 11(1-2):107-119.

Schirmer K, Dixon DG, Greenberg BM, Bols NC. 1998. Ability of 16 priority PAHs to be directly cytotoxic to a cell line from the rainbow trout gill. Toxicology 127(1-3):129-141.

Stern S, Adiseshaiah P, Crist R. 2012. Autophagy and lysosomal dysfunction as emerging mechanisms of nanomaterial toxicity. Particle and Fibre Toxicology 9(1):20.

Tanneberger K, Knöbel M, Busser FJM, Sinnige TL, Hermens JLM, Schirmer K. 2012. Predicting Fish Acute Toxicity Using a Fish Gill Cell Line-Based Toxicity Assay. Environmental Science & Technology 47(2):1110-1119.

Tedesco S, Doyle H, Blasco J, Redmond G, Sheehan D. 2010. Oxidative stress and toxicity of gold nanoparticles in Mytilus edulis. Aquatic Toxicology 100(2):178-186.

Teeguarden JG, Hinderliter PM, Orr G, Thrall BD, Pounds JG. 2007. Particokinetics in vitro: Dosimetry considerations for in vitro nanoparticle toxicity assessments. Toxicological Sciences 95(2):300-312.

Truong L, Zaikova T, Richman EK, Hutchison JE, Tanguay RL. 2011. Media ionic strength impacts embryonic responses to engineered nanoparticle exposure. Nanotoxicology 6(7):691-699.

Visual MINTEQ ver. 3.0. 2011. Department of Land and Water Resources Engineering, KTH, Sweden. http://www2.lwr.kth.se/English/OurSoftware/vminteq/.

Wijnhoven SWP, Peijnenburg WJGM, Herberts CA, Hagens WI, Oomen AG, Heugens EHW, Roszek B, Bisschops J, Gosens I, Van De Meent D and others. 2009. Nano-silver – a review of available data and knowledge gaps in human and environmental risk assessment. Nanotoxicology 3(2):109-138.

Wood CM, Playle RC, Hogstrand C. 1999. Physiology and modeling of mechanisms of silver uptake and toxicity in fish. Environmental Toxicology and Chemistry 18(1):71-83.

Woodrow Wilson International Centre for Scholars. 2013. Project on Emerging Nanotechnologies. Consumer Products Inventory of Nanotechnology Products. Accessed June 2013 from the website: http://www.nanotechproject.org/inventories/consumer/.

Yang X, Gondikas AP, Marinakos SM, Auffan M, Liu J, Hsu-Kim H, Meyer JN. 2011. Mechanism of Silver Nanoparticle Toxicity Is Dependent on Dissolved Silver and Surface Coating in Caenorhabditis elegans. Environmental Science & Technology 46(2):1119-1127.

Chapter 3 Silver nanoparticle-protein interactions in intact rainbow trout gill cells

Upon contact with biota, nanoparticles can bind proteins, which coat the nanoparticles and form a nanoparticle-protein corona. This corona therefore is what cells of an organism "see"; thus, the protein corona plays a key role in the interaction of nanoparticles with cells and organisms. The research presented here focused on silver nanoparticle (AgNP) uptake and interaction with proteins in cells of the rainbow trout (*Oncorhynchus mykiss*) gill cell line, RTgill-W1. Uptake studies confirmed that RTgill-W1 cells internalize AgNP via an energy-depend pathway and store the AgNP in endocytic compartments, which include lysosomes and endosomes. With subcellular fractionation, the AgNP-protein corona was recovered from these intact subcellular compartments. Proteins acquired from the AgNP-protein corona were identified by mass spectrometry and analysed with Gene Ontology. A total of 383 proteins were identified in this way and broadly classified as belonging to cell membrane functions, endocytosis, vesicle-mediated transport and stress-response pathways. Of particular interest was the identification of "ATPase Na^+/K^+ transporting protein" and "Rab Family Small GTPases" as these were previously implied to bind to nanoparticles. Based on the uptake experiments and the identity of proteins extracted from the AgNP corona, an initial mechanism of AgNP uptake and toxicity was derived. This is the first study that focuses on the interaction of industrial nanoparticles with proteins in living cells. The method established to isolate the nanoparticles-protein corona from living cells can be broadly applied to other nanoparticle-cell interaction studies.

3.1 Introduction

After being taken up by vertebrate cells via endocytic processes, nanoparticles accumulate in different endocytic compartments such as endosomes and lysosomes (Iversen et al. 2011). Endocytic uptake routes and lysosome-related degradation processes play a vital role in cellular metabolism and homeostasis (Kroemer and Jaattela 2005). Overloading these compartments with an exogenous stressor, such as nanoparticles, can lead to lysosomal dysfunction and other injuries in cells (Stern et al. 2012). Lysosome membrane permeabilization and destabilization are common causes of lysosome dysfunction, which can induce oxidative stress, lysosomal alkalization and osmotic swelling (Futerman and van Meer 2004; Stern et al. 2012; Xia et al. 2007). Indeed, an *in vitro* study showed lysosomal membrane integrity to be more strongly affected than cellular metabolic activity and membrane integrity in fish gill cells exposed to silver nanoparticles (AgNP) (Yue et al. 2015; Chapter 2 of this thesis).

Due to the nanoparticles' extremely high surface to volume ratio, nanoparticles have a very active surface chemistry in comparison to bulk biomaterials; hence, upon entry into cells, a variety of biomolecules may adsorb to the nanoparticle surface and reduce the nanoparticle surface energy by physical adsorption or chemical reactions (Lynch and Dawson 2008; Mahmoudi et al. 2011; Monopoli et al. 2011; Nel et al. 2009; Walczyk et al. 2010). Based on their abundance and diversity, proteins are thought to play a dominant role in such types of interactions, coating the nanoparticles surface with a so-called protein corona. Thus, it is the NP-protein corona, not the bare nanoparticles surface, that influences the interaction of nanoparticles with constituents in cells (Monopoli et al. 2012). In turn, corona-forming proteins may be depleted from the cellular machinery and be structurally and/or functionally impaired.

That proteins which adsorb to nanoparticle surfaces are prone to alterations has been demonstrated using isolated proteins or protein mixtures extracted from cells. After adsorbing to a gold nanoparticle surface, the structure of serum albumin was different from the native form (Wang et al. 2011). The activity of tryptophanase (TNase) from *E. coli* extract was significantly inhibited by AgNP due to high affinity binding to the enzyme active site (Wigginton et al. 2010). Yet, knowledge of nanoparticle interactions with proteins in intact cells is scarce. Two recent studies made use of the unique magnetic property of magnetite nanoparticles to recover the protein corona by magnetic separation from intact cells and identified the recovered proteins by mass spectrometry (Bertoli et al. 2014; Hofmann et al. 2014). No previous study has attempted to determine the proteins that

bind in living cells to industrially used, high production volume nanoparticles, such as AgNP. Which kind of proteins adsorb to the surface of AgNP after cellular uptake? Can these proteins explain mechanisms of AgNP cytotoxicity?

To address these questions, we here explore the uptake, fate and interactions of AgNP with proteins in intact cells of the rainbow trout (*Oncorhynchus mykiss*) gill cell line, RTgill-W1 (Bols et al. 1994). These cells can survive in a low ionic strength exposure medium (d-L15/ex), which can stabilize AgNP in suspension and allows to more closely mimic the aquatic environment a gill cell would face (Yue et al. 2015; Chapter 2). We have previously demonstrated that AgNP elicit a particle-specific effect in RTgill-W1 cells. Specifically, lysosomal membrane integrity was significantly more sensitive than cell membrane integrity and cellular metabolic activity upon exposure to AgNP. Moreover, scavenging silver ions stemming from AgNP dissolution by a strong silver ion ligand, cysteine, only partially prevented the AgNP impact on the lysosomes, further corroborating the particle specific toxicity (Yue et al. 2015; Chapter 2). These findings led us to hypothesize that AgNP-induced toxicity to RTgill-W1 cells may be elicited via lysosome related pathways and involve binding of lysosomal proteins to the AgNP. We now exploited this system to isolate the AgNP protein corona from intact cells. To do this, we first confirmed the presence of AgNP in membrane-bound compartments and then performed subcellular fractionation of RTgill-W1 cells by means of density gradient centrifugation. The AgNP-protein corona was subsequently isolated from intact cellular compartments enriched in silver and the corona composition analyzed.

This work mainly focused on the initial stage of AgNP interaction with cells in order to capture early stages of binding where both the cellular compartments were intact for AgNP-corona isolation as well as AgNP clearly discernible in the cells. Such conditions were identified after 2 h of exposure, which was then chosen as the longest exposure time for all steps performed in this work.

3.2   Results

3.2.1   Cell viability and silver content in RTgill-W1 cells after exposure

The toxicity of AgNP and silver ions, using $AgNO_3$ as control, was quantified after 2 h of exposure (Figure 3.1, Table 3.1). $AgNO_3$ induced higher toxicity than AgNP to RTgill-W1 cells as a function of total silver (Figure 3.1A). In AgNP exposures, lysosomal membrane integrity was similarly affected as cell membrane integrity and cellular metabolic activity, which is in contrast to the results observed in AgNP exposures for 24 h (Yue et al., 2015; Chapter 2). Based on the dissolved silver content in the exposure medium, d-L15/ex (Table S3.1), re-calculation of the 2 h exposure concentration-response curves as a function of dissolved silver showed that AgNP elicited a higher toxicity than $AgNO_3$ (Figure 3.1B), indicating that the AgNP still elicited a particle-specific effect to the cells.
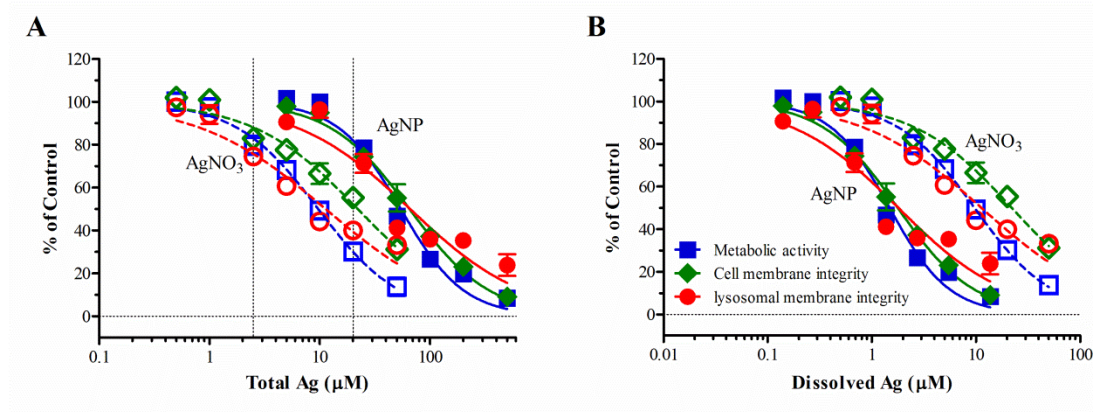
Figure 3.1 Toxicity of AgNP and $AgNO_3$ to RTgill-W1 cells.

A: Toxicity of AgNP and $AgNO_3$ as a function of total silver in the d-L15/ex medium for 2 h exposures. B: Toxicity of AgNP and $AgNO_3$ as a function of dissolved silver in the d-L15/ex medium for 2 h. Average and standard deviation of three independent experiments is shown (n=3). The endpoints measured are metabolic activity (■), cell membrane integrity (♦) and lysosomal integrity (●). Solid lines represent AgNP effects and dashed lines represent $AgNO_3$ effects. 2.5 µM $AgNO_3$ and 20 µM AgNP, indicated by dotted vertical lines, were selected for subsequent experiments.

Table 3.1 EC50 Values, Corresponding 95% Confidence Intervals, Hill slope and R^2 of AgNP and $AgNO_3$ concentration-response curves for 2 h exposures of RTgill-W1 cells.

		EC50 (µM)	95% confidence interval	Hill Slope	R^2
AgNP	Metabolic activity	54.20	48.11-61.06	-1.519	0.9760
	Cell membrane integrity	64.89	59.70-70.54	-1.195	0.9888
	Lysosomal membrane integrity	65.83	49.76-87.08	-0.838	0.8849
$AgNO_3$	Metabolic activity	9.681	8.916-10.51	-1.167	0.9885
	Cell membrane integrity	22.00	18.91-25.59	-0.917	0.9636
	Lysosomal membrane integrity	11.26	9.085-13.95	-0.754	0.9317

EC 50 values were tested by Two-way ANOVA and no significant differences were found, n=3.

The cellular uptake of AgNP by RTgill-W1 cells was quantified by inductively coupled plasma mass spectrometry (ICP-MS) (Figure 3.2, Supplementary Figure S3.1). Much more silver accumulated over 24 h compared to 2 h of exposures for both AgNP and $AgNO_3$. An about 2.5-10 fold higher accumulation of AgNP compared to $AgNO_3$ was observed for the same external total silver concentration for both time points.
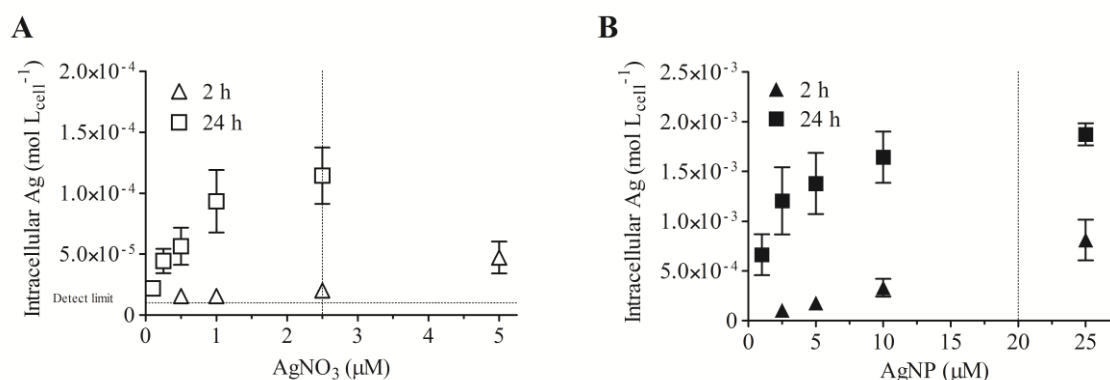
Figure 3.2 Uptake of AgNP and $AgNO_3$ in RTgill-W1 cells.

Internal silver (mol/cell) were quantified by ICP-MS after exposure of RTgill-W1 cells to $AgNO_3$ (A) and AgNP (B) for 2 h and 24 h. 2.5 μM $AgNO_3$ (grid line in panel A X axis) and 20 μM AgNP (grid line in panel B X axis) were selected for the later experiments. Data were presented as mean ± standard deviation, n=3.

Based on the toxicity results, similarly toxic concentrations of $AgNO_3$ and AgNP were chosen for subsequent experiments. These concentrations were 2.5 μM for $AgNO_3$ and 20 μM for AgNP. These concentrations caused a 20% effect on the cells (Figure 3.1A) but were at the same time high enough for efficient quantification by mass spectrometry (Figure 3.2).

3.2.2   Localization of AgNP in RTgill-W1 cells

AgNP were found in the endosomes and lysosomes and other endocytic compartments in transmission electron microscopy (TEM) images (Figure 3.3A, E, F). Energy-Dispersive X-ray (EDX) confirmed that high electron density dots were silver (Figure 3.3A-B). As demonstrated in Figure 3.3C-F, significant uptake of AgNP occurred in cells at 19℃ compared to cells incubated at 4℃.
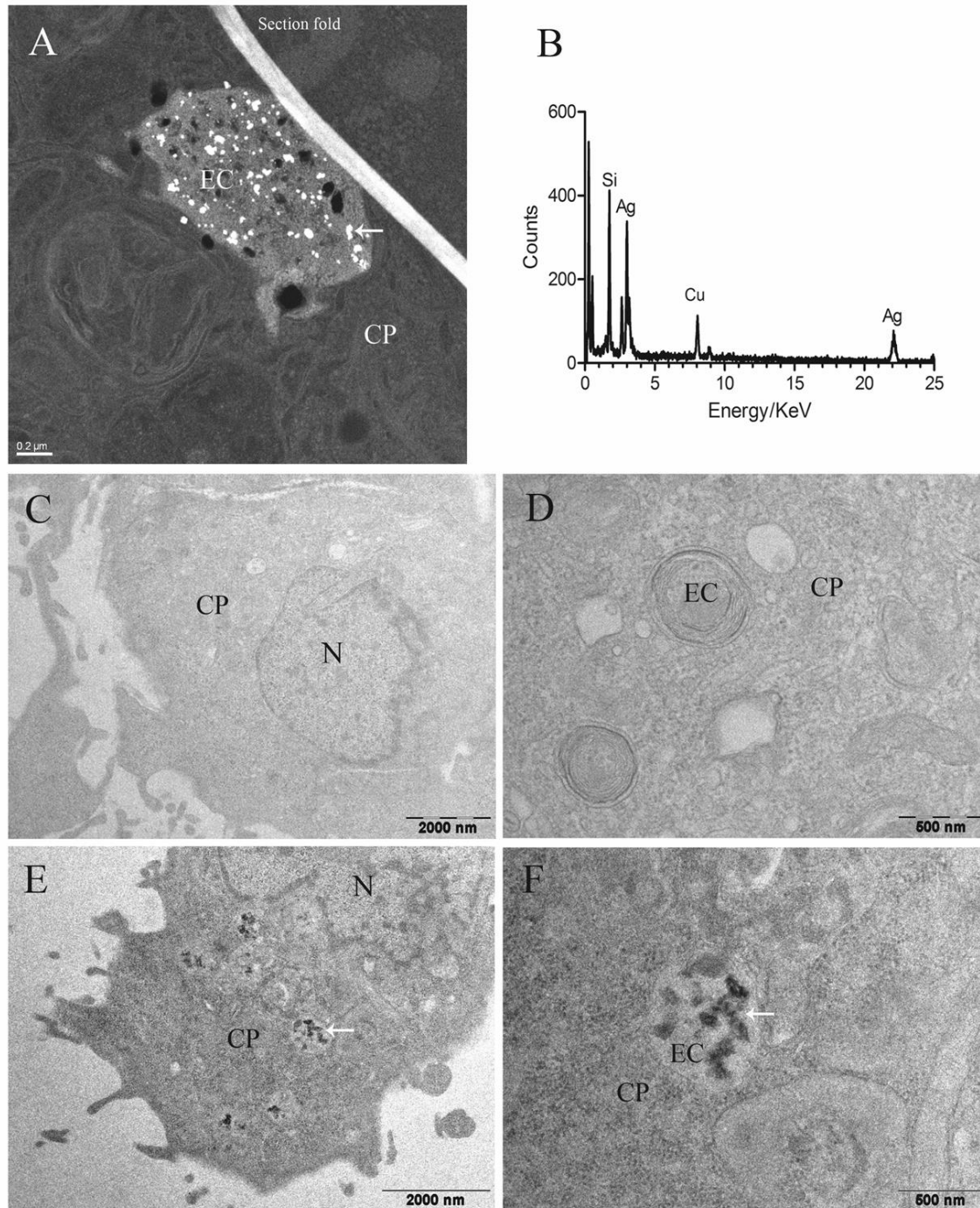
Figure 3.3 Localization and identification of AgNP in RTgill-W1 cells under varying exposure conditions.

A and B: scanning transmission electron microscope image of AgNP in a RTgill-W1 cell organelle and the AgNP EDX spectrum associated with it. C and D: transmission electron microscopy images of RTgill-W1 cells after exposure to AgNP for 0.5 h at 4℃. E and F: TEM images of RTgill-W1 cells after exposure to AgNP for 0.5 h at 19℃. CP: cytoplasm. N: nucleus. EC: endocytic compartment. White arrows show the AgNP in cells.

To further study the AgNP containing compartments, subcellular fractionation of RTgill-W1 cells was performed with density gradient centrifugation (Figure 3.4, Figure S3.2). After lysis of cells and centrifugation, the lysate was separated by density gradient centrifugation in an OptiPrep™ gradient buffer. Acid phosphatase assay and LysoTracker staining indicated that intact lysosomes and endosomes were enriched in a low density band (Fraction 1-3, endosome-lysosome fractions) (Figure 3.5, Figure S3.3). Nuclei, mitochondria, peroxisomes and some membrane debris were found in a high density band (Fraction 8-10, cell membrane-mitochondria-nucleus fractions).
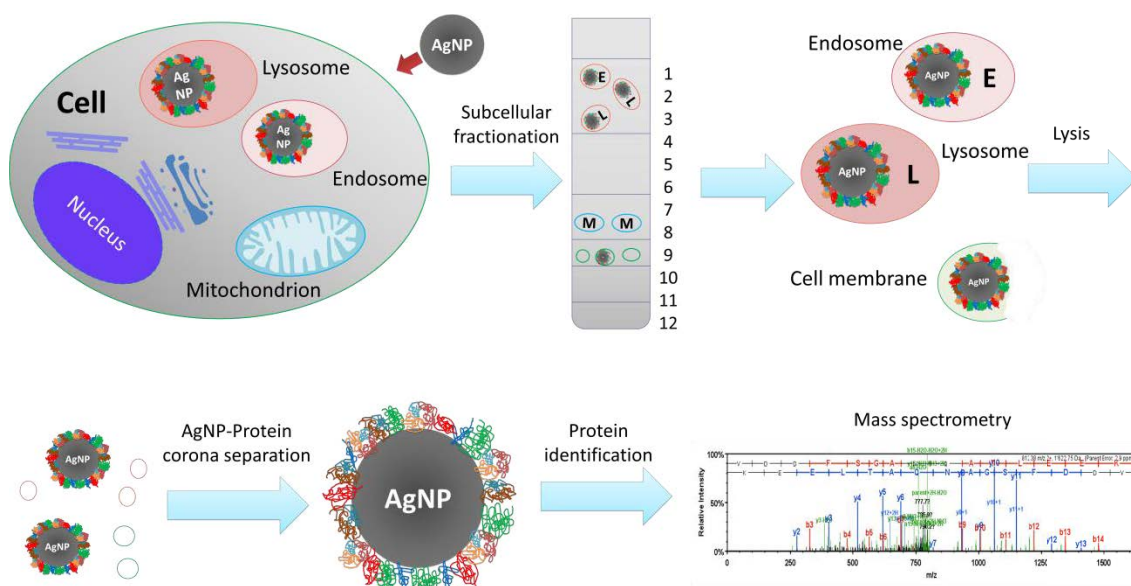
Figure 3.4 Scheme of AgNP-protein corona isolation from intact cells.

After exposure to AgNP/AgNO$_3$, RTgill-W1 cells were lysed and separated in a density gradient buffer with 15% to 30% Optiprep and ultracentrifuged at 145 000 × g for 2 h. Different fractions were collected and tested for total protein concentration, acid phosphatase activity (biomarker for endo-lysosome compartments) and silver content. LysoTracker staining was used to check for the intactness of the endo-lysosome compartments. The AgNP-protein coronas were separated from lysate of intact cell compartments by centrifugation. The corona proteins were identified with label-free quantitative mass spectrometry.

The silver content in each fraction was measured by ICP-MS. The silver content was enriched in both the endosome-lysosome fractions and the cell membrane-mitochondria-nucleus fractions in AgNP exposures (Figure 3.5). In contrast, in the AgNO$_3$ exposures, very low levels of silver were seen in the cell membrane-mitochondria-nucleus fractions while the silver content was below the limit of detection in the endosome-lysosome fractions.
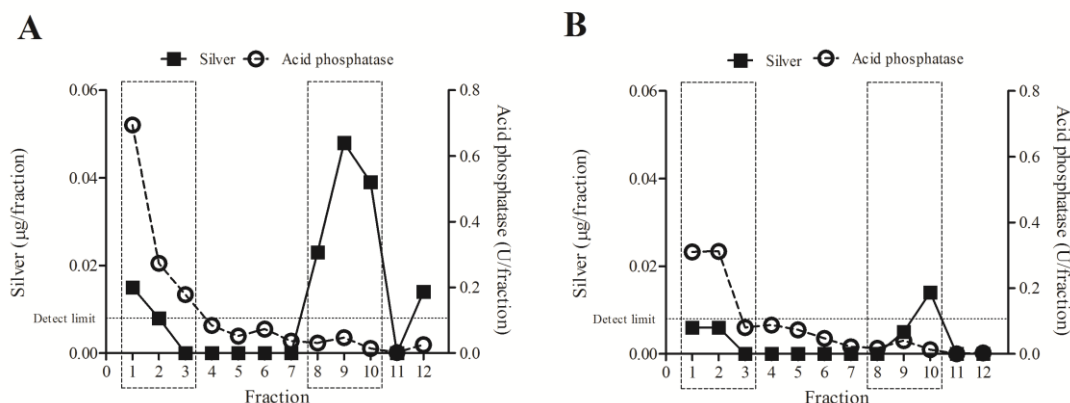
Figure 3.5 Silver content and acid phosphatase activity distribution in subcellular fractions isolated from AgNP or AgNO$_3$ exposed cells.

A: cell fractions from AgNP exposed cells. B: cell fractions from AgNO$_3$ exposed cells. Fraction 1-3, endosome-lysosome fractions; Fraction 8-10, cell membrane-mitochondria-nucleus fractions.

Taking different parameters, i.e. protein content, acid phosphatase activity and silver content together, the endosome-lysosome fractions and cell membrane-mitochondria-nucleus fractions were harvested for AgNP-protein corona isolation. Samples from AgNO$_3$ exposures served as control.

3.2.3   Proteins identified from the AgNP corona

Relevant fractions containing the intact cellular compartments enriched in AgNP were lysed by freezing and thawing in TBS with 1% CHAPS. The AgNP-protein corona was pelleted from the lysates by centrifugation. Proteins in the AgNP-protein corona were identified by a label-free quantitative mass spectrometry approach with nano-LC-MS/MS. A total of 1223 proteins were identified in both AgNP and AgNO$_3$ exposures. Among those, 383 proteins were found to specifically bind to AgNP in the RTgill-W1 cells, using an enrichment factor of at least two, relative to AgNO$_3$ exposures, as the cut-off value (Supplementary Spectra counts of Proteins file). An additional experiment was performed to offer further proof of the identity of proteins binding to AgNP. Here, AgNP was added to extracts of fractions separated as described above but from untreated cells. After incubation of these extracts, the same protocol was used for AgNP-protein corona separation and protein identification. Among the proteins detected in the isolations starting from intact, exposed cells, 82 proteins were confirmed in this AgNP-extraction experiment.

In order to test whether protein adsorption was correlated to cysteine abundance in proteins, a strong silver ion ligand, cysteine abundance was compared between bound proteins and unbound proteins from the AgNP-extraction experiment (Supplementary, cysteine abundance analysis).

Bound proteins were identified in AgNP-protein corona isolated from incubation of AgNP with cell extracts. Unbound proteins were identified from control extracts which never exposed to silver. No statistically relevant trend was observed for linking protein adsorption and cysteine abundance by t-test.

To identify protein functions and potential pathways of the 383 proteins isolated from the AgNP corona, protein ontology was applied. Proteins not included in protein ontology analysis were checked in UniProt. Proteins identified from the AgNP corona were found to belong to the cell membrane, cytoplasm, endoplasmic reticulum (ER), endosome, Golgi, lysosome, mitochondrion and nucleus (Table S3.2-6). Two biological pathways were identified that relate to AgNP uptake: endocytosis pathways (GO:0006897~endocytosis, Table S3.4) and vesicle-mediated transport pathway (GO:0016192~vesicle-mediated transport, Table S3.5). Based on these results, the interaction of AgNP with RTgill-W1 cells was reconstructed along three main routes of interaction: cell membrane and adhesion, uptake and vesicle trafficking as well as stress response (Figure 3.6).
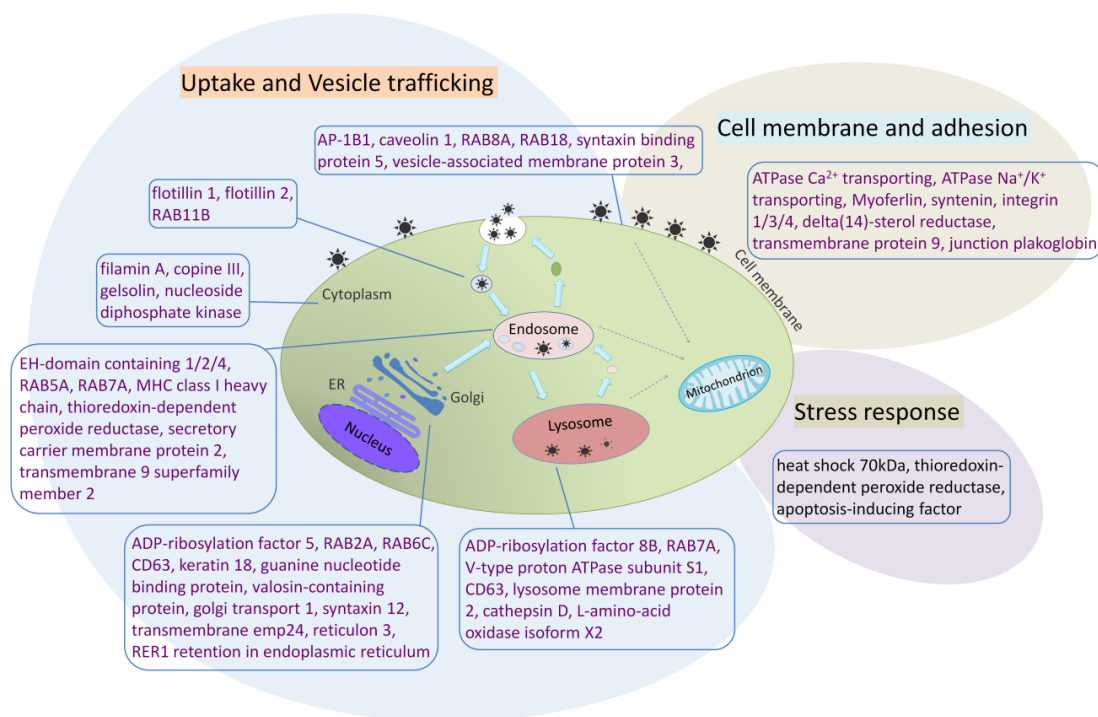
Figure 3.6 Reconstruction of AgNP interaction with RTgill-W1 cells.

Proteins identified from AgNP-proteins corona were analyzed with DAVID ontology and classified as belonging to cell membrane functions (cell membrane and adhesion section) as well as endocytosis and vesicle-mediated transport pathways (uptake and vesicle trafficking). Several proteins related to cellular stress response were listed in stress response section. ER: endoplasmic reticulum.

3.3 Discussion

In this study, the ability of RTgill-W1 cells to take up AgNP was explored and used to isolate and identify the proteins that bound to AgNP upon trafficking in intact cells. On this basis, the events following AgNP uptake into cells and ensuing toxicity can be, for the first time, described in the context of the AgNP-protein corona.

AgNP entered RTgill-W1 cells via endocytic pathways, which was confirmed by different lines of evidence. First, the fact that much more silver uptake was observed for AgNP exposures compared to $AgNO_3$ at the same external silver concentration means that RTgill-W1 cells take up AgNP and Ag^+ via different routes. Previous research indicated that cells take up Ag^+ via some Cu^+ transporters in mammalian cells (Bertinato et al. 2010) and algae (Pillai et al. 2014). In contrast, AgNP uptake was demonstrated in human mesenchymal stem cells to be via endocytic pathways (Greulich et al. 2011). Furthermore, the cellular uptake of AgNP was temperature- and therefore energy–dependent, pointing toward active uptake, as is the case for endocytic processes. Finally, the silver content after AgNP exposure was particularly high in the endosome-lysosome fractions. As for the high silver signal in the cell membrane-mitochondria-nucleus fractions, it is difficult to conclude that AgNP accumulate in mitochondria and nuclei because AgNP was never seen in these organelles in TEM images. One explanation might be that the cell membrane-mitochondria-nucleus fraction also contained some endocytosis related organelles which were overloaded with AgNP and cell membrane debris containing AgNP. Then, due to large amounts of AgNP, these fragments would have a significantly higher density than the endosome-lysosome fraction and therefore elute in the cell membrane-mitochondria-nucleus fractions.

The cell membrane is the first location where cells interact with AgNP. Proteins located in the cell membrane are responsible for substance and signal transport between the exterior and the interior of a cell, they maintain cell structure, as well as support adhesion. Several plasma membrane transport proteins were identified from the AgNP-protein corona formed in RTgill-W1 cells. One of them is the ATPase Na^+/K^+ transporting protein, which regulates the exchange of sodium and potassium ions across the plasma membrane (Table S3.3). Schultz *et al* reported that citrate coated AgNP, which is the same coating of AgNP as used in this work, led to significant inhibition of Na^+/K^+ ATPase activity in juvenile rainbow trout gill. Compared to fish exposed to silver ions, AgNP showed a nano-specific effect to sodium influx in rainbow trout (Schultz et al. 2012). Other cell membrane proteins, such as myoferlin and junction plakoglobin, participate in cell junction formation, adhe-

sion and vesicular trafficking (Bernatchez et al. 2009; Cowin et al. 1986). Binding to AgNP could impair the function of these membrane proteins and disrupt the cell membrane, which was also seen for exposures to RTgill-W1 cells, reflected in the cell viability measurements.

Following contact with the cell membrane, the AgNP are apparently engulfed by RTgill-W1 cells via endocytosis, as also illustrated by the proteins eluted from the protein corona. Indeed, the endocytotic pathway and vesicle-mediated transport pathway were highlighted by the gene ontology analysis. Identified proteins include adaptor-related protein complex 1(AP-1B1), caveolin 1, flotillin 1 and flotillin 2, EH-domain containing protein 1/2/4, and Rab Family Small GTPases (RAB5A, RAB7A, RAB18).

AP-1B1 is a necessary factor in the clathrin-mediated endocytosis by facilitating both the recruitment of clathrin to membranes and the recognition of sorting signals of clathrin-coated vesicles (Canton and Battaglia 2012). Two other proteins participating in clathrin-coated vesicle formation, namely syntaxin binding protein 5 and RAB5A, were also identified in the AgNP-protein corona. Greulich and colleagues reported that several specific clathrin-mediated endocytosis inhibitors reduced the AgNP uptake by human mesenchymal stem cells (Greulich et al. 2011). However, also caveolin 1, a biomarker of caveolae-mediated endocytosis, was identified from the protein corona. This finding points to a possible clathrin-independent uptake in this study in addition to a clathrin-dependent pathway. Flotillin 1 and flotillin 2 form flotillin vesicles and mediate a clathrin-independent, caveolae-like endocytotic pathway (Meister and Tikkanen 2014; Vercauteren et al. 2011). Knockdown of these proteins decreased magnetic nanoparticle uptake in HeLa cells (Hofmann et al. 2014).

Once inside the cells, vesicles carrying AgNP were apparently transported to different compartments, e.g. early endosome and multi-vesicular bodies. For example, in addition to clathrin-coated vesicle formation, RAB5A is also required for the fusion of plasma membranes and early endosome intracellular membrane trafficking. RAB7A is a dominant marker of late endosomes and lysosomes and plays a key role in the regulation of endo-lysosomal trafficking (Grant and Donaldson 2009). Live cell imaging by fluorescence microscopy revealed that polystyrene particles travelled in HeLa Kyoto cells and retinal pigment epithelial cells from early endosomes (marked with fluorescence labeled RAB5) to late endosomes and lysosomes (marked with fluorescence labeled RAB7) (Sandin et al. 2012; Vercauteren et al. 2011). RAB5A and RAB7A were also identified in the corona of magnetic nanoparticles separated from HeLa cells (Hofmann et al. 2014).

AgNP were stored in late endosomes and lysosomes and led to lysosome dysfunction. Several previous studies showed that nanoparticles co-localized with different endosome or lysosome protein markers (Hofmann et al. 2014; Sandin et al. 2012; Wang et al. 2013). As a confirmation of these previous studies, we identified a number of proteins associated with these compartments: lysosome membrane protein 2, Cathepsin D, and L-amino-acid oxidase isoform X2 (Table S6). Vacuolar ATP synthase 16 kDa proteolipid subunit was another important protein identified in the AgNP-protein corona. It is a hydrogen ion transport protein with proton-transporting ATPase activity in lysosomes. This protein is a subunit of the membrane integral V0 complex of vacuolar ATPase (v-ATPase). Coupled with ATP hydrolysis, v-ATPase is responsible for acidifying lysosomes and late endosomes. Ma *et al* found that gold nanoparticles cause lysosome alkalinization through dissociation of v-ATPase in normal rat kidney cells (Ma et al. 2011).

Finally, trafficking of AgNP in cells seems to be a stress condition under which cells may synthesize different proteins to protect the cells from damage. Indeed, several stress response proteins were identified from the AgNP-protein corona, such as heat shock 70kDa, thioredoxin-dependent peroxide reductase, and apoptosis-inducing factor. SiO_2 nanoparticles induced increased thioredoxin reductase levels in human epidermal keratinocytes; the enzyme is involved in redox regulation and protection of radical-sensitive enzymes from oxidative damage (Passagne et al. 2012).

As discussed in previous work, cysteine abundance did not increase within identified from the proteins in AgNP-protein corona (Eigenheer et al. 2014). This was opposite to the hypothesis that the silver–thiol bond could enhance the protein binding to the AgNP surface. Thus, AgNP properties other than dissolved silver appear more important for protein binding.

Overall, this is the first study to focus on industrial nanoparticle interaction with proteins in living cells. With subcellular fractionation, the AgNP-protein corona was recovered from intact subcellular compartments and mechanisms of AgNP toxicity to fish gill cells were interpreted from the identity of proteins deduced. AgNP were taken up by RTgill-W1 cells via endocytosis pathways and transported via an endosome-lysosome pathway. In lysosomes, AgNP appear to have affected the lysosome function by interacting with v-ATPase. Furthermore, cell membrane proteins, like ATPase Na^+/K^+ transporting protein, were also found in the AgNP-protein corona, which affords an explanation for the cell membrane toxicity. While this study dealt with the identification of the proteins, how they may be affected in their structure and/or function is currently not known. Studying such

interactions would be very useful to further pin-down the mechanisms that nanoparticles have in cells. The protein list established here can serve as a guide to prioritize such kind of investigations.

3.4   Material and Methods

3.4.1   RTgill-W1 culture and toxicity measurement

RTgill-W1 cells were routinely cultivated in L15 medium (Invitrogen, Basel, Switzerland), supplemented with 5% fetal bovine serum (FBS, Gold, PAA Laboratories GmbH, Austria) and 1% penicillin/streptomycin (Sigma-Aldrich, Buchs, Switzerland) in 75 cm^2 flasks. The L15 medium containing these supplements is termed "complete L15".

For exposure to AgNP and $AgNO_3$, cells were seeded in 24-well microtiter plates, 25 cm^2 or 300 cm^2 flasks and cultured in L15 complete medium. After being fully confluent, cell monolayers were washed with d-L15/ex, a simple buffer that supports short-term RTgill-W1 cell survival and stabilizes AgNP in suspension (Yue et al. 2015; Chapter 2). Then, AgNP or $AgNO_3$ suspension in the d-L15/ex medium was added. Exposure was done at 4℃ or 19℃ in the dark for 0.5-2 h. Toxicity was assessed by three measurements: Alamar Blue (AB, Invitrogen, Basel, Switzerland) was used to measure the cellular metabolic activity; 5-carboxyfluorescein diacetate acetoxymethyl ester (CFDA-AM, Invitrogen, Basel, Switzerland) to measure the cell membrane integrity; Neutral Red (NR, Sigma-Aldrich, Buchs, Switzerland) to measure the lysosomal membrane integrity (Schirmer et al. 1997; Schirmer et al. 1998; Tanneberger et al. 2012).

3.4.2   Uptake of AgNP by RTgill-W1 cells and cell-internal distribution

To prepare samples for electron microscopy, confluent RTgill-W1 cells were exposed to AgNP in 24-well plates. Cells were sequentially washed with PBS, 0.5 mM Cysteine in PBS for 5 min, and Versene (Invitrogen/Gibco, Germany) to remove loosely bound AgNP and dissolved silver located on the cell surface. Washed cells were fixed by glutaraldehyde and paraformaldehyde and postfixed by osmium tetroxide (OsO_4). After uranyl acetate block staining, samples were dehydrated with a gradient of ethanol and embedded in Epon. Ultrathin sections were cut with a Leica microtome and placed on carbon coated copper grids. Images were taken for transmission electron microscopy (TEM, FEI Morgagni 268, 100 kV). A scanning transmission electron microscope (STEM, Hitachi HD-2700) was used to perform the Energy dispersive X-ray spectroscopy (EDX) analyses.

To quantify the cell associated silver, RTgill-W1 cells were cultured in 25 cm^2 flasks until confluency and then exposed to AgNP and $AgNO_3$ in d-L15/ex medium. After exposure, AgNP and $AgNO_3$ suspension were discarded and cells were washed as described above with PBS and 0.5 mM Cys in PBS for 5 min to remove the silver loosely adsorbed on the cell surface. Cells were then washed twice

with Versene and trypsinized. Detached cells were re-suspended in L15 completed medium. Cell suspensions were centrifuged at 1 000 × g for 3 min to pellet the cells. Cell pellets were re-suspended in 550 µL PBS and the cell density counted by an electronic cell counter (CASY1 TCC, Schärfe System, Germany). A volume of 500 µL cell supernatant was digested with 4.5 mL of 65% HNO_3 in a high-performance microwave digestion unit (MLS-1200 MEGA, Oberwil, Switzerland) at a maximal temperature of 195 °C for 20 min. The digests were diluted 50-times and measured by ICP-MS (Element 2 High Resolution Sector Field ICP-MS; Thermo Finnigan, Bremen, Germany). The reliability of the measurements was determined using specific water references (M105A, IFA-Tull, Austria).

3.4.3   Subcellular fractionation

Isolation of intact cell compartments was based on a lysosome enrichment kit (Thermo Fisher scientific, No. 89839, USA). All fractionation steps and subsequent NP-protein corona isolation work was performed at 4 °C or on ice and all isolation buffers were added with protease inhibitor (Halt™ Protease Inhibitor Single-Use Cocktail EDTA-Free, Thermo Fisher scientific, No. 78425, USA) in order to minimize protein degradation.

About 3 x 10^8 RTgill-W1 cells were used for this work. After washing with 0.5 mM cysteine solution in PBS, cells treated with silver or untreated cells were harvested with trypsin digestion and centrifuged to pellet the cells as described above. Cell pellets were suspended in lysis buffer and lysed by sonication (LABSONIC® M, Sartorius AG, Germany), 90W, 10 sec for 2 times. Trypan blue staining was used to check the percentage of broken cells and ensure that at least 80% of cells were lysed. The cell lysate was centrifuged at 500 × g for 10 min to spin down unbroken cells and big fragments such as some remaining nuclei. The centrifuged lysate was loaded in a density gradient buffer with 15% to 30% Optiprep and ultra-centrifuged at 145,000 × g for 2 h (CENTRIKON T-2000, KONTRON Instruments, Switzerland). After centrifugation, several bands formed in the gradient. These bands were separated into 12 fractions according to density (F1-F12, low density - high density). Each fraction was mixed with 2-3 volumes of PBS to decrease fraction density and centrifuged at 18,000 × g for 30 minutes. Pellets were surface washed with 200 µL gradient dilution buffer and centrifuged at 18,000 × g for 30 minutes. Each pellet was tested for protein concentration, acid phosphatase activity, silver content and LysoTracker staining.

Protein assay was performed with bradford assay (Coomassie Plus™ (Bradford) Assay Kit, Thermo Fisher scientific, No.23236, USA). Acid phosphatase activity was checked with an acid phosphatase

assay kit (Sigma, CS0740, USA). Silver content was measured with ICP-MS as described above. Lysotracker (LysoTracker® Red DND-99, L7528, Invitrogen, United States) can stain intact acidic cell compartments such as late endosomes and lysosomes. LysoTracker staining was used to distinguish the endosome and lysosome in different fractions and check the intactness of the isolated cell compartments. After that, each pellet was frozen at -80 °C for subsequent work.

3.4.4   AgNP-Protein corona isolation

The protein corona was isolated in two different approaches. The first was the isolation after intact cells were exposed and subcellular fractions isolated as described above. The second approach was to fractionate cells as described above and expose those fraction extracts to AgNP.

<u>Isolation after exposure to AgNP or AgNO$_3$ of intact cells:</u> Selected cell compartment pellets were lysed in 200 μL 1% CHAPS (3-[(3-Cholamidopropyl)dimethylammonio]-1-propanesulfonate, Sigma, C5849) in TBS (Tris-NaCl) buffer by freezing at -80 °C and thawing at 25 °C for 3 times. After vortex-ing at maxim speed for 1 min, each sample was centrifuged at 500 × g for 10 minutes to remove larger debris. Supernatants were transferred to a new eppendorf protein LoBind tube and centri-fuged at 10,000 × g for 45 minutes. After removing the supernatant with the unbound proteins, 50 μL TBS was added to each pellet and centrifuged at 10,000 × g for 30 minutes for washing. The re-sulting supernatant was again removed; the pellet now contained the AgNP-protein corona. The same procedure was followed after AgNO$_3$ exposure as a control.

Isolation after exposure to AgNP of cell fraction extracts To confirm the proteins that bind to AgNP in intact cells, the same cell compartments were isolated and extracted from unexposed cells and subsequently incubated with AgNP. Thus, cell compartments pelleted from the same density gradi-ent fractions were lysed in the same way as above with the exception of CHAPS, which was de-creased to 0.25%. After centrifugation of the debris, supernatants (extracted proteins) were quanti-fied by Nanodrop 2000 (Thermo Fisher Scientific) at A280 and direct detect system (Merck Milli-pore). A concentration of 0.1 mg/mL AgNP and 1 mg/mL extract proteins were incubated for 2 h in 19 °C. Then, the same protocol as described above and below was applied to isolate and identify the AgNP-protein corona.

3.4.5   Protein identification

To detached proteins from the AgNP-protein corona, 35-50 μL TBS with 1% SDS and 50 mM DTT were added to each sample and incubated at 95 °C for 15 min. Samples were centrifuged at room

temperature for 15 min at 18,000 × g to pellet AgNP. Supernatants containing isolated proteins were collected and quantified by Nanodrop and direct detect system. All samples were stored at - 20 °C for further analysis.

In order to identify the corona proteins by mass spectrometry, recovered protein samples were run in SDS-PAGE for a short time to remove CHAPS. Protein bands were excised and digested in-gel with trypsin and analyzed by electrospray liquid chromatography mass spectrometry (LC MS/MS) with a label-free quantitative mass spectrometry approach. The MS raw data were analyzed by Scaffold 4 (version 4.3.4) and searched to rainbow trout protein recordings in NCBI.

3.4.6   Protein ontology analysis

After data evaluation of the MS spectra, >2-fold enriched proteins in AgNP samples were selected for further analysis. All selected proteins in rainbow trout were blasted to the human data base in NCBI in order to get the relative human protein GI number and a better protein functional annotation from human data than with fish. In this work, as we aimed to investigate the interaction of AgNP with aquatic organisms, the rainbow trout gill cell line was selected as model. However, the genome information for rainbow trout is still limited. Therefore, as long as analysis has to rely on NCBI database alone, certain proteins not recorded there are lost. This might, for example, explain why we did not find as many proteins from the endocytic pathways as previous work with human cell lines (Hofmann et al. 2014). All identified human proteins were forwarded to DAVID protein ontology analysis (Huang et al. 2008; http://david.abcc.ncifcrf.gov/). Functional annotation clustering was performed using DAVID ontology analysis. Cluster enrichment and *p*-values for each item in clusters were calculated.

3.5   Supplementary Material
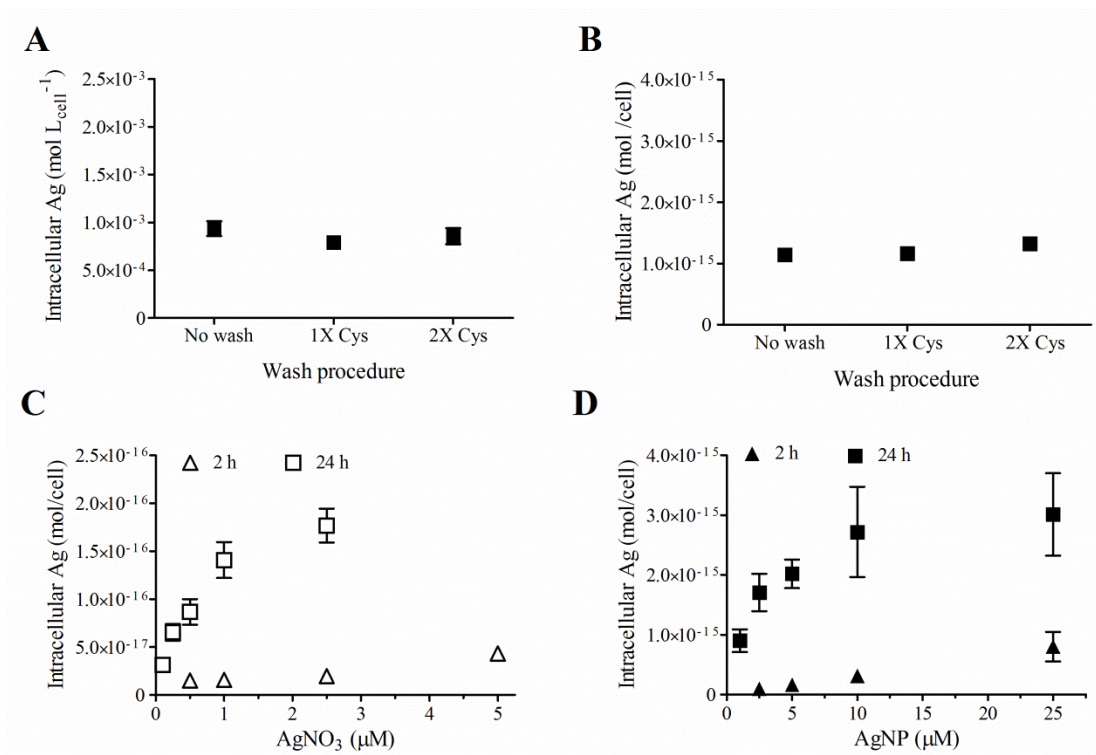
Figure S3.1 Intracellular silver content in RTgill-W1cells by ICP-MS.

Internal silver content were represented by (mol/L_{cell}, A) and (mol/cell, B) after different times 0.5 mM Cys solution washing. Internal silver (mol/cell) after exposed RTgill-W1 cells to $AgNO_3$ (C) and AgNP (D) for 2 h and 24 h.

A: Isolation of AgNP-protein corona from AgNP treated intact cells. (Intact S)
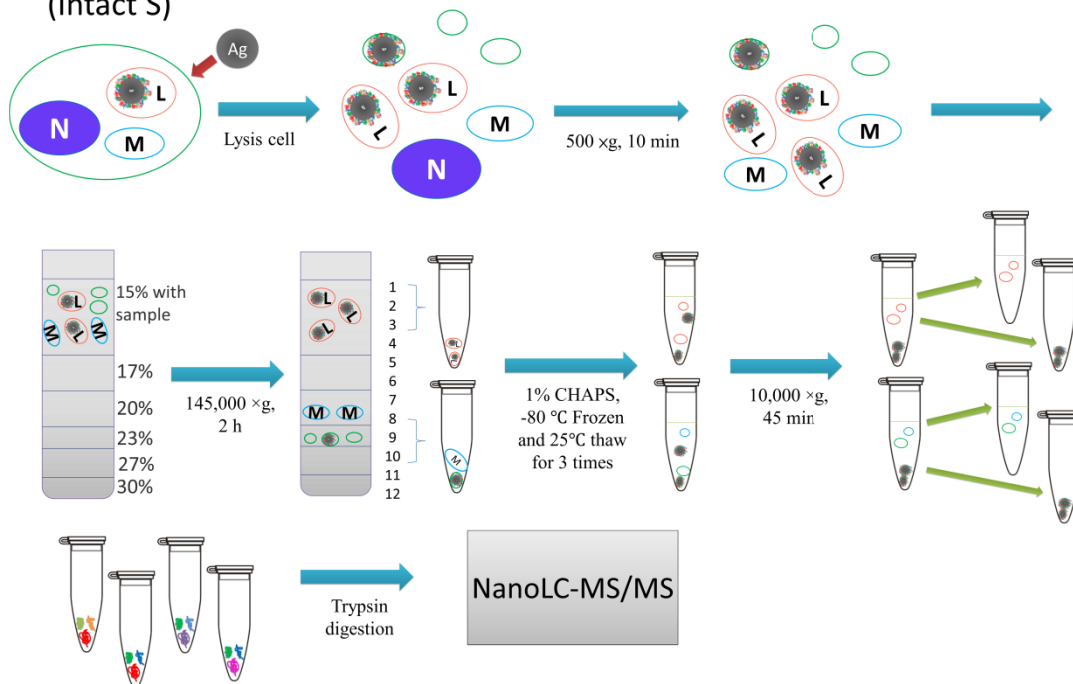
B: Isolation of AgNP-protein corona from AgNP-organelles extraction incubation. (Extra S)
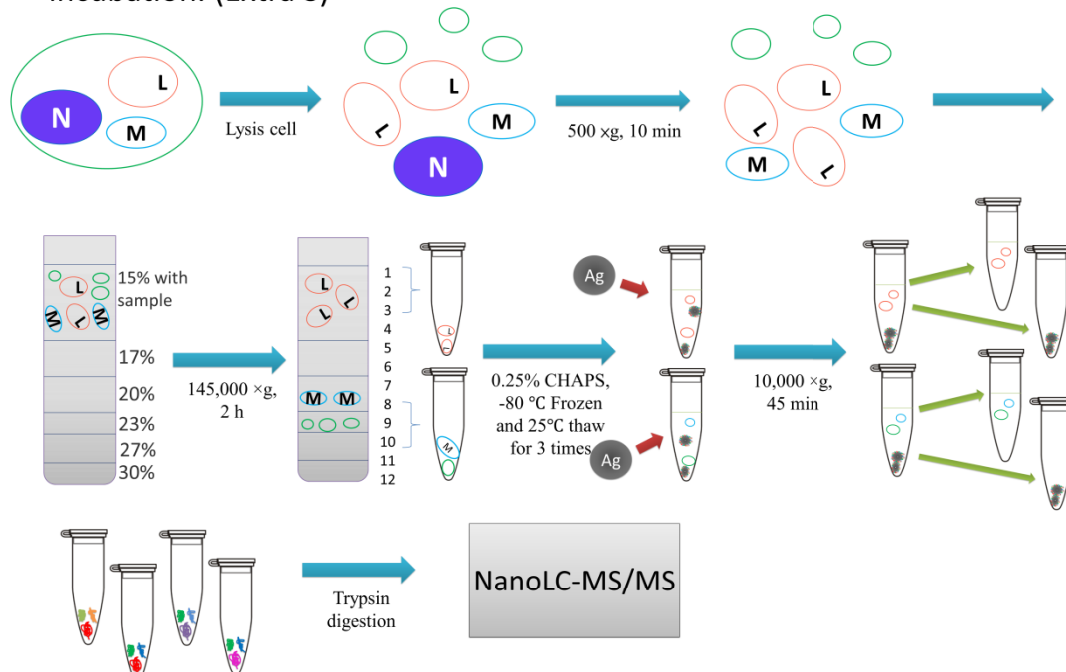
Figure S3.2 Schematic overview of AgNP-Protein corona separation workflow.

A: Separating AgNP-Protein from RTgill-W1 cells after exposed to 20 μM AgNP for 2 h. B: Separating AgNP-Protein from RTgill-W1 cell fractions extracts after incubating with AgNP. Density gradient buffer: 15-30% Optiprep buffer.
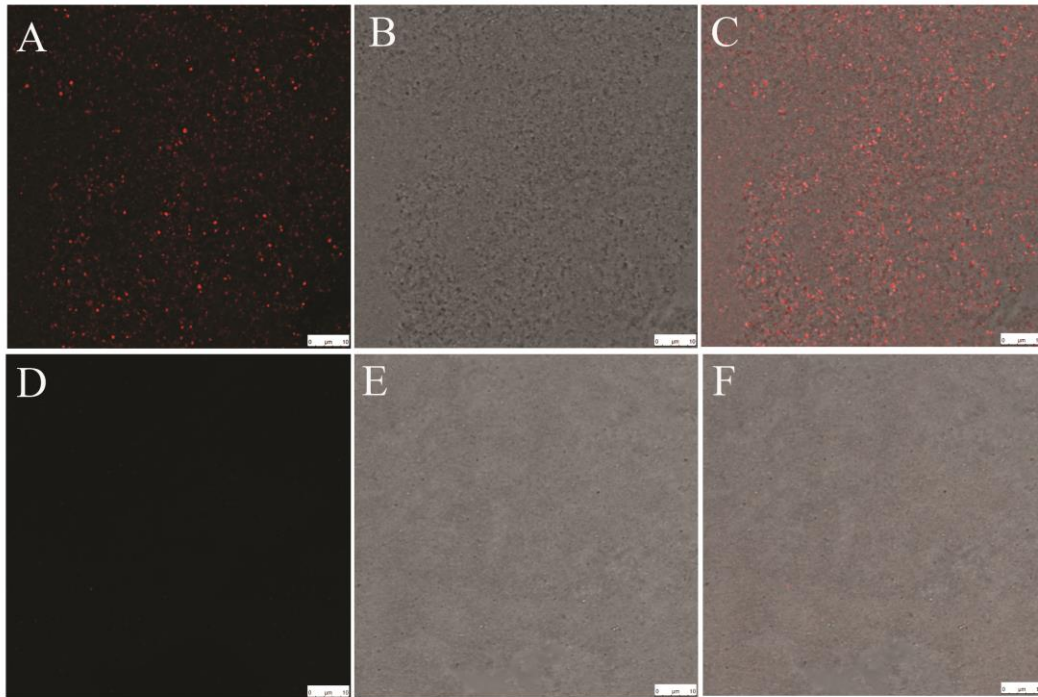
Figure S3.3 Cell organelles in fractions by LysoTracker staining.

A-C: samples from fraction 1-3, endosome-lysosome fractions. D-F: samples from fraction 8-10, cell membrane-mitochondria-nucleus fractions. A and D: LysoTacker red fluorescence images. B and E: Bright field images. C and F: merge fluorescence images with bright field image.

Table S3.1 Dissolution of AgNP in d-L15/ex after incubation with RTgill-W1 cells for 2 h.

Dissolved silver	25 uM	100 uM
Centrifugal Ultrafiltration	0.57%	0.26%
Ultra-centrifugation	6.87%	3.23%
Average	2.73%	

Table S3.2 Overview of proteins identified from AgNP-protein corona.

| Sample preparation | Proteins identified from AgNP-protein corona | | | Proteins identified from control |
	Intact S	Extra S	Intact S + Extra S	Extra S control
Total proteins from AgNP-protein corona	383	236	82	
Proteins included in GO analysis	266			
Proteins in cell membrane	34			
Proteins in lysosome	7			
Proteins in endocytosis pathway	9			
Proteins in vesicle-mediated transport pathway	29			
Proteins for cysteine abundances analysis		236		154

Table S3.3 DAVID ontology analysis of proteins.

All the proteins were enriched > 2-fold in the AgNP sample compared to the AgNO$_3$ sample. Total: 35 clusters.

Annotation Cluster 1	Enrichment Score: 18.75				
Category	Term	Count	p Value	Fold Enrich-rich-ment	Benja-mini
SP_PIR_KEYWORDS	mitochondrion	59	3.7E-25	5.13	6.6E-23
GOTERM_CC_FAT	GO:0044429~mitochondrial part	55	4.8E-23	4.94	1.7E-20
GOTERM_CC_FAT	GO:0005739~mitochondrion	71	2.6E-21	3.49	4.6E-19
GOTERM_CC_FAT	GO:0031967~organelle envelope	53	1.2E-20	4.57	1.5E-18
GOTERM_CC_FAT	GO:0031975~envelope	53	1.4E-20	4.56	1.3E-18
GOTERM_CC_FAT	GO:0031090~organelle membrane	70	1.9E-20	3.42	1.3E-18
GOTERM_CC_FAT	GO:0031966~mitochondrial membrane	41	7.8E-19	5.57	4.6E-17
GOTERM_CC_FAT	GO:0005740~mitochondrial envelope	42	1.0E-18	5.36	5.2E-17
GOTERM_CC_FAT	GO:0019866~organelle inner membrane	32	8.2E-14	5.20	3.6E-12
GOTERM_CC_FAT	GO:0005743~mitochondrial inner membrane	29	2.9E-12	5.07	1.0E-10
Annotation Cluster 2	Enrichment Score: 10.81				
Category	Term	Count	p Value	Fold Enrich-rich-ment	Benja-mini
SP_PIR_KEYWORDS	mitochondrion	59	3.7E-25	5.13	6.6E-23
GOTERM_CC_FAT	GO:0044429~mitochondrial part	55	4.8E-23	4.94	1.7E-20
GOTERM_CC_FAT	GO:0005739~mitochondrion	71	2.6E-21	3.49	4.6E-19
SP_PIR_KEYWORDS	transit peptide	34	2.2E-14	5.17	2.6E-12
UP_SEQ_FEATURE	transit peptide:Mitochondrion	32	5.3E-13	4.92	4.6E-10
GOTERM_CC_FAT	GO:0031980~mitochondrial lumen	22	1.5E-09	5.18	4.7E-08
GOTERM_CC_FAT	GO:0005759~mitochondrial matrix	22	1.5E-09	5.18	4.7E-08
GOTERM_CC_FAT	GO:0070013~intracellular organelle lumen	51	1.6E-03	1.53	1.6E-02
GOTERM_CC_FAT	GO:0031974~membrane-enclosed lumen	52	2.4E-03	1.50	2.2E-02
GOTERM_CC_FAT	GO:0043233~organelle lumen	51	2.6E-03	1.50	2.4E-02
GOTERM_CC_FAT	GO:0031981~nuclear lumen	23	8.7E-01	0.85	1.0E+00
Annotation Cluster 3	Enrichment Score: 7.04				
Category	Term	Count	p Value	Fold Enrich-rich-ment	Benja-mini
SP_PIR_KEYWORDS	nucleotide-binding	65	4.2E-14	2.79	3.0E-12
GOTERM_MF_FAT	GO:0000166~nucleotide binding	78	1.1E-11	2.14	1.4E-09
GOTERM_MF_FAT	GO:0017076~purine nucleotide binding	70	2.6E-11	2.25	2.7E-09
GOTERM_MF_FAT	GO:0032555~purine ribonucleotide binding	66	2.5E-10	2.21	2.2E-08
GOTERM_MF_FAT	GO:0032553~ribonucleotide binding	66	2.5E-10	2.21	2.2E-08
SP_PIR_KEYWORDS	atp-binding	40	5.8E-06	2.18	9.5E-05
GOTERM_MF_FAT	GO:0001883~purine nucleoside binding	50	6.2E-06	1.92	4.6E-04
GOTERM_MF_FAT	GO:0001882~nucleoside binding	50	7.4E-06	1.91	4.9E-04
GOTERM_MF_FAT	GO:0030554~adenyl nucleotide binding	48	2.0E-05	1.87	9.7E-04

Category	Term	Count	p Value	Fold Enrich-ment	Benja-mini
GOTERM_MF_FAT	GO:0005524~ATP binding	44	8.6E-05	1.83	3.5E-03
GOTERM_MF_FAT	GO:0032559~adenyl ribonucleotide binding	44	1.2E-04	1.81	4.1E-03
UP_SEQ_FEATURE	nucleotide phosphate-binding region:ATP	24	7.8E-03	1.79	3.6E-01
Annotation Cluster 4	**Enrichment Score: 6.58**				
Category	Term	Count	p Value	Fold Enrich-rich-ment	Benja-mini
SP_PIR_KEYWORDS	P-loop	19	3.0E-14	11.84	2.7E-12
SP_PIR_KEYWORDS	nucleotide binding	18	1.1E-13	12.16	6.4E-12
GOTERM_MF_FAT	GO:0005525~GTP binding	31	3.0E-13	5.13	1.6E-10
GOTERM_MF_FAT	GO:0019001~guanyl nucleotide binding	31	5.9E-13	4.99	1.6E-10
GOTERM_MF_FAT	GO:0032561~guanyl ribonucleotide binding	31	5.9E-13	4.99	1.6E-10
GOTERM_MF_FAT	GO:0003924~GTPase activity	23	3.5E-12	6.71	6.2E-10
SP_PIR_KEYWORDS	gtp-binding	26	5.1E-12	5.71	2.3E-10
SP_PIR_KEYWORDS	GTP binding	14	6.3E-12	15.11	2.5E-10
UP_SEQ_FEATURE	nucleotide phosphate-binding region:GTP	21	6.0E-09	5.11	2.6E-06
SP_PIR_KEYWORDS	prenylated cysteine	8	1.8E-08	25.15	4.5E-07
SP_PIR_KEYWORDS	prenylation	14	2.6E-07	6.49	5.8E-06
UP_SEQ_FEATURE	short sequence motif:Effector region	11	8.0E-07	8.32	2.3E-04
SP_PIR_KEYWORDS	methylation	16	1.4E-06	4.78	2.7E-05
UP_SEQ_FEATURE	lipid moiety-binding region:S-geranylgeranyl cysteine	11	1.5E-06	7.75	3.3E-04
INTERPRO	IPR005225:Small GTP-binding protein	14	2.0E-06	5.41	3.8E-04
GOTERM_BP_FAT	GO:0007264~small GTPase mediated signal transduction	19	5.0E-06	3.63	8.6E-04
INTERPRO	IPR001806:Ras GTPase	12	7.9E-06	5.74	1.1E-03
INTERPRO	IPR013753:Ras	11	2.4E-05	5.68	2.8E-03
SMART	SM00175:RAB	7	8.5E-05	9.47	3.7E-03
SP_PIR_KEYWORDS	lipoprotein	23	8.6E-05	2.59	1.2E-03
INTERPRO	IPR003579:Ras small GTPase, Rab type	7	3.5E-04	7.41	2.8E-02
BIOCARTA	h_rabPathway:Rab GTPases Mark Targets In The Endocytotic Machinery	5	5.2E-04	11.74	7.1E-02
SP_PIR_KEYWORDS	membrane trafficking	4	1.3E-03	18.08	1.3E-02
GOTERM_CC_FAT	GO:0009898~internal side of plasma membrane	15	2.4E-03	2.54	2.2E-02
GOTERM_BP_FAT	GO:0007242~intracellular signaling cascade	35	4.7E-03	1.62	1.3E-01
INTERPRO	IPR002078:RNA polymerase sigma factor 54, interaction	3	1.2E-02	17.61	2.8E-01
UP_SEQ_FEATURE	propeptide:Removed in mature form	7	1.0E-01	2.20	9.1E-01
GOTERM_CC_FAT	GO:0031225~anchored to membrane	5	5.9E-01	1.22	9.3E-01
Annotation Cluster 5	**Enrichment Score: 6.36**				
Category	Term	Count	p Value	Fold Enrich-rich-ment	Benja-mini
GOTERM_CC_FAT	GO:0042470~melanosome	18	5.1E-13	10.82	2.0E-11
GOTERM_CC_FAT	GO:0048770~pigment granule	18	5.1E-13	10.82	2.0E-11
GOTERM_CC_FAT	GO:0031410~cytoplasmic vesicle	27	1.6E-04	2.25	2.4E-03
GOTERM_CC_FAT	GO:0031982~vesicle	27	3.1E-04	2.16	3.8E-03

GOTERM_CC_FAT	GO:0016023~cytoplasmic membrane-bounded vesicle	23	6.2E-04	2.24	6.8E-03
GOTERM_CC_FAT	GO:0031988~membrane-bounded vesicle	23	9.4E-04	2.17	9.7E-03
Annotation Cluster 6	**Enrichment Score: 5.47**				
Category	Term	Count	*p* Value	Fold Enrich-ment	Benja-mini
INTERPRO	IPR016040:NAD(P)-binding domain	15	8.4E-08	6.46	4.9E-05
SP_PIR_KEYWORDS	nad	14	2.3E-06	5.36	4.1E-05
UP_SEQ_FEATURE	nucleotide phosphate-binding region:NAD	9	1.0E-05	8.51	1.5E-03
UP_SEQ_FEATURE	binding site:NAD	7	6.4E-05	10.06	7.9E-03
Annotation Cluster 7	**Enrichment Score: 5.37**				
Category	Term	Count	*p* Value	Fold Enrich-ment	Benja-mini
SP_PIR_KEYWORDS	mitochondrion outer membrane	12	2.9E-09	12.40	8.1E-08
GOTERM_CC_FAT	GO:0005741~mitochondrial outer membrane	12	8.4E-07	7.13	2.3E-05
GOTERM_CC_FAT	GO:0031968~organelle outer membrane	12	3.6E-06	6.17	8.4E-05
GOTERM_CC_FAT	GO:0019867~outer membrane	12	5.2E-06	5.94	1.1E-04
GOTERM_BP_FAT	GO:0007005~mitochondrion organization	7	3.1E-02	2.96	4.2E-01
Annotation Cluster 8	**Enrichment Score: 4.85**				
Category	Term	Count	*p* Value	Fold Enrich-ment	Benja-mini
SMART	SM00244:PHB	6	2.7E-07	38.09	2.4E-05
INTERPRO	IPR001107:Band 7 protein	6	9.8E-07	29.80	2.8E-04
PIR_SUPERFAMILY	PIRSF005651:membrane protease subunits, stomatin/prohibitin homologs	3	1.1E-02	18.11	6.1E-01
Annotation Cluster 9	**Enrichment Score: 4.77**				
Category	Term	Count	*p* Value	Fold Enrich-ment	Benja-mini
GOTERM_CC_FAT	GO:0005626~insoluble fraction	37	2.1E-06	2.36	5.3E-05
GOTERM_CC_FAT	GO:0000267~cell fraction	43	3.7E-06	2.12	8.1E-05
GOTERM_CC_FAT	GO:0005624~membrane fraction	35	6.6E-06	2.31	1.3E-04
GOTERM_CC_FAT	GO:0005792~microsome	15	1.4E-04	3.38	2.3E-03
GOTERM_CC_FAT	GO:0042598~vesicular fraction	15	1.9E-04	3.29	2.8E-03
Annotation Cluster 10	**Enrichment Score: 4.51**				
Category	Term	Count	*p* Value	Fold Enrich-ment	Benja-mini
GOTERM_BP_FAT	GO:0006091~generation of precursor metabo-lites and energy	24	4.0E-09	4.47	6.2E-06
GOTERM_BP_FAT	GO:0009060~aerobic respiration	9	1.0E-07	14.99	5.2E-05
SP_PIR_KEYWORDS	tricarboxylic acid cycle	7	2.9E-07	24.10	5.9E-06
GOTERM_BP_FAT	GO:0045333~cellular respiration	12	7.8E-07	7.21	2.4E-04
GOTERM_BP_FAT	GO:0046356~acetyl-CoA catabolic process	7	1.8E-06	17.75	4.1E-04
GOTERM_BP_FAT	GO:0006099~tricarboxylic acid cycle	7	1.8E-06	17.75	4.1E-04

GOTERM_BP_FAT	GO:0009109~coenzyme catabolic process	7	4.0E-06	15.70	7.7E-04
GOTERM_BP_FAT	GO:0015980~energy derivation by oxidation of organic compounds	13	6.6E-06	5.26	1.0E-03
UP_SEQ_FEATURE	nucleotide phosphate-binding region:NAD	9	1.0E-05	8.51	1.5E-03
GOTERM_BP_FAT	GO:0051187~cofactor catabolic process	7	1.2E-05	13.17	1.5E-03
GOTERM_BP_FAT	GO:0006084~acetyl-CoA metabolic process	7	1.2E-05	13.17	1.5E-03
GOTERM_BP_FAT	GO:0043648~dicarboxylic acid metabolic process	7	2.1E-05	12.01	2.3E-03
KEGG_PATHWAY	hsa00020:Citrate cycle (TCA cycle)	7	8.7E-05	9.11	1.2E-02
GOTERM_BP_FAT	GO:0051186~cofactor metabolic process	13	1.3E-04	3.89	1.3E-02
GOTERM_BP_FAT	GO:0006734~NADH metabolic process	4	2.6E-04	29.16	2.2E-02
GOTERM_BP_FAT	GO:0006732~coenzyme metabolic process	11	3.0E-04	4.19	2.4E-02
GOTERM_BP_FAT	GO:0043603~cellular amide metabolic process	7	3.7E-04	7.29	2.8E-02
GOTERM_BP_FAT	GO:0006103~2-oxoglutarate metabolic process	4	5.4E-04	23.32	3.6E-02
GOTERM_BP_FAT	GO:0046496~nicotinamide nucleotide metabolic process	6	5.6E-04	8.75	3.5E-02
GOTERM_BP_FAT	GO:0006769~nicotinamide metabolic process	6	5.6E-04	8.75	3.5E-02
GOTERM_BP_FAT	GO:0009820~alkaloid metabolic process	6	6.3E-04	8.53	3.8E-02
GOTERM_BP_FAT	GO:0019362~pyridine nucleotide metabolic process	6	7.1E-04	8.33	4.1E-02
GOTERM_BP_FAT	GO:0019674~NAD metabolic process	5	7.9E-04	11.66	4.3E-02
GOTERM_BP_FAT	GO:0006733~oxidoreduction coenzyme metabolic process	6	1.9E-03	6.73	7.2E-02
GOTERM_BP_FAT	GO:0019748~secondary metabolic process	7	2.3E-03	5.17	8.1E-02
Annotation Cluster 11	**Enrichment Score: 4.46**				
Category	Term	Count	*P Value*	Fold Enrichment	Benjamini
SP_PIR_KEYWORDS	oxidoreductase	33	1.1E-11	4.25	4.0E-10
GOTERM_BP_FAT	GO:0055114~oxidation reduction	33	4.2E-08	3.01	3.2E-05
INTERPRO	IPR016040:NAD(P)-binding domain	15	8.4E-08	6.46	4.9E-05
UP_SEQ_FEATURE	binding site:Substrate	17	4.3E-06	4.11	7.4E-04
SP_PIR_KEYWORDS	nadp	10	3.2E-04	4.64	4.0E-03
INTERPRO	IPR002347:Glucose/ribitol dehydrogenase	6	1.3E-03	7.31	6.7E-02
INTERPRO	IPR002198:Short-chain dehydrogenase/reductase SDR	6	2.1E-03	6.57	9.0E-02
PIR_SUPERFAMILY	PIRSF000092:short-chain dehydrogenase	4	3.1E-03	13.00	4.1E-01
UP_SEQ_FEATURE	active site:Proton acceptor	15	7.7E-02	1.64	8.8E-01
UP_SEQ_FEATURE	nucleotide phosphate-binding region:NADP	4	7.8E-02	3.99	8.7E-01
Annotation Cluster 12	**Enrichment Score: 4.35**				
Category	Term	Count	*P Value*	Fold Enrichment	Benjamini
GOTERM_MF_FAT	GO:0050662~coenzyme binding	14	7.6E-06	4.76	4.4E-04
GOTERM_MF_FAT	GO:0048037~cofactor binding	16	1.3E-05	3.95	6.8E-04
GOTERM_MF_FAT	GO:0051287~NAD or NADH binding	6	9.3E-04	7.85	2.6E-02
Annotation Cluster 13	**Enrichment Score: 3.49**				
Category	Term	Count	*P Value*	Fold Enrich-	Benjamini

Category	Term	Count	P Value	Fold Enrichment	Benjamini
				rich-ment	
SP_PIR_KEYWORDS	tricarboxylic acid cycle	7	2.9E-07	24.10	5.9E-06
GOTERM_BP_FAT	GO:0006099~tricarboxylic acid cycle	7	1.8E-06	17.75	4.1E-04
GOTERM_BP_FAT	GO:0046356~acetyl-CoA catabolic process	7	1.8E-06	17.75	4.1E-04
GOTERM_BP_FAT	GO:0009109~coenzyme catabolic process	7	4.0E-06	15.70	7.7E-04
GOTERM_BP_FAT	GO:0006084~acetyl-CoA metabolic process	7	1.2E-05	13.17	1.5E-03
GOTERM_BP_FAT	GO:0051187~cofactor catabolic process	7	1.2E-05	13.17	1.5E-03
KEGG_PATHWAY	hsa00020:Citrate cycle (TCA cycle)	7	8.7E-05	9.11	1.2E-02
GOTERM_MF_FAT	GO:0051287~NAD or NADH binding	6	9.3E-04	7.85	2.6E-02
UP_SEQ_FEATURE	site:Critical for catalysis	3	1.9E-03	43.11	1.4E-01
INTERPRO	IPR019818:Isocitrate/isopropylmalate dehydrogenase, conserved site	3	2.3E-03	38.74	8.5E-02
GOTERM_MF_FAT	GO:0004448~isocitrate dehydrogenase activity	3	2.5E-03	36.92	6.4E-02
GOTERM_BP_FAT	GO:0006102~isocitrate metabolic process	3	2.8E-03	34.99	9.0E-02
INTERPRO	IPR001804:Isocitrate/isopropylmalate dehydrogenase	3	3.4E-03	32.28	1.2E-01
UP_SEQ_FEATURE	metal ion-binding site:Magnesium or manganese	3	2.3E-02	12.68	5.9E-01
SP_PIR_KEYWORDS	manganese	4	3.5E-01	1.90	7.8E-01
GOTERM_MF_FAT	GO:0030145~manganese ion binding	4	4.6E-01	1.60	9.9E-01
Annotation Cluster 14	**Enrichment Score: 3.24**				
Category	Term	Count	P Value	Fold Enrichment	Benjamini
GOTERM_CC_FAT	GO:0012505~endomembrane system	32	5.4E-05	2.19	9.9E-04
GOTERM_CC_FAT	GO:0005783~endoplasmic reticulum	35	2.1E-04	1.95	2.9E-03
GOTERM_CC_FAT	GO:0044432~endoplasmic reticulum part	18	2.7E-04	2.77	3.4E-03
SP_PIR_KEYWORDS	endoplasmic reticulum	23	3.8E-04	2.33	4.4E-03
GOTERM_CC_FAT	GO:0005789~endoplasmic reticulum membrane	13	4.6E-03	2.58	3.8E-02
GOTERM_CC_FAT	GO:0042175~nuclear envelope-endoplasmic reticulum network	13	7.0E-03	2.45	5.1E-02
Annotation Cluster 15	**Enrichment Score: 3.14**				
Category	Term	Count	P Value	Fold Enrichment	Benjamini
GOTERM_CC_FAT	GO:0030062~mitochondrial tricarboxylic acid cycle enzyme complex	4	1.2E-04	35.65	2.0E-03
GOTERM_CC_FAT	GO:0045239~tricarboxylic acid cycle enzyme complex	4	2.1E-04	30.56	2.8E-03
GOTERM_CC_FAT	GO:0045240~dihydrolipoyl dehydrogenase complex	3	3.3E-03	32.09	2.8E-02
GOTERM_CC_FAT	GO:0005947~mitochondrial alpha-ketoglutarate dehydrogenase complex	3	3.3E-03	32.09	2.8E-02
Annotation Cluster 16	**Enrichment Score: 2.89**				
Category	Term	Count	P Value	Fold Enrichment	Benjamini
GOTERM_BP_FAT	GO:0046395~carboxylic acid catabolic process	10	1.2E-04	5.25	1.2E-02
GOTERM_BP_FAT	GO:0016054~organic acid catabolic process	10	1.2E-04	5.25	1.2E-02

Category	Term	Count	P Value	Fold Enrichment	Benjamini
GOTERM_BP_FAT	GO:0009083~branched chain family amino acid catabolic process	4	7.3E-04	21.20	4.1E-02
GOTERM_BP_FAT	GO:0009081~branched chain family amino acid metabolic process	4	2.3E-03	14.58	7.9E-02
KEGG_PATHWAY	hsa00280:Valine, leucine and isoleucine degradation	6	4.2E-03	5.50	6.3E-02
GOTERM_BP_FAT	GO:0009063~cellular amino acid catabolic process	6	6.1E-03	5.15	1.5E-01
GOTERM_BP_FAT	GO:0009310~amine catabolic process	6	1.1E-02	4.49	2.2E-01
Annotation Cluster 17	**Enrichment Score: 2.87**				
Category	Term	Count	P Value	Fold Enrichment	Benjamini
SP_PIR_KEYWORDS	transport	53	1.8E-08	2.29	4.4E-07
SP_PIR_KEYWORDS	protein transport	24	2.9E-07	3.58	6.1E-06
GOTERM_BP_FAT	GO:0016192~vesicle-mediated transport	29	5.9E-07	2.94	2.3E-04
GOTERM_BP_FAT	GO:0008104~protein localization	37	8.9E-07	2.45	2.3E-04
GOTERM_BP_FAT	GO:0045184~establishment of protein localization	32	7.2E-06	2.43	1.0E-03
GOTERM_BP_FAT	GO:0015031~protein transport	31	1.6E-05	2.37	1.9E-03
GOTERM_BP_FAT	GO:0046907~intracellular transport	26	1.5E-04	2.31	1.3E-02
GOTERM_BP_FAT	GO:0034613~cellular protein localization	17	1.9E-03	2.41	7.3E-02
GOTERM_BP_FAT	GO:0070727~cellular macromolecule localization	17	2.0E-03	2.39	7.5E-02
GOTERM_BP_FAT	GO:0006605~protein targeting	10	1.2E-02	2.71	2.3E-01
GOTERM_BP_FAT	GO:0006886~intracellular protein transport	14	1.2E-02	2.18	2.3E-01
GOTERM_BP_FAT	GO:0033365~protein localization in organelle	8	1.3E-02	3.20	2.4E-01
GOTERM_BP_FAT	GO:0017038~protein import	7	2.5E-02	3.12	3.7E-01
GOTERM_BP_FAT	GO:0006839~mitochondrial transport	5	3.0E-02	4.23	4.2E-01
GOTERM_BP_FAT	GO:0051170~nuclear import	5	6.4E-02	3.31	6.0E-01
GOTERM_BP_FAT	GO:0006626~protein targeting to mitochondrion	3	1.1E-01	5.15	7.3E-01
GOTERM_BP_FAT	GO:0070585~protein localization in mitochondrion	3	1.1E-01	5.15	7.3E-01
GOTERM_BP_FAT	GO:0006606~protein import into nucleus	4	1.8E-01	2.71	8.5E-01
GOTERM_BP_FAT	GO:0034504~protein localization in nucleus	4	2.2E-01	2.48	8.8E-01
GOTERM_BP_FAT	GO:0006913~nucleocytoplasmic transport	5	2.8E-01	1.87	9.1E-01
GOTERM_BP_FAT	GO:0051169~nuclear transport	5	2.8E-01	1.85	9.2E-01
Annotation Cluster 18	**Enrichment Score: 2.70**				
Category	Term	Count	P Value	Fold Enrichment	Benjamini
UP_SEQ_FEATURE	repeat:Solcar 1	7	9.9E-05	9.31	1.1E-02
UP_SEQ_FEATURE	repeat:Solcar 2	7	9.9E-05	9.31	1.1E-02
INTERPRO	IPR018108:Mitochondrial substrate/solute carrier	7	2.2E-04	8.07	2.1E-02
UP_SEQ_FEATURE	repeat:Solcar 3	6	6.9E-04	8.45	6.4E-02
INTERPRO	IPR001993:Mitochondrial substrate carrier	6	1.2E-03	7.45	6.7E-02
GOTERM_BP_FAT	GO:0055085~transmembrane transport	20	4.1E-03	2.05	1.2E-01
INTERPRO	IPR002067:Mitochondrial carrier protein	4	8.1E-03	9.57	2.1E-01

INTERPRO	IPR002113:Adenine nucleotide translocator 1	3	6.0E-02	7.45	6.8E-01
PIR_SUPERFAMILY	PIRSF002458:ADP,ATP carrier protein	3	1.6E-01	4.23	1.0E+00
Annotation Cluster 19	**Enrichment Score: 2.60**				
Category	Term	Count	*P Value*	Fold Enrich-rich-ment	Benja-mini
GOTERM_CC_FAT	GO:0005856~cytoskeleton	45	2.5E-04	1.74	3.2E-03
GOTERM_CC_FAT	GO:0043232~intracellular non-membrane-bounded organelle	65	8.2E-03	1.34	5.9E-02
GOTERM_CC_FAT	GO:0043228~non-membrane-bounded orga-nelle	65	8.2E-03	1.34	5.9E-02
Annotation Cluster 20	**Enrichment Score: 2.54**				
Category	Term	Count	P Value	Fold Enrich-rich-ment	Benja-mini
SP_PIR_KEYWORDS	mitochondrion inner membrane	18	1.6E-09	6.74	4.7E-08
GOTERM_CC_FAT	GO:0044455~mitochondrial membrane part	14	5.6E-07	5.99	1.6E-05
GOTERM_MF_FAT	GO:0015077~monovalent inorganic cation transmembrane transporter activity	10	4.6E-05	5.92	2.0E-03
GOTERM_MF_FAT	GO:0015078~hydrogen ion transmembrane transporter activity	9	1.0E-04	6.15	3.8E-03
GOTERM_MF_FAT	GO:0022890~inorganic cation transmembrane transporter activity	11	1.7E-04	4.48	5.6E-03
KEGG_PATHWAY	hsa05012:Parkinson's disease	11	1.1E-03	3.47	5.0E-02
KEGG_PATHWAY	hsa00190:Oxidative phosphorylation	11	1.2E-03	3.41	3.4E-02
SP_PIR_KEYWORDS	oxidative phosphorylation	5	1.3E-03	10.33	1.3E-02
GOTERM_BP_FAT	GO:0006119~oxidative phosphorylation	8	1.4E-03	4.76	6.1E-02
KEGG_PATHWAY	hsa04260:Cardiac muscle contraction	8	2.8E-03	4.14	4.9E-02
SP_PIR_KEYWORDS	respiratory chain	6	3.0E-03	6.11	2.5E-02
KEGG_PATHWAY	hsa05016:Huntington's disease	12	4.5E-03	2.69	5.6E-02
SP_PIR_KEYWORDS	membrane-associated complex	4	9.5E-03	9.04	6.5E-02
GOTERM_MF_FAT	GO:0004129~cytochrome-c oxidase activity	4	1.0E-02	8.79	1.6E-01
GOTERM_MF_FAT	GO:0015002~heme-copper terminal oxidase activity	4	1.0E-02	8.79	1.6E-01
GOTERM_MF_FAT	GO:0016676~oxidoreductase activity, acting on heme group of donors, oxygen as acceptor	4	1.0E-02	8.79	1.6E-01
GOTERM_MF_FAT	GO:0016675~oxidoreductase activity, acting on heme group of donors	4	1.0E-02	8.79	1.6E-01
GOTERM_CC_FAT	GO:0070469~respiratory chain	6	1.3E-02	4.28	8.4E-02
KEGG_PATHWAY	hsa05010:Alzheimer's disease	10	1.8E-02	2.48	1.7E-01
SP_PIR_KEYWORDS	mitochondrial inner membrane	3	2.8E-02	11.42	1.5E-01
GOTERM_CC_FAT	GO:0005746~mitochondrial respiratory chain	5	3.1E-02	4.18	1.6E-01
GOTERM_BP_FAT	GO:0022900~electron transport chain	6	4.6E-02	3.07	5.2E-01
SP_PIR_KEYWORDS	electron transport	5	5.0E-02	3.62	2.2E-01
GOTERM_BP_FAT	GO:0022904~respiratory electron transport chain	4	9.6E-02	3.64	7.0E-01
SP_PIR_KEYWORDS	electron transfer	3	1.5E-01	4.34	4.9E-01
GOTERM_BP_FAT	GO:0042775~mitochondrial ATP synthesis coupled electron transport	3	2.5E-01	3.12	9.0E-01
GOTERM_BP_FAT	GO:0042773~ATP synthesis coupled electron transport	3	2.5E-01	3.12	9.0E-01

Annotation Cluster 21	Enrichment Score: 2.28				
Category	Term	Count	*P Value*	Fold Enrich-rich-ment	Benja-mini
SP_PIR_KEYWORDS	cytoskeleton	21	5.4E-04	2.39	5.9E-03
SP_PIR_KEYWORDS	actin binding	5	2.2E-03	9.04	1.9E-02
GOTERM_MF_FAT	GO:0008092~cytoskeletal protein binding	18	3.4E-03	2.20	8.2E-02
SP_PIR_KEYWORDS	actin-binding	10	7.4E-03	2.93	5.4E-02
SMART	SM00033:CH	5	9.8E-03	5.90	1.3E-01
GOTERM_MF_FAT	GO:0003779~actin binding	12	1.7E-02	2.26	2.3E-01
INTERPRO	IPR001715:Calponin-like actin-binding	5	2.3E-02	4.61	4.3E-01
Annotation Cluster 22	Enrichment Score: 2.21				
Category	Term	Count	*P Value*	Fold Enrich-rich-ment	Benja-mini
GOTERM_BP_FAT	GO:0030036~actin cytoskeleton organization	13	5.1E-04	3.35	3.5E-02
GOTERM_BP_FAT	GO:0030029~actin filament-based process	13	9.1E-04	3.15	4.6E-02
GOTERM_BP_FAT	GO:0007015~actin filament organization	6	7.7E-03	4.86	1.7E-01
GOTERM_BP_FAT	GO:0007010~cytoskeleton organization	16	8.0E-03	2.14	1.8E-01
GOTERM_CC_FAT	GO:0005925~focal adhesion	6	4.2E-02	3.15	2.0E-01
GOTERM_CC_FAT	GO:0005924~cell-substrate adherens junction	6	4.8E-02	3.03	2.2E-01
Annotation Cluster 23	Enrichment Score: 2.16				
Category	Term	Count	*P Value*	Fold Enrich-rich-ment	Benja-mini
GOTERM_MF_FAT	GO:0004579~dolichyl-diphosphooligosaccharide-protein glycotrans-ferase activity	4	3.3E-04	27.35	1.0E-02
GOTERM_MF_FAT	GO:0004576~oligosaccharyl transferase activity	4	4.6E-04	24.61	1.3E-02
GOTERM_BP_FAT	GO:0018279~protein amino acid N-linked glycosylation via asparagine	4	5.4E-04	23.32	3.6E-02
GOTERM_BP_FAT	GO:0018196~peptidyl-asparagine modification	4	5.4E-04	23.32	3.6E-02
GOTERM_CC_FAT	GO:0008250~oligosaccharyltransferase com-plex	4	6.9E-04	21.39	7.4E-03
GOTERM_CC_FAT	GO:0005789~endoplasmic reticulum mem-brane	13	4.6E-03	2.58	3.8E-02
GOTERM_BP_FAT	GO:0006487~protein amino acid N-linked glycosylation	5	6.6E-03	6.63	1.6E-01
GOTERM_CC_FAT	GO:0042175~nuclear envelope-endoplasmic reticulum network	13	7.0E-03	2.45	5.1E-02
GOTERM_BP_FAT	GO:0009101~glycoprotein biosynthetic pro-cess	7	5.4E-02	2.58	5.6E-01
GOTERM_BP_FAT	GO:0009100~glycoprotein metabolic process	8	5.9E-02	2.31	5.9E-01
GOTERM_BP_FAT	GO:0006486~protein amino acid glycosylation	6	6.8E-02	2.73	6.2E-01
GOTERM_BP_FAT	GO:0070085~glycosylation	6	6.8E-02	2.73	6.2E-01
GOTERM_BP_FAT	GO:0043413~biopolymer glycosylation	6	6.8E-02	2.73	6.2E-01
KEGG_PATHWAY	hsa00510:N-Glycan biosynthesis	4	1.0E-01	3.51	5.2E-01
Annotation Cluster 24	Enrichment Score: 2.14				
Category	Term	Count	*P Value*	Fold Enrich-	Benja-mini

				rich-ment	
SP_PIR_KEYWORDS	membrane	138	6.6E-11	1.60	2.2E-09
SP_PIR_KEYWORDS	transmembrane	82	4.7E-02	1.19	2.1E-01
UP_SEQ_FEATURE	transmembrane region	80	7.2E-02	1.17	8.9E-01
GOTERM_CC_FAT	GO:0031224~intrinsic to membrane	96	8.4E-01	0.94	9.9E-01
UP_SEQ_FEATURE	topological domain:Cytoplasmic	42	8.5E-01	0.89	1.0E+00
GOTERM_CC_FAT	GO:0016021~integral to membrane	91	8.9E-01	0.92	1.0E+00
Annotation Cluster 25	**Enrichment Score: 2.05**				
Category	Term	Count	*P Value*	Fold Enrich-rich-ment	Benja-mini
GOTERM_BP_FAT	GO:0046395~carboxylic acid catabolic process	10	1.2E-04	5.25	1.2E-02
GOTERM_BP_FAT	GO:0016054~organic acid catabolic process	10	1.2E-04	5.25	1.2E-02
GOTERM_BP_FAT	GO:0030258~lipid modification	7	1.1E-03	5.92	5.3E-02
GOTERM_BP_FAT	GO:0006635~fatty acid beta-oxidation	4	1.2E-02	8.33	2.3E-01
GOTERM_BP_FAT	GO:0006631~fatty acid metabolic process	9	2.1E-02	2.65	3.4E-01
GOTERM_BP_FAT	GO:0009062~fatty acid catabolic process	4	2.3E-02	6.48	3.6E-01
GOTERM_BP_FAT	GO:0034440~lipid oxidation	4	2.9E-02	5.98	4.1E-01
GOTERM_BP_FAT	GO:0019395~fatty acid oxidation	4	2.9E-02	5.98	4.1E-01
GOTERM_BP_FAT	GO:0044242~cellular lipid catabolic process	4	1.4E-01	3.07	7.9E-01
GOTERM_BP_FAT	GO:0016042~lipid catabolic process	5	3.4E-01	1.69	9.4E-01
Annotation Cluster 26	**Enrichment Score: 2.04**				
Category	Term	Count	*P Value*	Fold Enrich-rich-ment	Benja-mini
GOTERM_CC_FAT	GO:0032592~integral to mitochondrial mem-brane	4	1.2E-03	17.83	1.2E-02
GOTERM_CC_FAT	GO:0031307~integral to mitochondrial outer membrane	3	4.9E-03	26.74	4.0E-02
GOTERM_CC_FAT	GO:0031306~intrinsic to mitochondrial outer membrane	3	6.8E-03	22.92	5.2E-02
GOTERM_CC_FAT	GO:0031301~integral to organelle membrane	7	2.7E-02	3.04	1.4E-01
GOTERM_CC_FAT	GO:0031300~intrinsic to organelle membrane	7	5.5E-02	2.56	2.4E-01
Annotation Cluster 27	**Enrichment Score: 2.03**				
Category	Term	Count	*P Value*	Fold Enrich-rich-ment	Benja-mini
GOTERM_MF_FAT	GO:0015077~monovalent inorganic cation transmembrane transporter activity	10	4.6E-05	5.92	2.0E-03
GOTERM_MF_FAT	GO:0015078~hydrogen ion transmembrane transporter activity	9	1.0E-04	6.15	3.8E-03
GOTERM_MF_FAT	GO:0022890~inorganic cation transmembrane transporter activity	11	1.7E-04	4.48	5.6E-03
GOTERM_BP_FAT	GO:0009141~nucleoside triphosphate meta-bolic process	10	4.1E-04	4.45	3.0E-02
GOTERM_BP_FAT	GO:0009205~purine ribonucleoside triphos-phate metabolic process	9	8.8E-04	4.49	4.6E-02
GOTERM_BP_FAT	GO:0009199~ribonucleoside triphosphate metabolic process	9	9.3E-04	4.45	4.5E-02
GOTERM_BP_FAT	GO:0009144~purine nucleoside triphosphate metabolic process	9	1.2E-03	4.30	5.3E-02

KEGG PATHWAY	hsa00190:Oxidative phosphorylation	11	1.2E-03	3.41	3.4E-02
GOTERM_BP_FAT	GO:0006163~purine nucleotide metabolic process	11	1.4E-03	3.45	6.0E-02
GOTERM_BP_FAT	GO:0006119~oxidative phosphorylation	8	1.4E-03	4.76	6.1E-02
GOTERM_BP_FAT	GO:0009206~purine ribonucleoside triphosphate biosynthetic process	8	1.4E-03	4.76	6.1E-02
GOTERM_BP_FAT	GO:0009145~purine nucleoside triphosphate biosynthetic process	8	1.5E-03	4.71	6.3E-02
GOTERM_BP_FAT	GO:0009201~ribonucleoside triphosphate biosynthetic process	8	1.5E-03	4.71	6.3E-02
GOTERM_BP_FAT	GO:0009142~nucleoside triphosphate biosynthetic process	8	1.8E-03	4.57	7.3E-02
GOTERM_BP_FAT	GO:0046034~ATP metabolic process	8	2.1E-03	4.44	7.7E-02
GOTERM_BP_FAT	GO:0009150~purine ribonucleotide metabolic process	9	2.5E-03	3.80	8.3E-02
GOTERM_BP_FAT	GO:0009259~ribonucleotide metabolic process	9	3.7E-03	3.57	1.1E-01
GOTERM_BP_FAT	GO:0006164~purine nucleotide biosynthetic process	9	3.9E-03	3.55	1.2E-01
GOTERM_BP_FAT	GO:0009152~purine ribonucleotide biosynthetic process	8	3.9E-03	3.99	1.1E-01
GOTERM_BP_FAT	GO:0006754~ATP biosynthetic process	7	4.2E-03	4.59	1.2E-01
GOTERM_BP_FAT	GO:0009260~ribonucleotide biosynthetic process	8	5.4E-03	3.76	1.4E-01
GOTERM_MF_FAT	GO:0042625~ATPase activity, coupled to transmembrane movement of ions	6	6.9E-03	4.99	1.4E-01
GOTERM_MF_FAT	GO:0042626~ATPase activity, coupled to transmembrane movement of substances	7	8.5E-03	3.95	1.6E-01
GOTERM_MF_FAT	GO:0043492~ATPase activity, coupled to movement of substances	7	8.9E-03	3.92	1.6E-01
GOTERM_MF_FAT	GO:0016820~hydrolase activity, acting on acid anhydrides, catalyzing transmembrane movement of substances	7	9.3E-03	3.88	1.6E-01
SP_PIR_KEYWORDS	atp synthesis	3	1.3E-02	16.69	8.6E-02
GOTERM_MF_FAT	GO:0015399~primary active transmembrane transporter activity	7	1.4E-02	3.53	2.1E-01
GOTERM_MF_FAT	GO:0015405~P-P-bond-hydrolysis-driven transmembrane transporter activity	7	1.4E-02	3.53	2.1E-01
GOTERM_BP_FAT	GO:0009165~nucleotide biosynthetic process	9	1.5E-02	2.82	2.6E-01
GOTERM_BP_FAT	GO:0034404~nucleobase, nucleoside and nucleotide biosynthetic process	9	1.8E-02	2.72	3.0E-01
GOTERM_BP_FAT	GO:0034654~nucleobase, nucleoside, nucleotide and nucleic acid biosynthetic process	9	1.8E-02	2.72	3.0E-01
GOTERM_MF_FAT	GO:0019829~cation-transporting ATPase activity	4	2.0E-02	6.84	2.6E-01
GOTERM_MF_FAT	GO:0016887~ATPase activity	12	2.0E-02	2.21	2.6E-01
GOTERM_BP_FAT	GO:0044271~nitrogen compound biosynthetic process	12	2.4E-02	2.15	3.6E-01
GOTERM_MF_FAT	GO:0046933~hydrogen ion transporting ATP synthase activity, rotational mechanism	3	2.7E-02	11.54	3.2E-01
SP_PIR_KEYWORDS	Hydrogen ion transport	4	2.8E-02	6.03	1.5E-01
GOTERM_BP_FAT	GO:0015986~ATP synthesis coupled proton transport	4	3.1E-02	5.83	4.2E-01
GOTERM_BP_FAT	GO:0015985~energy coupled proton transport, down electrochemical gradient	4	3.1E-02	5.83	4.2E-01
GOTERM_MF_FAT	GO:0042623~ATPase activity, coupled	10	3.3E-02	2.26	3.5E-01
GOTERM_CC_FAT	GO:0033178~proton-transporting two-sector ATPase complex, catalytic domain	3	4.3E-02	8.91	2.0E-01

Category	Term	Count	P Value	Fold Enrichment	Benjamini
GOTERM_CC_FAT	GO:0005753~mitochondrial proton-transporting ATP synthase complex	3	4.8E-02	8.44	2.2E-01
GOTERM_BP_FAT	GO:0034220~ion transmembrane transport	4	5.1E-02	4.76	5.4E-01
GOTERM_CC_FAT	GO:0016469~proton-transporting two-sector ATPase complex	4	5.1E-02	4.75	2.3E-01
GOTERM_MF_FAT	GO:0046961~proton-transporting ATPase activity, rotational mechanism	3	5.3E-02	8.03	4.6E-01
GOTERM_CC_FAT	GO:0045259~proton-transporting ATP synthase complex	3	5.7E-02	7.64	2.4E-01
GOTERM_BP_FAT	GO:0015992~proton transport	4	8.6E-02	3.82	6.7E-01
GOTERM_BP_FAT	GO:0006818~hydrogen transport	4	9.3E-02	3.70	6.9E-01
GOTERM_BP_FAT	GO:0006811~ion transport	18	1.6E-01	1.37	8.3E-01
GOTERM_MF_FAT	GO:0015662~ATPase activity, coupled to transmembrane movement of ions, phosphorylative mechanism	3	2.1E-01	3.48	8.9E-01
SP_PIR_KEYWORDS	ion transport	11	2.8E-01	1.38	6.9E-01
GOTERM_BP_FAT	GO:0006812~cation transport	11	4.7E-01	1.16	9.8E-01
GOTERM_BP_FAT	GO:0015672~monovalent inorganic cation transport	6	6.4E-01	1.10	9.9E-01
Annotation Cluster 28	**Enrichment Score: 2.03**				

Category	Term	Count	P Value	Fold Enrichment	Benjamini
GOTERM_BP_FAT	GO:0016044~membrane organization	16	2.3E-03	2.45	8.0E-02
SP_PIR_KEYWORDS	endosome	10	2.5E-03	3.46	2.2E-02
GOTERM_BP_FAT	GO:0006897~endocytosis	9	3.5E-02	2.39	4.6E-01
GOTERM_BP_FAT	GO:0010324~membrane invagination	9	3.5E-02	2.39	4.6E-01
Annotation Cluster 29	**Enrichment Score: 1.97**				

Category	Term	Count	P Value	Fold Enrichment	Benjamini
INTERPRO	IPR012335:Thioredoxin fold	8	9.6E-04	5.11	6.0E-02
UP_SEQ_FEATURE	short sequence motif:Prevents secretion from ER	6	1.3E-03	7.31	1.1E-01
INTERPRO	IPR017936:Thioredoxin-like	5	2.2E-03	8.97	8.7E-02
INTERPRO	IPR000886:Endoplasmic reticulum, targeting sequence	5	5.0E-03	7.17	1.5E-01
GOTERM_CC_FAT	GO:0005793~ER-Golgi intermediate compartment	5	6.9E-03	6.52	5.2E-02
GOTERM_MF_FAT	GO:0003756~protein disulfide isomerase activity	3	8.7E-03	20.51	1.6E-01
GOTERM_MF_FAT	GO:0016864~intramolecular oxidoreductase activity, transposing S-S bonds	3	8.7E-03	20.51	1.6E-01
GOTERM_MF_FAT	GO:0016862~intramolecular oxidoreductase activity, interconverting keto- and enol-groups	3	1.1E-02	18.46	1.7E-01
GOTERM_CC_FAT	GO:0005788~endoplasmic reticulum lumen	6	1.7E-02	4.01	9.8E-02
SP_PIR_KEYWORDS	Redox-active center	4	2.0E-02	6.89	1.1E-01
GOTERM_BP_FAT	GO:0045454~cell redox homeostasis	5	2.3E-02	4.63	3.6E-01
INTERPRO	IPR017937:Thioredoxin, conserved site	3	6.0E-02	7.45	6.8E-01
INTERPRO	IPR013766:Thioredoxin domain	3	6.5E-02	7.17	6.9E-01
GOTERM_MF_FAT	GO:0016860~intramolecular oxidoreductase activity	3	1.3E-01	4.86	7.4E-01
Annotation Cluster 30	**Enrichment Score: 1.96**				

Category	Term	Count	P Value	Fold Enrich-rich-ment	Benja-mini
SP_PIR_KEYWORDS	calcium binding	8	5.6E-04	5.62	5.9E-03
INTERPRO	IPR018247:EF-HAND 1	12	5.7E-04	3.57	4.0E-02
INTERPRO	IPR018249:EF-HAND 2	11	1.9E-03	3.30	8.8E-02
INTERPRO	IPR011992:EF-Hand type	11	3.8E-03	3.01	1.2E-01
UP_SEQ_FEATURE	calcium-binding region:2	7	5.4E-03	4.37	2.8E-01
SMART	SM00054:EFh	7	7.4E-03	4.04	1.2E-01
UP_SEQ_FEATURE	calcium-binding region:1	7	8.3E-03	3.99	3.6E-01
SP_PIR_KEYWORDS	EF hand	5	9.4E-03	6.03	6.6E-02
UP_SEQ_FEATURE	calcium-binding region:3	4	1.3E-02	7.98	4.6E-01
UP_SEQ_FEATURE	domain:EF-hand 2	8	1.4E-02	3.16	4.5E-01
UP_SEQ_FEATURE	domain:EF-hand 1	8	1.4E-02	3.16	4.5E-01
SP_PIR_KEYWORDS	calcium	20	1.6E-02	1.80	9.8E-02
INTERPRO	IPR002048:Calcium-binding EF-hand	7	2.4E-02	3.16	4.2E-01
UP_SEQ_FEATURE	domain:EF-hand 3	5	4.2E-02	3.82	8.0E-01
UP_SEQ_FEATURE	domain:EF-hand 4	4	4.9E-02	4.87	8.2E-01
SP_PIR_KEYWORDS	calcium	20	1.6E-02	1.80	9.8E-02
GOTERM_MF_FAT	GO:0005509~calcium ion binding	21	1.1E-01	1.41	7.1E-01
INTERPRO	IPR018248:EF hand	4	3.2E-01	1.99	9.9E-01
Annotation Cluster 31	**Enrichment Score: 1.92**				
Category	Term	Count	P Value	Fold Enrich-rich-ment	Benja-mini
KEGG PATHWAY	hsa04670:Leukocyte transendothelial migration	10	2.3E-03	3.42	5.3E-02
KEGG PATHWAY	hsa04360:Axon guidance	10	4.2E-03	3.13	5.8E-02
KEGG PATHWAY	hsa04062:Chemokine signaling pathway	8	1.8E-01	1.73	6.4E-01
Annotation Cluster 32	**Enrichment Score: 1.81**				
Category	Term	Count	P Value	Fold Enrich-rich-ment	Benja-mini
INTERPRO	IPR012335:Thioredoxin fold	8	9.6E-04	5.11	6.0E-02
UP SEQ FEATURE	domain:GST C-terminal	4	1.1E-02	8.71	4.2E-01
INTERPRO	IPR010987:Glutathione S-transferase, C-terminal-like	3	7.3E-02	6.68	7.1E-01
INTERPRO	IPR017933:Glutathione S-transferase/chloride channel, C-terminal	3	7.8E-02	6.46	7.3E-01
Annotation Cluster 33	**Enrichment Score: 1.76**				
Category	Term	Count	P Value	Fold Enrich-rich-ment	Benja-mini
UP_SEQ_FEATURE	domain:EH	3	1.9E-03	43.11	1.4E-01
SMART	SM00027:EH	3	7.3E-03	22.51	1.5E-01
SMART	SM00053:DYNc	3	1.0E-02	19.05	1.2E-01
INTERPRO	IPR000261:EPS15 homology (EH)	3	1.2E-02	17.61	2.8E-01
INTERPRO	IPR001401:Dynamin, GTPase region	3	1.7E-02	14.90	3.5E-01

UP_SEQ_FEATURE	domain:EF-hand	3	1.1E-01	5.26	9.2E-01
KEGG_PATHWAY	hsa04144:Endocytosis	8	1.7E-01	1.75	6.3E-01
Annotation Cluster 34	**Enrichment Score: 1.73**				
Category	Term	Count	*P Value*	Fold Enrich-rich-ment	Benja-mini
SP_PIR_KEYWORDS	endosome	10	2.5E-03	3.46	2.2E-02
GOTERM_CC_FAT	GO:0005768~endosome	13	1.5E-02	2.21	9.2E-02
KEGG_PATHWAY	hsa04144:Endocytosis	8	1.7E-01	1.75	6.3E-01
Annotation Cluster 35	**Enrichment Score: 1.72**				
Category	Term	Count	*P Value*	Fold Enrich-rich-ment	Benja-mini
GOTERM_CC_FAT	GO:0016323~basolateral plasma membrane	14	1.1E-04	3.69	1.9E-03
GOTERM_CC_FAT	GO:0005912~adherens junction	9	8.5E-03	3.11	5.9E-02
GOTERM_CC_FAT	GO:0070161~anchoring junction	9	1.5E-02	2.80	9.1E-02
GOTERM_CC_FAT	GO:0030055~cell-substrate junction	7	1.8E-02	3.34	1.0E-01
GOTERM_CC_FAT	GO:0005925~focal adhesion	6	4.2E-02	3.15	2.0E-01
GOTERM_CC_FAT	GO:0005924~cell-substrate adherens junction	6	4.8E-02	3.03	2.2E-01
GOTERM_CC_FAT	GO:0030054~cell junction	15	1.0E-01	1.55	3.7E-01
SP_PIR_KEYWORDS	cell junction	8	3.1E-01	1.45	7.4E-01
Annotation Cluster 73	**Enrichment Score: 0.6975542091836765**				
Category	Term	Count	*P Value*	Fold Enrich-rich-ment	Benja-mini
SP_PIR_KEYWORDS	lysosome	6	5.6E-02	2.91	2.4E-01
GOTERM_CC_FAT	GO:0005770~late endosome	4	8.6E-02	3.82	3.3E-01
KEGG_PATHWAY	hsa04142:Lysosome	5	3.2E-01	1.72	7.8E-01
GOTERM_CC_FAT	GO:0005773~vacuole	7	3.3E-01	1.49	7.3E-01
GOTERM_CC_FAT	GO:0000323~lytic vacuole	6	3.6E-01	1.52	7.6E-01
GOTERM_CC_FAT	GO:0005764~lysosome	6	3.6E-01	1.52	7.6E-01

Table S3.4 Proteins in cell membrane.

Protein GI number[#]	Gene Name
4502101	annexin A1
51895795	annexin A13
48255959	ATPase, Ca++ transporting, plasma membrane 4
21361181	ATPase, Na+/K+ transporting, alpha 1 polypeptide
4502281	ATPase, Na+/K+ transporting, beta 3 polypeptide
4502565	calpain, small subunit 1
16357472	cell division cycle 42 (GTP binding protein, 25kDa); cell division cycle 42 pseudo-gene 2
7330335	chloride intracellular channel 4
124107616	claudin 23
170650661	ectonucleotide pyrophosphatase/phosphodiesterase 1
4503571	enolase 1, (alpha)
45387945	family with sequence similarity 62 (C2 domain containing), member B
94538362	flotillin 2
73486658	glutamic-oxaloacetic transaminase 2, mitochondrial (aspartate aminotransferase 2)
21614499	hypothetical protein LOC100129652; ezrin
19743813	integrin, beta 1 (fibronectin receptor, beta polypeptide, antigen CD29 includes MDF2, MSK12)
4506787	IQ motif containing GTPase activating protein 1
5031815	lysyl-tRNA synthetase
19718759	myoferlin
124494247	myosin IC
29171736	phosphatidic acid phosphatase type 2A
190358517	RAB11B, member RAS oncogene family
10880989	RAB18, member RAS oncogene family
16933567	RAB8A, member RAS oncogene family
7661678	RAP1B, member of RAS oncogene family
10835049	ras homolog gene family, member A
5454028	related RAS viral (r-ras) oncogene homolog
41872583	Rho-associated, coiled-coil containing protein kinase 2
166795299	solute carrier family 2 (facilitated glucose transporter), member 1
38016911	stomatin
189217915	syntaxin binding protein 5 (tomosyn)
223029410	talin 1
4759300	vesicle-associated membrane protein 3 (cellubrevin)
4507879	voltage-dependent anion channel 1; similar to voltage-dependent anion channel 1

All the proteins in this list were selected manually based on the information from Unitprot database.

[#] These protein GI number is from human being data base.

Table S3.5 Proteins in endocytosis pathway.

Annotation Cluster 28	Enrichment Score: 2.03
GOTERM_BP_FAT	GO:0006897~endocytosis
Protein GI number#	Gene Name
30240932	EH-domain containing 1
21361462	EH-domain containing 2
21264315	EH-domain containing 4
10880989	RAB18, member RAS oncogene family
19923262	RAB5A, member RAS oncogene family
34147513	RAB7A, member RAS oncogene family
260436862	adaptor-related protein complex 1, beta 1 subunit
15451856	caveolin 1, caveolae protein, 22kDa
4557797	nucleoside diphosphate kinase

[#] These protein GI number is from human being data base.

Table S3.6 Proteins in vesicle-mediated transport pathway.

Annotation Cluster 17	Enrichment Score: 2.87
GOTERM_BP_FAT	GO:0016192~vesicle-mediated transport
Protein GI number#	Gene Name
4502209	ADP-ribosylation factor 5
30240932	EH-domain containing 1
21361462	EH-domain containing 2
21264315	EH-domain containing 4
10880989	RAB18, member RAS oncogene family
4506365	RAB2A, member RAS oncogene family
19923262	RAB5A, member RAS oncogene family
38679888	RAB6C, member RAS oncogene family; RAB6A, member RAS oncogene family; hypothetical LOC100130819; RAB6C-like
34147513	RAB7A, member RAS oncogene family
16933567	RAB8A, member RAS oncogene family
116812591	RER1 retention in endoplasmic reticulum 1 homolog (S. cerevisiae)
260436862	adaptor-related protein complex 1, beta 1 subunit
15451856	caveolin 1, caveolae protein, 22kDa
4503015	copine III
21361625	exocyst complex component 2
31083351	exocyst complex component 3
116063573, 160420317	filamin A, alpha (actin binding protein 280)
38044288	gelsolin (amyloidosis, Finnish type)
7705636	golgi transport 1 homolog B (S. cerevisiae)
5729850	guanine nucleotide binding protein (G protein), alpha inhibiting activity polypeptide 3
4557888	keratin 18; keratin 18 pseudogene 26; keratin 18 pseudogene 19
4557797	non-metastatic cells 1, protein (NM23A) expressed in; NME1-NME2 readthrough transcript; non-metastatic cells 2, protein (NM23B) expressed in
5174655, 41393604	reticulon 3
5730031	secretory carrier membrane protein 2
28933465	syntaxin 12
189217915	syntaxin binding protein 5 (tomosyn)
98986464	transmembrane emp24-like trafficking protein 10 (yeast)
6005942	valosin-containing protein
4759300	vesicle-associated membrane protein 3 (cellubrevin)

These protein GI number is from human being data base.

Table S3.7 Proteins in lysosome.

Annotation Cluster 73	Enrichment Score: 0.7
SP_PIR_KEYWORDS KEGG_PATHWAY	lysosome
Protein GI number#	Gene Name
8922601	ADP-ribosylation factor-like 8B
17136148	ATPase, H+ transporting, lysosomal accessory protein 1 (V-type proton ATPase subunit S1)
4502679	CD63 molecule
34147513	RAB7A, member RAS oncogene family
4503143	cathepsin D
23821023	L-amino-acid oxidase isoform X2 (interleukin 4 induced 1)
5031631	lysosome membrane protein 2 (scavenger receptor class B, member 2)

These protein GI number is from human being data base.

References

Bernatchez PN, Sharma A, Kodaman P, Sessa WC. 2009. Myoferlin is critical for endocytosis in endothelial cells. American Journal of Physiology - Cell Physiology 297(3):C484-C492.

Bertinato J, Cheung L, Hoque R, Plouffe LJ. 2010. Ctr1 transports silver into mammalian cells. Journal of Trace Elements in Medicine and Biology 24(3):178-184.

Bertoli F, Davies G-L, Monopoli MP, Moloney M, Gun'ko YK, Salvati A, Dawson KA. 2014. Magnetic Nanoparticles to Recover Cellular Organelles and Study the Time Resolved Nanoparticle-Cell Interactome throughout Uptake. Small 10(16):3307-3315.

Bols NC, Barlian A, Chirinotrejo M, Caldwell SJ, Goegan P, Lee LEJ. 1994. Development of a Cell-Line from Primary Cultures of Rainbow-Trout, Oncorhyrzchus Mykiss (Walbaum), Gills. Journal of Fish Diseases 17(6):601-611.

Canton I, Battaglia G. 2012. Endocytosis at the nanoscale. Chemical Society Reviews 41(7):2718-2739.

Cowin P, Kapprell H-P, Franke WW, Tamkun J, Hynes RO. 1986. Plakoglobin: A protein common to different kinds of intercellular adhering junctions. Cell 46(7):1063-1073.

Eigenheer R, Castellanos ER, Nakamoto MY, Gerner KT, Lampe AM, Wheeler KE. 2014. Silver nanoparticle protein corona composition compared across engineered particle properties and environmentally relevant reaction conditions. Environmental Science: Nano.

Futerman AH, van Meer G. 2004. The cell biology of lysosomal storage disorders. Nat Rev Mol Cell Biol 5(7):554-565.

Grant BD, Donaldson JG. 2009. Pathways and mechanisms of endocytic recycling. Nat Rev Mol Cell Biol 10(9):597-608.

Greulich C, Diendorf J, Simon T, Eggeler G, Epple M, Köller M. 2011. Uptake and intracellular distribution of silver nanoparticles in human mesenchymal stem cells. Acta Biomaterialia 7(1):347-354.

Hofmann D, Tenzer S, Bannwarth MB, Messerschmidt C, Glaser S-F, Schild H, Landfester K, Mailänder V. 2014. Mass Spectrometry and Imaging Analysis of Nanoparticle-Containing Vesicles Provide a Mechanistic Insight into Cellular Trafficking. ACS Nano 8(10):10077-10088.

Huang DW, Sherman BT, Lempicki RA. 2008. Systematic and integrative analysis of large gene lists using DAVID bioinformatics resources. Nat. Protocols 4(1):44-57.

Iversen T-G, Skotland T, Sandvig K. 2011. Endocytosis and intracellular transport of nanoparticles: Present knowledge and need for future studies. Nano Today 6(2):176-185.

Kroemer G, Jaattela M. 2005. Lysosomes and autophagy in cell death control. Nat Rev Cancer 5(11):886-897.

Lu J, Liong M, Sherman S, Xia T, Kovochich M, Nel A, Zink J, Tamanoi F. 2007. Mesoporous Silica Nanoparticles for Cancer Therapy: Energy-Dependent Cellular Uptake and Delivery of Paclitaxel to Cancer Cells. NanoBiotechnology 3(2):89-95.

Lynch I, Dawson KA. 2008. Protein-nanoparticle interactions. Nano Today 3(1-2):40-47.

Ma X, Wu Y, Jin S, Tian Y, Zhang X, Zhao Y, Yu L, Liang X-J. 2011. Gold Nanoparticles Induce Autophagosome Accumulation through Size-Dependent Nanoparticle Uptake and Lysosome Impairment. Acs Nano 5(11):8629-8639.

Mahmoudi M, Lynch I, Ejtehadi MR, Monopoli MP, Bombelli FB, Laurent S. 2011. Protein–Nanoparticle Interactions: Opportunities and Challenges. Chemical Reviews 111(9):5610-5637.

Meister M, Tikkanen R. 2014. Endocytic trafficking of membrane-bound cargo: a flotillin point of view. Membranes 4(3):356-371.

Monopoli MP, Aberg C, Salvati A, Dawson KA. 2012. Biomolecular coronas provide the biological identity of nanosized materials. Nature Nanotechnology 7(12):779-786.

Monopoli MP, Walczyk D, Campbell A, Elia G, Lynch I, Baldelli Bombelli F, Dawson KA. 2011. Physical–Chemical Aspects of Protein Corona: Relevance to in Vitro and in Vivo Biological Impacts of Nanoparticles. Journal of the American Chemical Society 133(8):2525-2534.

Nel AE, Madler L, Velegol D, Xia T, Hoek EMV, Somasundaran P, Klaessig F, Castranova V, Thompson M. 2009. Understanding biophysicochemical interactions at the nano-bio interface. Nat Mater 8(7):543-557.

Passagne I, Morille M, Rousset M, Pujalté I, L'Azou B. 2012. Implication of oxidative stress in size-dependent toxicity of silica nanoparticles in kidney cells. Toxicology 299(2–3):112-124.

Pillai S, Behra R, Nestler H, Suter MJF, Sigg L, Schirmer K. 2014. Linking toxicity and adaptive responses across the transcriptome, proteome, and phenotype of Chlamydomonas reinhardtii exposed to silver. Proceedings of the National Academy of Sciences 111(9):3490-3495.

Sandin P, Fitzpatrick LW, Simpson JC, Dawson KA. 2012. High-Speed Imaging of Rab Family Small GTPases Reveals Rare Events in Nanoparticle Trafficking in Living Cells. ACS Nano 6(2):1513-1521.

Schirmer K, Chan AGJ, Greenberg BM, Dixon DG, Bols NC. 1997. Methodology for demonstrating and measuring the photocytotoxicity of fluoranthene to fish cells in culture. Toxicology in Vitro 11(1-2):107-119.

Schirmer K, Dixon DG, Greenberg BM, Bols NC. 1998. Ability of 16 priority PAHs to be directly cytotoxic to a cell line from the rainbow trout gill. Toxicology 127(1-3):129-141.

Schultz AG, Ong KJ, MacCormack T, Ma G, Veinot JGC, Goss GG. 2012. Silver Nanoparticles Inhibit Sodium Uptake in Juvenile Rainbow Trout (Oncorhynchus mykiss). Environmental Science & Technology 46(18):10295-10301.

Stern S, Adiseshaiah P, Crist R. 2012. Autophagy and lysosomal dysfunction as emerging mechanisms of nanomaterial toxicity. Particle and Fibre Toxicology 9(1):20.

Tanneberger K, Knöbel M, Busser FJM, Sinnige TL, Hermens JLM, Schirmer K. 2012. Predicting Fish Acute Toxicity Using a Fish Gill Cell Line-Based Toxicity Assay. Environmental Science & Technology 47(2):1110-1119.

Vercauteren D, Deschout H, Remaut K, Engbersen JFJ, Jones AT, Demeester J, De Smedt SC, Braeckmans K. 2011. Dynamic Colocalization Microscopy To Characterize Intracellular Trafficking of Nanomedicines. ACS Nano 5(10):7874-7884.

Walczyk D, Bombelli FB, Monopoli MP, Lynch I, Dawson KA. 2010. What the Cell "Sees" in Bionanoscience. Journal of the American Chemical Society 132(16):5761-5768.

Wang J, Jensen UB, Jensen GV, Shipovskov S, Balakrishnan VS, Otzen D, Pedersen JS, Besenbacher F, Sutherland DS. 2011. Soft Interactions at Nanoparticles Alter Protein Function and Conformation in a Size Dependent Manner. Nano Letters 11(11):4985-4991.

Wang Z, Liu S, Ma J, Qu G, Wang X, Yu S, He J, Liu J, Xia T, Jiang G-B. 2013. Silver Nanoparticles Induced RNA Polymerase-Silver Binding and RNA Transcription Inhibition in Erythroid Progenitor Cells. Acs Nano 7(5):4171-4186.

Wigginton NS, Titta Ad, Piccapietra F, Dobias J, Nesatyy VJ, Suter MJF, Bernier-Latmani R. 2010. Binding of Silver Nanoparticles to Bacterial Proteins Depends on Surface Modifications and Inhibits Enzymatic Activity. Environmental Science & Technology 44(6):2163-2168.

Xia T, Kovochich M, Liong M, Zink JI, Nel AE. 2007. Cationic Polystyrene Nanosphere Toxicity Depends on Cell-Specific Endocytic and Mitochondrial Injury Pathways. ACS Nano 2(1):85-96.

Yue Y, Behra R, Sigg L, Fernández Freire P, Pillai S, Schirmer K. 2015. Toxicity of silver nanoparticles to a fish gill cell line: Role of medium composition. Nanotoxicology 9(1):54-63.

Chapter 4 Silver nanoparticles inhibit fish gill cell proliferation in protein-free culture medium

While short-term exposures of vertebrate cells, such as from fish, can be performed in simple serum-free media, long-term cultures generally require addition of growth factors and proteins, normally supplied with a serum supplement. However, proteins are known to alter nanoparticle properties by binding to nanoparticles. Therefore, in order to be able to study nanoparticle-cell interactions for extended periods, the rainbow trout (*Oncorhynchus mykiss*) gill cell line, RTgill-W1, was adapted to proliferate in a commercial serum-free medium, InVitrus VP-6. The newly adapted cell strain was named RTgill-W1-pf (protein free). These cells proliferate at a speed similar to the RTgill-W1 cells cultured in a fully supplemented medium containing 5% fetal bovine serum. As well, they were successfully cryopreserved in liquid nitrogen and fully recovered after thawing. Yet, senescence set in after about 10 passages in InVitrus VP-6 medium, revealing that, unlike the "wild-type" RTgill-W1 strain, they no longer comprise a permanent cell line. The RTgill-W1-pf cell line was subsequently applied to investigate the effect of silver nanoparticles (AgNP) on cell proliferation over a period of twelve days. Indeed, cell proliferation was inhibited by AgNP. This effect correlated with high levels of silver being associated with the cells. The new cell line, RTgill-W1-pf, which can proliferate in serum free medium and therefore might better represent gill cell exposures in the organism *in vivo*, offers novel opportunities to study nanoparticle-cell interactions without serum protein interference.

4.1 Introduction

Toxicological research, such as nanotoxicology, benefits from both *in vivo* and *in vitro* experimental models. The main *in vitro* models are cell cultures including primary cultures, cell lines with limited capacity to proliferate and continuous cell lines (Bols et al. 2005; Nogueira et al. 2014). Compared to the complex biological environment of an *in vivo* model, *in vitro* models, i.e. cells taken from organisms and cultured in a defined environment, offer several advantages. Cell cultures are ideal for understanding the toxic mechanisms induced by nanoparticles and other chemicals to cells. Many processes that are difficult to quantify or visualize *in vivo* can be observed in cell culture models. *In vitro* nanoparticle toxicity studies thus far revealed that nanoparticles can induce oxidative stress, apoptosis and genotoxicity, among other effects, and are therefore useful to explore the mechanisms underlying nanoparticle toxicity (Schirmer 2014; Schultz et al. 2014). In addition to providing mechanistic insights, cell cultures have several other advantages, such as easy handling, comparatively low costs, high reproducibility and the potential to scale up for high-throughput or high-content analysis. Finally, cell cultures can contribute to a reduction or even replacement of animals in toxicological research. Tanneberger *et al* tested 35 organic chemicals for short-term, acute toxicity to a rainbow trout (*Oncorhynchus mykiss*) gill cell line, RTgill-W1, and found a very good agreement between *in vivo* and *in vitro* effective concentrations (Tanneberger et al. 2012). Based on these promising results, an international round-robin test is currently performed with the aim to establish the RTgill-W1 based assay as an alternative to the acute fish toxicity test (Schirmer and Knöbel, personal communication).

However, certain limitations also apply to cell cultures. For example, as of now it has been impossible to explore nanoparticles effects in cultured fish cells over long exposure times in the absence of a serum supplement to, e.g., quantify the nanoparticles' effect on cell proliferation. Indeed, most cell cultures require serum, which is an undefined supplement providing growth factors and hormones for cell attachment, growth and proliferation (Barnes and Sato 1980; Sato 1975).

Under various circumstances, a serum supplement is justifiable owing to the original organism physiological, e.g. when attempting to mimic endothelial cells lining blood vessels. However, for epithelia that comprise a barrier to the out-side environment, such as the gill of fish, the interface with cells is quite different. To account for this, several studies have explored the tolerance of the RTgill-W1 rainbow trout cell line to ion composition and strength. Schirmer *et al* developed an L15/ex exposure medium containing only salts, galactose and pyruvate to provide an isotonic envi-

ronment and a source of energy while excluding medium components such as vitamins and aromatic amino acids from basal medium, Leibovitz's L15 (L15) (Schirmer et al. 1997). Furthermore, the fish gill cell line is known to be quite tolerant to osmotic differences (Dayeh et al. 2002; Yue et al. 2015; Chapter 2). However, the gill cells still need serum for long term maintenance and cell proliferation. Previous research clearly demonstrated that proteins do not only bind to nanoparticles in cells (see Chapter 3) but also that they bind if present together with nanoparticles in exposure medium. For example, fetal bovine serum (FBS) stabilized tungsten carbide (WC) and cobalt-doped tungsten carbide (WC-Co) nanoparticle suspensions in cell culture media (Bastian et al. 2009; Kühnel et al. 2009; Meißner et al. 2010). Moreover, Bertoli *et al* reported that serum proteins, binding to nanoparticles and forming a corona, were stable and preserved as nanoparticles traveled through the cells (Bertoli et al. 2014). Having a cell model that grows and proliferates in the absence of serum, which is rare in aquatic environment, would therefore be very useful to study the impact of nanoparticles on cells over extended times.

Since the pioneering work of Hayashi and Sato in 1976 , where they adapted a rat pituitary cell line in a defined serum-free medium supplemented with hormones, a number of serum free medium formulations have been developed for mammalian cell lines and for primary cultures (Grillberger et al. 2009; Hayashi and Sato 1976; van der Valk et al. 2010). Yet, adaption of fish cell lines to serum-free medium has thus far been reported only once; Ackermann and Fent published on the adaptation of the rainbow trout gonad cell line (RTG-2) to a serum-free medium, Turbo Doma (Cell Culture Technologies, Switzerland), resulting in similar growth rates as under serum-containing conditions (Ackermann and Fent 1998).

The aim of the current work was to adapt the RTgill-W1 cells to growth in serum-free medium. Two commercially available serum- and protein-free media were investigated: Turbo Doma and InVitrus VP-6 (Cell Culture Technologies, Switzerland). Both media have been developed for mammalian cell culture. Turbo Doma is a protein-free and chemically defined medium developed for the cultivation of hybridomas and myeloma cell lines. InVitrus VP-6 is likewise protein-free and chemically defined and propagated as medium for mammalian kidney and fibroblast cell lines. Only the InViturs medium proved capable of supporting long-term culture of a newly derived RTgill-W1 cell strain. With this new RTgill-W1-based cell line, the impact of AgNP on cell proliferation was explored.

4.2 Results

4.2.1 Adaptation of RTgill-W1 cells in protein-free cell culture medium

RTgill-W1 cells were cultured in two commercial serum- and protein-free cell culture media: Turbo Doma and InVitrus VP-6. The strategy for adaptation was to place the cells in these media initially in the presence of 5% fetal bovine serum (FBS), which is used for routine culture of RTgill-W1 cells, and then gradually lower the FBS content if the cells are able to proliferate in the respective medium conditions to confluency until the FBS, finally, was completely removed (Figure 4.1). When doing so, the "wild-type" RTgill-W1 cells responded differently to the two media. In the case of the Turbo Doma medium, cells proliferated as long as FBS was present but died within a couple of days as soon as the FBS was completely removed. However, the InVitrus VP-6 medium allowed for a more sustained culture. In this medium, it was possible to culture the cells to confluency at 5% FBS and then further lower the FBS concentration to 2.5, 1 and finally 0.5%. After reaching confluency in 0.5% FBS in 25 cm^2 culture flaks, cells were placed in 25 cm^2 flasks in InVitrus VP-6 medium without FBS. At this step, most of the cells died but some cells survived and formed clumps from which new cells grew out (Figure 4.2A). Proliferation was extremely slow for these cells; half of the culture medium was exchanged with fresh InVitrus VP-6 medium every seven days. After about 6 months, the cells growing out from the clumps started to proliferate faster and finally reached confluency. This culture was termed passage 1 of the newly derived cell line, RTgill-W1-pf (protein free). After passaging, i.e. transfer into two new 25 cm^2 flasks, proliferation rate further increased to reach confluency within 15 days (Figure 4.2B). From passage three on, the new gill cell line grew steadily and reached confluency every six days (Figure 4.2C-D).
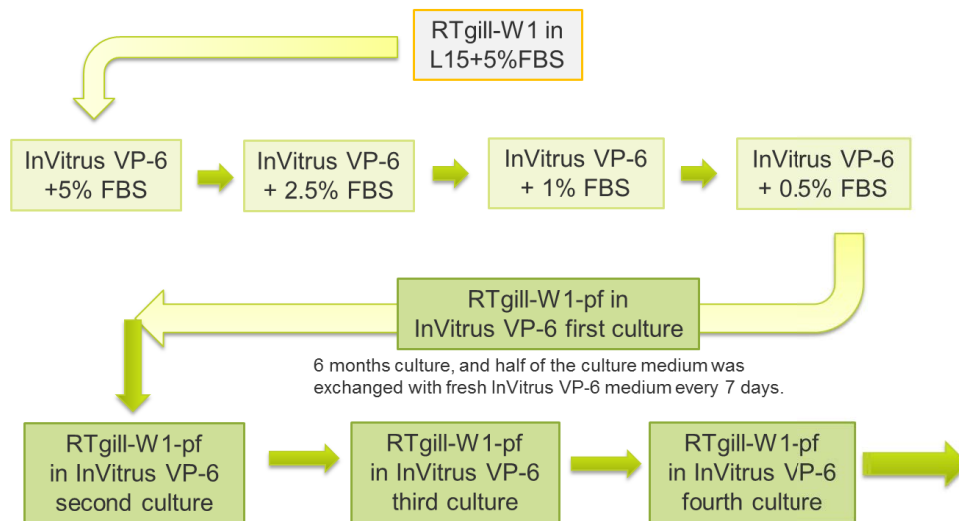
Figure 4.1 Scheme of RTgill-W1 cell adaptation in protein free cell culture medium.

The adaption begun with culturing RTgill-W1 in InVitrus VP-6 medium with 5% FBS and then step-wise lowering the FBS concentration to 2.5, 1 and 0.5%. After reaching confluency in 0.5% FBS, cells were placed in InVitrus VP-6 medium without FBS. In the InVitrus VP-6 medium without FBS, cells proliferation was very slow and reached confluency in 6 months. This culture was named passage 1 of the newly derived cell line, RTgill-W1-pf (protein free). Then, RTgill-W1-pf cells were split once (1 flask to 2 flasks) in 1-2 weeks. All the cells were cultured in 25 cm^2 flasks. Another medium, Turbo Doma, only supported cell proliferation until the medium with 0.5% serum step.
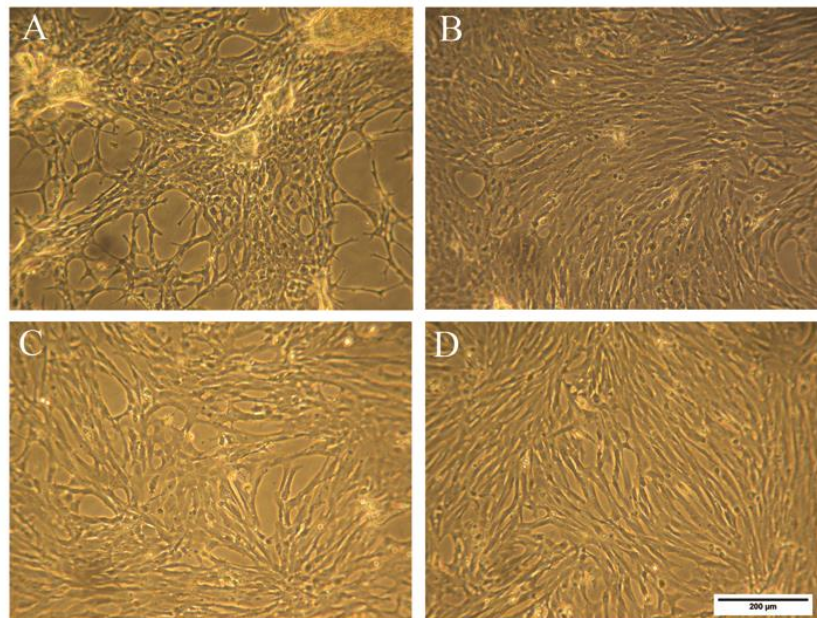

Figure 4.2 Appearance of the newly evolving RTgill-W1-pf cell line during the adaptation period.

A: Cells in passage 1 cultured for 6 months; cell clumps were observed in this passage; B: Cells in passage 2 cultured for 15 days; with passaging and over time, cell clumps disappeared from the culture; C: Cells in passage 3 cultured for 7 days; and D: Cells in passage 4 cultured for 7 days.

4.2.2   Characterization of the RTgill-W1-pf cell line

Compared to the original, "wild-type" RTgill-W1 cells grown in L15 medium supplemented with 5% FBS, the new RTgill-W1-pf cells are similar in size when in suspension (average cell diameter: 13.5 µm for RTgill-W1 and 13.8 µm RTgill-W1-pf) but appear more spread when growing as monolayer in the cell culture flasks. Doubling time of the RTgill-W1-pf cell line in InVitrus VP-6 medium was determined to be six days based on a 21 day cell proliferation experiment (Figure 4.3A).

Inasmuch as the premise was to culture the RTgill-W1-pf in protein-free medium, the total protein concentration in the medium of proliferating cultures was measured (Figure 4.3B). As expect, no protein was detectable in pure InVitrus VP-6 medium. However, after the cells were incubated for three to twelve days, the protein concentration in cell culture medium reached protein levels of between 5-22 µg/mL, which comprises 1-5% of the protein concentration measured in routine, RTgill-W1 cell culture medium, i.e. L15 medium containing 5% FBS.
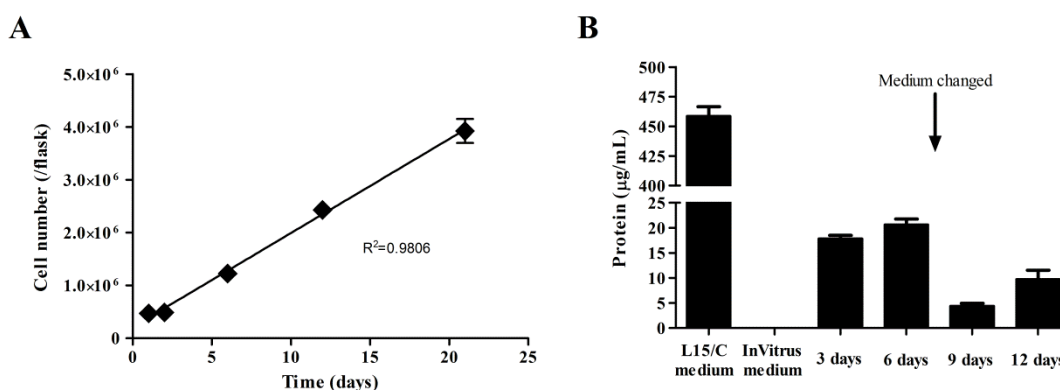

Figure 4.3 Characterization of the newly derived RTgill-W1-pf cell culture.

A: RTgill-W1-pf cell growth over time in InVitrus VP-6 medium. Cell number was counted by electronic cell counting (Casy). Cell doubling time was six days. For counting, the cell diameter range was set to 7.5 - 25 µm. B: Total protein concentration in cell culture medium over time. The protein concentration on day nine was much lower than on day six because of a fresh medium exchange on day six after sampling. The protein concentration was also significantly lower on day twelve than on day six despite the same incubation time. One-way ANOVA with Dunnett's multiple comparison test compared to day six, n=3. This was likely due to the dead and detached cells after seeding, which might have increased the medium protein concentration on day six.

To obtain an easily accessible stock of RTgill-W1-pf cells, confluent cells were not only sub-cultured but also preserved in 10% FBS and 10% DMSO in InVitrus VP-6 medium in liquid nitrogen. Frozen

cells were successfully thawed in InVitrus VP-6 medium containing 5% FBS. Then, a step-wise reduction of the serum concentration to 2.5, to 1, to 0.5% was again necessary. Once the FBS was completely removed, RTgill-W1-pf cells resumed proliferation to the same extent as cells never frozen. However, whether frozen or not, it was found that the RTgill-W1-pf cells entered senescence and completely dislodged from the culture surface and died after about ten passages.

4.2.3   Exposure of RTgill-W1-pf to AgNP

Particle characterization: The average AgNP diameter in the original stock suspension is 19.4±0.4 nm and the zeta potential -30±0.9 mV (Yue et al. 2015). Once placed in InVitrus VP-6 medium, the particles quickly and strongly agglomerated. Transmission electron microscopy (TEM) revealed large AgNP agglomerates (Figure 4.4A-B). The AgNP size increased to 800-1500 nm after one day in the medium (Figure 4.4C). The zeta potential increased to around -15 mV (Figure 4.4D).
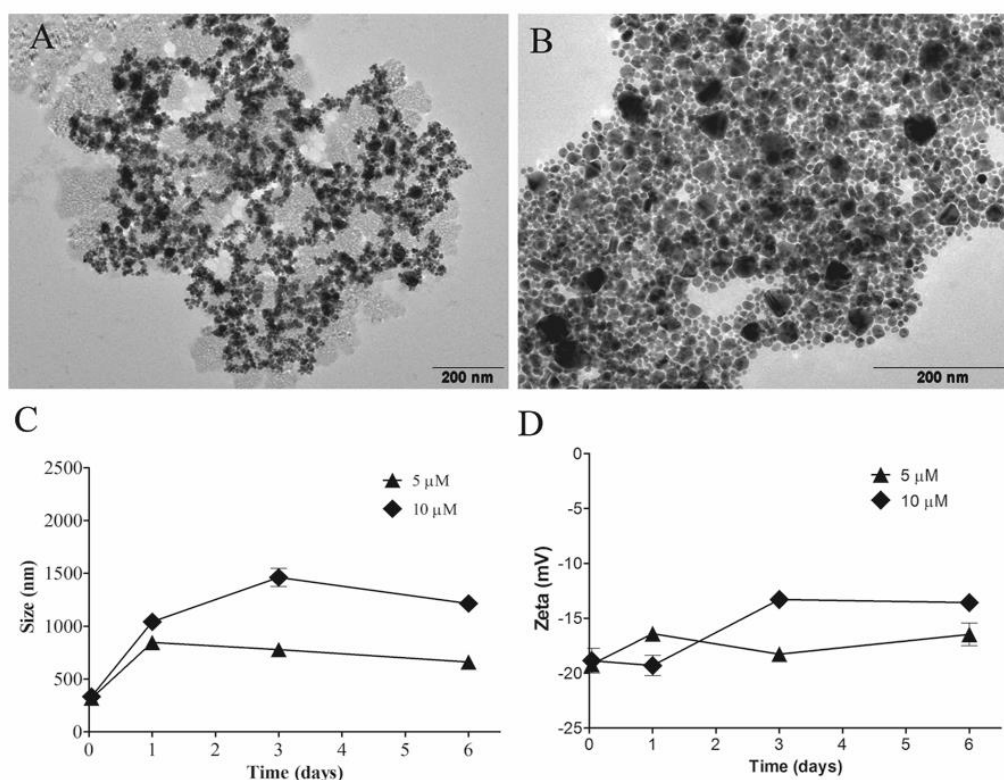
Figure 4.4 AgNP in InVitus medium over time.

A-B: TEM images of AgNP present in InVitrus VP-6 medium for 15 min, which refers to the first time point in Figure 4.4C. A: Overview of AgNP agglomeration in InVitrus VP-6 medium; B: magnified view of AgNP in InVitrus VP-6 medium. C: Size of AgNP in InVitrus VP-6 medium as determined by Zetasizer. D: Zeta potential of AgNP in InVitrus VP-6 medium measured by Zetasizer. Data were presented as mean ± standard deviation, n=3.

<u>Short-term toxicity (impact on cell viability):</u> RTgill-W1-pf cells were exposed to AgNP for three days and impact on cell viability measured focusing on cellular metabolic activity, cell membrane integrity and lysosomal membrane integrity (Figure 4.5). All three cell viability parameters responded similarly with no significant differences between the EC50 values (Table 4.1). To compare with the impact of silver ion exposure, cells were likewise exposed and assessed upon addition of $AgNO_3$. The resulting concentration response again was very similar, displaying no significant differences in the EC50 values for either measure of cell viability or for AgNP vs. $AgNO_3$ (Table 4.1). From the AgNP concentration response curves it was deduced that the highest AgNP concentration yielding no significant impact on cell viability was 2.5 µM while 5% impact on cell viability were seen for the 10 µM AgNP concentration. These two concentrations were chosen for subsequent long-term experiments.
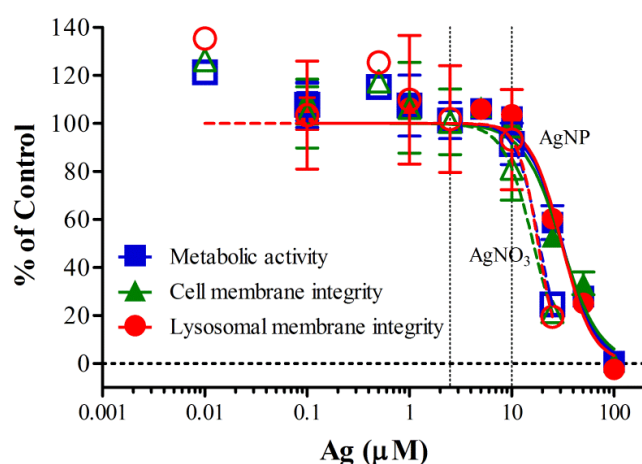

Figure 4.5 AgNP toxicity to RTgill-W1-pf cells measured after three days of exposure.

Solid lines: AgNP exposures; Dashed lines: $AgNO_3$ exposures. 2.5 µM and 10 µM of AgNP were selected for the long term exposures (indicated by dotted vertical lines). Data were presented as mean ± standard deviation, n=3.

Table 4.1 EC50 Values, Corresponding 95% Confidence Intervals, Hill slope and R^2 of AgNP and $AgNO_3$ concentration-response curves after exposure for three days.

		EC50 (µM)	95% confidence interval	Hill Slope	R^2
	Metabolic activity	31.14	27.44 - 35.35	-2.605	0.9655
AgNP	Cell membrane integrity	30.60	26.20 - 35.74	-2.311	0.9541
	Lysosomal membrane integrity	30.79	27.79 - 34.11	-2.864	0.9756
	Metabolic activity	18.65	14.86 - 23.41	-3.813	0.8394
$AgNO_3$	Cell membrane integrity	16.26	12.19 - 21.69	-3.027	0.7877
	Lysosomal membrane integrity	18.14	11.62 - 28.30	-4.419	0.6525

EC 50 values were test by Two-way ANOVA and no significant differences were found, n=3.

Long-term toxicity (impact on cell proliferation): Cell proliferation on long-term AgNP exposure was monitored by counting cell number in 25 cm^2 flasks over time (Figure 4.6A). Under control conditions, cell number increased exponentially over time and had increased by about 6.3-fold after exposure for twelve days. For the 2.5 µM AgNP concentration, cell number increased in a manner comparable to the control until day nine. However, at day twelve, total cell number had increased to only about 4.6-fold. Finally, for the 10 µM AgNP concentration, a slower increase in cell number was visible already at day six. After twelve days, cell number had increased by about 3.5-fold. A phase-contrast image of the cells after nine days of exposure under the three different conditions is depicted in Figure 4.7.
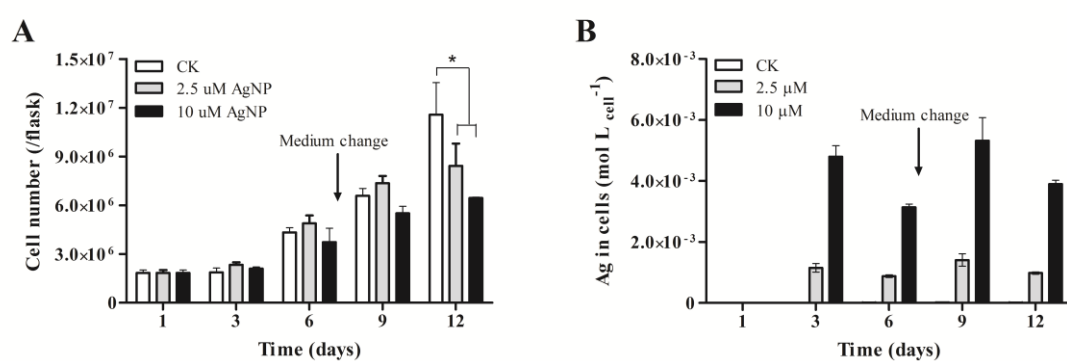
Figure 4.6 Long-term exposure of RTgill-W1-pf cells to AgNP for twelve days.

A: RTgill-W1-pf cell number in controls and after exposure to AgNP. * RTgill-W1-pf cell numbers in 2.5 and 10 AgNP exposures were significantly lower than cell numbers in CK (control; without AgNP exposure), $p < 0.05$, two-way ANOVA, n=3. B: Cell associated silver quantified in RTgill-W1-pf cells after exposure to AgNP or a silver-free control (CK). Data were presented as mean ± standard deviation, n=3.
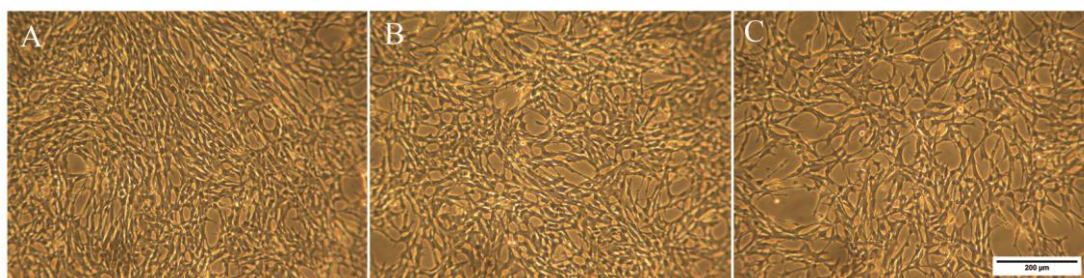
Figure 4.7 Phase-contrast images of RTgill-W1-pf exposed to AgNP for nine days.

A: CK, control cells without AgNP exposure; B: Cells exposed to 2.5 µM AgNP; C: Cells exposed to 10 µM.

In a parallel batch of identically treated cells, cell-associated silver content was measured at each time point by inductively coupled plasma mass spectrometry (ICP-MS). Inasmuch as the cell culture medium in the long-term exposures was completely exchanged every six days, cells were extracted at the end of each of these periods, i.e. before the medium change, starting with a cysteine wash to remove any loosely bound silver. Silver content per cell stayed constant for the low exposure concentration, while an initial steep increase in cell-associated silver concentration was followed by a stabilization for the exposure to 10 µM (Figure 4.6B).

4.3 Discussion

This study focused on the establishment of a new RTgill-W1 cell strain able to proliferate in a serum- and protein-free culture medium. The resulting RTgill-W1-pf cell line allowed for the first time to study a long-term nanoparticle effect in an *in vitro* cell culture system without interference by serum proteins or other, undefined serum constituents.

RTgill-W1-pf cells resulted from adaptation to InVitrus VP-6 medium. Compared to L15 medium for wild type RTgill-W1 cells, the InVitrus VP-6 medium contains much more metabolic precursors than the L15. For example, InVitrus VP-6 contains trace elements such as Fe, Cu and Zn and lipid precursors (fatty acids), such as linoleic acid. The major C-source in InVitrus VP-6 is glucose, not galactose/pyruvate as in L15. InVitrus VP-6 is buffered with sodium hydrogen carbonate while the L15 is buffered with phosphates. The exact composition of the InVitrus medium is not available from the company but it is clearly protein-free as also demonstrated from the protein measurements performed here. RTgill-W1-pf cells divide in InVitrus VP-6 medium with a doubling time (6 days) similar to the original RTgill-W1 cells (7 days) grown in L15 medium supplemented with 5% FBS. In the work by Ackermann and Fent, the RTG-2 cells doubling time was 1.8 days in original culture medium (EM: DMEM/F12 (1: l) medium with 5% serum) and 2.4 days in Turbo Doma (serum-free medium) (Ackermann and Fent 1998). Yet, this Turbo Doma medium was not successful for adaptation of RTgill-W1 cells. In summary, while the InVitrus medium proved very valuable for adaptation of the RTgill-W1 cells, the unavailability of information on each of its ingredients remains a limitation of its applications. This, together with the inability of the RTgill-W1 cells to proliferate in Turbo Doma medium, points toward the need for developing a fish-cell specific medium. Few previous studies have focused on the detailed nutritional requirements of fish cells. For instance, Bols *et al* found that glutamine was not required in L15 medium for fish cell lines (Bols et al. 1994). However, to date, no completely defined culture medium for fish cells has been established.

Despite the success of adapting the gill cells to the InVitrus VP-6 medium, cells could only be cultured in this medium for about ten passages before the cells started to senesce and die. Thus, the RTgill-W1-pf cell line, opposite to the wild-type RTgill-W1 cell line, does not have the ability to grow in InVitrus VP-6 medium indefinitely. Nevertheless, up to passage ten, the RTgill-W1-pf cell line can be used to study the toxicity of nanoparticles or potentially other agents without serum protein interference. Moreover, the cells can be frozen and thawed so that a continuous supply of RTgill-W1-pf cell material can be assured.

The three-day short-term toxicity of AgNP and AgNO$_3$ in the InVitrus VP-6 medium differed in several aspects from that in the simple buffers applied for up to 24 h as described in Chapter 2 (Yue et al. 2015). Firstly, based on total silver concentration, there was no significant difference in toxicity between the particle and the silver ion exposures after three days, whereas significant differences were found in the 24 h exposures (Chapter 2; Yue et al., 2015). The similar toxicity for AgNP and AgNO$_3$ implied that AgNP toxicity was mainly due to dissolved silver. One possible explanation is that AgNP were degraded in cellular compartments after uptake. As discussed in Chapter 3, AgNP were transported in endocytic compartments such as endosomes and lysosomes, which have an acidic environment and in this way increase AgNP dissolution (Behra et al. 2013; Liu and Hurt 2010; Odzak et al. 2015; Setyawati et al. 2014). Another reason might be that organic compounds, such as amino acids in the InVitrus VP-6 medium, can bind silver ions and thereby also increase the AgNP dissolution (Shi et al. 2014). Therefore it can be postulated that, during three days of exposure, most of the AgNP were transformed to dissolved silver and induced very similar effects to RTgill-W1-pf cells. Another observed difference between the three day cell viability measurements is that metabolic activity, cell- and lysosomal membrane integrity were similarly affected whereas lysosomal membrane integrity was the most affected by AgNP after 24 h of exposure (Chapter 2; Yue et al. 2015). This difference likely also is linked to the dynamic nature of the nanoparticle-cell interaction. After 2 h of exposure, AgNP were recoverable from the endocytic-lysosomal compartment (Chapter 3), and this locally increased accumulation of AgNP in these compartments apparently to the higher sensitivity of lysosomal membrane integrity as measured after the 24 h exposure (Chapter 2, Yue et al., 2015). However, if in the three days exposures, most of AgNP were dissolved in lysosomes as discussed above, they are expected to induce a similar toxicity pattern as AgNO$_3$ in the cells.

Application of the RTgill-W1-pf cell line allowed the impact of AgNP on cell proliferation to be quantified. Indeed, both 2.5 µM and 10 µM AgNP led to significant inhibition of cell proliferation over twelve days as compared to the unexposed control cells. While the AgNP were presented to the cells in the absence of protein in the medium, protein-AgNP in the exposure medium cannot be excluded or prevented over the course of the experiment. This is because cells secrete proteins into the medium during their culture (Knowles et al. 1980). The identity of these proteins, and whether this identity differs if cells are exposed to nanoparticles or not, remains an interesting aspect of future investigations. Sisco *et al.* identified proteins derived from cultured neonatal rat cardiac fibro-

blasts in gold nanorods-protein coronas, which formed in this cell culture medium previously "conditioned" with cells (Sisco et al. 2014).

The cell associated silver contents in the InVitrus VP-6 medium exposed for twelve days were compared to that in the simple buffer applied for 24 h as described in Chapter 3. In 2.5 µM AgNP exposures, cell associated silver was very similar between the twelve days and the 24 h exposures. At 10 µM AgNP, cells exposed for twelve days had 2-3 times higher cell associated silver than in the 24 h exposures. AgNP strongly agglomerated in InVitrus VP-6 medium with a size range from 800 - 1500 nm, while AgNP in the simple buffer for 24 h exposure was much more stable with a size below 100 nm. Previous research on nanoparticles behavior in different media indicates that large nanoparticle agglomerates in the size range found in the InVitrus medium, settle down fast from the suspension (Cho et al. 2011; Hinderliter et al. 2010). Therefore, the deposition likely increased the interaction between AgNP and cells as well as raised the cell associated silver contents in InVitrus VP-6 medium. Yet, such an increase was not observed at the low, 2.5 µM AgNP exposures. Again, proteins secreted from the cells may have contributed to AgNP stabilization over time of RTgill-W1-pf culture in the InVitrus medium.

To conclude, work presented here led to the development of a new *in vitro* cell model, the RTgill-W1-pf cell line, which is suitable for long-term toxicological studies under serum- and protein-free culture condition. One previous study already reported different cell stress responses on the molecular level on short- or long-term exposures to AgNP in cell culture medium with serum (Comfort et al. 2014). Thus, it is worth to explore cell responses in RTgill-W1-pf cell on the molecular level, which may provide new insights into the long-term consequences of particle exposure. Compared to nanotoxicity studies in cell culture medium with serum, the new system offers an opportunity to investigate the original nanoparticle interaction with cells. Other stressors, such as man-made organic chemicals, can likewise be studied in this system without protein interference. Serum has, for example, been reported to influence the cellular response of cytochrome P450 monooxygenases (Hammond and Fry 1994; Nakama et al. 1995), which are important enzymes in biotransformation of many organic chemicals. What is more, unlike cells of internal tissues and organs, which are surrounded by a biofluid environment, i.e. the blood or lymph, fish gills face, at least on the apical side, the fresh water. Thus, the RTgill-W1-pf cells might better represent the exposures experienced by gill cells in the organism *in vivo*.

4.4   Material and Methods

4.4.1   Routine RTgill-W1 culture

RTgill-W1 cells were routinely cultivated in 75 cm^2 flasks (TPP, Trasadingen, Switzerland) in Leibovitz's L15 (L15) complete medium, i.e. L15 medium (Invitrogen, Basel, Switzerland) supplemented with 5% fetal bovine serum (FBS, Gold, PAA Laboratories GmbH, Austria) and 1% penicillin/streptomycin (Sigma-Aldrich, Buchs, Switzerland; 10 000 U/ml penicillin, 10 mg/ml streptomycin). Cells were maintained at 19 ℃ in normal atmosphere and split once (1 flask to 2 flasks) in 1-2 weeks. Confluent cells were washed twice with Versene (Invitrogen/Gibco, Germany), detached by trypsin (0.25% in phosphate-buffered saline, Biowest, Germany) and trypsin digestion stopped with complete L15 medium. The cell suspension was centrifuged at 1 000 × g for 3 min. The resulting cell pellet was re-suspended with fresh, complete medium and divided into new flasks.

4.4.2   Adaptation to serum-free medium

Two commercial serum- and protein- free culture media were tested for their suitability to sustain RTgill-W1 cell survival and proliferation: Turbo Doma and InVitrus VP-6 (Cell Culture Technologies, Switzerland). These media were routinely supplemented with 1% penicillin/streptomycin to prevent microbial contamination. To initiate adaptation, a selection procedure was designed that was comprised of: i) splitting confluent "wild-type" RTgill-W1 cells into 25 cm^2 flasks (TPP, Trasadingen, Switzerland) in complete L15 medium with 5% FBS allowing attachment for 24 h; ii) replacing the culture medium with the experimental, protein-free culture media containing 2.5% FBS; iii) allowing the cells to adapt at 19 ℃ in normal atmosphere with a weekly 50% media exchange until confluency was reached; iv) splitting the cells as described above but then placing them in the experimental media containing 1% FBS, changing the medium every week until confluency was reached, then placing them in medium containing 0.5% before serum was completely omitted. From this point on, cells were grown in serum-free medium and medium was changed routinely every seven days. In this way, one cell line strain was able to proliferate in the In Vitrus medium. This strain was termed RTgill-W1-pf (protein-free).

4.4.3   Characterization of RTgill-W1-pf

To measure RTgill-W1-pf cell proliferation and doubling time, cells were seeded in 25 cm^2 flasks with a density of 4*10^4 cells cm^{-2}. After 1, 3, 6, 9, 12, 21 days, cells were dislodged with trypsin and counted with an electric field multi-channel cell counting device (CASY1 TCC, Schärfe System, Ger-

many). To visualize cell morphology, cells were checked under the microscope as well as the cell di-ameter and volume measured with the CASY cell counting device.

Protein content was determined in the cell culture medium with or without incubation with cells. The cells were first pelleted and 2 mL medium from the supernatant was precipitated with Metha-nol-Chloroform. Specifically, 2 mL supernatant were mixed with 4 mL methanol in a new tube, then 1 mL of chloroform was added and the suspension well mixed. Then, 2 mL of deionized water were added into the mixture which produced a milky suspension. This suspension was vigorously mixed for 5 sec, and then centrifuged at 4 000 × g for 5 min at room temperature. A white pellet was formed on the interface between the oil (lower) and water (upper) phases. The band was carefully removed, while the lower and upper phases were discarded. The pellet was washed by adding 500 µL methanol, followed by centrifugation at 4 000 × g for 2 min at room temperature. The resulting supernatant was removed and the pellets dried for 15-30 min on air. Pellets were re-dissolved in re-solubilization buffer (9 M urea, 2 M thiourea, 0.1 M Tris-HCl, pH 8.5.). Protein concentrations were then measured by the Bradford method with Coomassie Plus™ (Bradford) Assay kit (Thermo Fisher Scientific, No. 23236).

4.4.4   Nanoparticle characterization

The citrated coated AgNP were purchased from NanoSys GmbH (Wolfhalden, Switzerland) as aque-ous suspension with a concentration of 1g/L (9.27 mM, pH=6.46). The AgNP were characterized when suspended in InVitrus VP-6 medium. The Z-average size and zeta potential of the AgNP were measured by dynamic light scattering (DLS) and electrophoretic mobility using a Zetasizer (Nano ZS, Malvern Instruments, UK). In addition, AgNP size and morphology in the InVitrus VP-6 medium were verified by transmission electron microscopy (TEM, FEI Morgagni 268, 100 kV).

4.4.5   Short-term exposure of RTgill-W1-pf to AgNP and AgNO$_3$

For short-term (three-day) exposure to AgNP and AgNO$_3$, confluent cells were used. Thus, cells were seeded in 24-well microtiter plates (Greiner Bio-One, Frickenhausen, Germany) at an initial cell density of $1.5*10^5$ cm^{-2} cells in each well in 1 mL of InVitrus VP-6 medium. After three days, the cells were fully confluent and used for toxicity assessment. One mL/well of AgNP or AgNO$_3$ suspen-sion in the InVitrus VP-6 medium was added. Exposure was done at 19℃ in the dark and lasted three days. Each experiment was performed three times independently with cells from different passages (n=3).

At the end of the exposure, toxicity was assessed by three indicators of cell viability: cellular metabolic activity, cell membrane integrity and the lysosomal membrane integrity (Schirmer et al. 1997; Schirmer et al. 1998). Alamar Blue (AB, Invitrogen, Basel, Switzerland) was used to measure the cellular metabolic activity; 5-carboxyfluorescein diacetate acetoxymethyl ester (CFDA-AM, Invitrogen, Basel, Switzerland) to measure the cell membrane integrity; Neutral Red (NR, Sigma-Aldrich, Buchs, Switzerland) to measure the lysosomal membrane integrity. After three days of cit-AgNP or AgNO$_3$ exposure, the exposure medium was discarded, cells were gently washed with 1 mL PBS, followed by adding 400 μL of AB and CFDA-AM working solution, containing 5% v/v AB and 4 μM CFDA-AM in PBS. After incubation for 30 min, fluorescence of each well was quantified by the Infinite M200 plate reader (TECAN, Männedorf, Switzerland) at respective excitation/emission wavelengths of 530/595 nm for AB and 485/530 nm for CFDA-AM. Thereafter, the AB/CFDA-AM working solution was discarded and 400 μL of NR solution, containing 1.5% v/v NR in PBS, were added and incubated for 60 min. Then, cells were fixed with 400 μL fixative (0.5% v/v formaldehyde and 1% w/v CaCl$_2$). Finally, NR was extracted from the lysosomes using 400 μL of an extraction solution (1% v/v acetic acid and 50% v/v ethanol) and gently shaken on a horizontal shaker (TiMix 2, Johanna Otto GmbH, Hechingen, Germany) for 10 min. NR fluorescence was measured at excitation/emission wavelengths of 530/645 nm using the same plate reader.

4.4.6   Long-term exposure of RTgill-W1-pf to AgNP

To expose RTgill-W1-pf cells to AgNP for prolonged times, i.e. to allow cell proliferation, cells were seeded in 25 cm^2 flask with density 8*10^4 cells cm^{-2} in InVitrus VP-6 medium. After incubation for 24 h to allow cell attachment, medium was exchanged with fresh InVitrus VP-6 medium containing 2.5 and 10 μM AgNP. This medium was replaced with fresh solutions after six days.

After 1, 3, 6, 9, 12 days of exposure, both cell-associated silver content and cell number were determined from the same flasks. First, cells were washed with 0.5 mM cysteine for 5 min to remove loosely bound silver from the cell surfaces. Then, cells were washed twice with Versene, detached by trypsin and trypsin digestion stopped with L15 containing 5% FBS. After centrifugation, cell pellets were re-suspended in 550 μL InVitrus VP-6 medium. 10 μL cell suspension was used to count cell number and volume with CASY cell counting device. Another 500 μL cell suspension was used to quantify the silver associated with cells. Thus, the 500 μL cell suspension was digested with 4.5 mL of 65% HNO$_3$ in a high-performance microwave digestion unit (MLS-1200 MEGA, Oberwil, Switzerland) at a maximal temperature of 195 °C for 20 min. The digests were diluted 50-times and meas-

ured by ICP-MS (Element 2 High Resolution Sector Field ICP-MS; Thermo Finnigan, Bremen, Germany). The reliability of the measurements was determined using specific water references (M105A, IFA-Tull, Austria).

References

Ackermann GE, Fent K. 1998. The adaptation of the permanent fish cell lines PLHC-1 and RTG-2 to FCS-free media results in similar growth rates compared to FCS-containing conditions. Marine Environmental Research 46(1-5):363-367.

Barnes D, Sato G. 1980. Serum-free cell culture: a unifying approach. Cell 22(3):649-655.

Bastian S, Busch W, Kuhnel D, Springer A, Meissner T, Holke R, Scholz S, Iwe M, Pompe W, Gelinsky M and others. 2009. Toxicity of tungsten carbide and cobalt-doped tungsten carbide nanoparticles in mammalian cells in vitro. Environ Health Perspect 117(4):530-6.

Behra R, Sigg L, Clift MJD, Herzog F, Minghetti M, Johnston B, Petri-Fink A, Rothen-Rutishauser B. 2013. Bioavailability of silver nanoparticles and ions: from a chemical and biochemical perspective. Journal of The Royal Society Interface 10(87).

Bertoli F, Davies G-L, Monopoli MP, Moloney M, Gun'ko YK, Salvati A, Dawson KA. 2014. Magnetic Nanoparticles to Recover Cellular Organelles and Study the Time Resolved Nanoparticle-Cell Interactome throughout Uptake. Small 10(16):3307-3315.

Bols N, Ganassin R, Tom D, Lee L. 1994. Growth of fish cell lines in glutamine-free media. Cytotechnology 16(3):159-166.

Bols NC, Dayeh VR, Lee LEJ, Schirmer K. 2005. Chapter 2 Use of fish cell lines in the toxicology and ecotoxicology of fish. Piscine cell lines in environmental toxicology. In: Mommsen TP, Moon TW, editors. Biochemistry and Molecular Biology of Fishes: Elsevier. p 43-84.

Cho EC, Zhang Q, Xia Y. 2011. The effect of sedimentation and diffusion on cellular uptake of gold nanoparticles. Nat Nano 6(6):385-391.

Comfort KK, Braydich-Stolle LK, Maurer EI, Hussain SM. 2014. Less Is More: Long-Term in Vitro Exposure to Low Levels of Silver Nanoparticles Provides New Insights for Nanomaterial Evaluation. Acs Nano.

Dayeh VR, Schirmer K, Bols NC. 2002. Applying whole-water samples directly to fish cell cultures in order to evaluate the toxicity of industrial effluent. Water Research 36(15):3727-3738.

Grillberger L, Kreil TR, Nasr S, Reiter M. 2009. Emerging trends in plasma-free manufacturing of recombinant protein therapeutics expressed in mammalian cells. Biotechnology Journal 4(2):186-201.

Hammond AH, Fry JR. 1994. Toxicity of precocene II in rat hepatocyte cultures: effects of serum and culture time. Toxicology Letters 70(3):337-342.

Hayashi I, Sato GH. 1976. Replacement of serum by hormones permits growth of cells in a defined medium. Nature 259(5539):132-134.

Hinderliter P, Minard K, Orr G, Chrisler W, Thrall B, Pounds J, Teeguarden J. 2010. ISDD: A computational model of particle sedimentation, diffusion and target cell dosimetry for in vitro toxicity studies. Particle and Fibre Toxicology 7(1):36.

Knowles BB, Howe CC, Aden DP. 1980. Human hepatocellular carcinoma cell lines secrete the major plasma proteins and hepatitis B surface antigen. Science 209(4455):497-499.

Kühnel D, Busch W, Meißner T, Springer A, Potthoff A, Richter V, Gelinsky M, Scholz S, Schirmer K. 2009. Agglomeration of tungsten carbide nanoparticles in exposure medium does not prevent uptake and toxicity toward a rainbow trout gill cell line. Aquatic Toxicology 93(2-3):91-99.

Liu J, Hurt RH. 2010. Ion Release Kinetics and Particle Persistence in Aqueous Nano-Silver Colloids. Environmental Science & Technology 44(6):2169-2175.

Meißner T, Kühnel D, Busch W, Oswald S, Richter V, Michaelis A, Schirmer K, Potthoff A. 2010. Physical-chemical characterization of tungsten carbide nanoparticles as a basis for toxicological investigations. Nanotoxicology 4(2):196-206.

Nakama A, Kuroda K, Yamada A. 1995. Induction of cytochrome P450-dependent monooxygenase in serum-free cultured Hep G2 cells. Biochemical Pharmacology 50(9):1407-1412.

Nogueira DR, Mitjans M, Rolim C, Vinardell MP. 2014. Mechanisms Underlying Cytotoxicity Induced by Engineered Nanomaterials: A Review of In Vitro Studies. Nanomaterials 4(2):454-484.

Odzak N, Kistler D, Behra R, Sigg L. 2015. Dissolution of metal and metal oxide nanoparticles under natural freshwater conditions. Environmental Chemistry 12(2):138-148.

Sato GH. 1975. The role of serum in cell culture. Biochemical actions of hormones 3:391-396.

Schirmer K. 2014. Chapter 6 - Mechanisms of Nanotoxicity. In: Jamie RL, Eugenia V-J, editors. Frontiers of Nanoscience: Elsevier. p 195-221.

Schirmer K, Chan AGJ, Greenberg BM, Dixon DG, Bols NC. 1997. Methodology for demonstrating and measuring the photocytotoxicity of fluoranthene to fish cells in culture. Toxicology in Vitro 11(1-2):107-119.

Schirmer K, Dixon DG, Greenberg BM, Bols NC. 1998. Ability of 16 priority PAHs to be directly cytotoxic to a cell line from the rainbow trout gill. Toxicology 127(1-3):129-141.

Schultz AG, Boyle D, Chamot D, Ong KJ, Wilkinson KJ, McGeer JC, Sunahara G, Goss GG. 2014. Aquatic toxicity of manufactured nanomaterials: challenges and recommendations for future toxicity testing. Environmental Chemistry 11(3):207-226.

Setyawati MI, Yuan X, Xie J, Leong DT. 2014. The influence of lysosomal stability of silver nanomaterials on their toxicity to human cells. Biomaterials 35(25):6707-6715.

Shi J, Sun X, Zou X, Zhang H. 2014. Amino acid-dependent transformations of citrate-coated silver nanoparticles: Impact on morphology, stability and toxicity. Toxicology Letters 229(1):17-24.

Sisco PN, Wilson CG, Chernak D, Clark JC, Grzincic EM, Ako-Asare K, Goldsmith EC, Murphy CJ. 2014. Adsorption of Cellular Proteins to Polyelectrolyte-Functionalized Gold Nanorods: A Mechanism for Nanoparticle Regulation of Cell Phenotype? PLoS ONE 9(2):e86670.

Tanneberger K, Knöbel M, Busser FJM, Sinnige TL, Hermens JLM, Schirmer K. 2012. Predicting Fish Acute Toxicity Using a Fish Gill Cell Line-Based Toxicity Assay. Environmental Science & Technology 47(2):1110-1119.

van der Valk J, Brunner D, De Smet K, Fex Svenningsen Å, Honegger P, Knudsen LE, Lindl T, Noraberg J, Price A, Scarino ML and others. 2010. Optimization of chemically defined cell culture media – Replacing fetal bovine serum in mammalian in vitro methods. Toxicology in Vitro 24(4):1053-1063.

Yue Y, Behra R, Sigg L, Fernández Freire P, Pillai S, Schirmer K. 2015. Toxicity of silver nanoparticles to a fish gill cell line: Role of medium composition. Nanotoxicology 9(1):54-63.

Chapter 5   Conclusions and outlook

The aim of this thesis was to explore the interaction of AgNP with rainbow trout gill cells. The main conclusions from this thesis can be summarized as follows:

- The exposure medium composition has an important influence on AgNP behaviour and toxicity to RTgill-W1 cells.
- AgNP can be taken up by RTgill-W1 cells via endocytic pathways and induce particle specific effects, specifically with regard to lysosome membrane integrity.
- Upon trafficking in the cells, a large number of proteins, mostly belonging to cell membrane functions as well as endocytosis and vesicle-mediated transport pathways, become associated with AgNP.
- AgNP inhibit fish gill cell proliferation in long term exposures in protein free medium.

In the following part, the most important outcomes and conclusions for AgNP interaction with fish gill cells are discussed in light of perspectives for further research.

This dissertation studied the role of cell exposure media composition on AgNP behaviour and toxicity to RTgill-W1 cells. The ionic strength and chloride concentration in the media influenced AgNP agglomeration, deposition and speciation of dissolved silver species, consequently altering the bioavailability and toxicity to RTgill-W1 cells. To allow AgNP interactions with the fish cells to be studied with nanoparticles well dispersed in the medium, a new exposure medium was developed, d-L15/ex, which has a low ionic strength and a low chloride concentration. This protein-free medium supported cell survival and stabilized the AgNP for at least 24 h, thus allowing small-size particles to be studied with respect to uptake and effects in cells without sedimentation of particles onto cells due to particle agglomeration. Based on its ionic strength, this medium also better mimics the freshwater environment than conventional culture media, and it offers an excellent platform to study cellular and molecular effects of nanoparticles on gill cells. For example, we know that dissolved silver and AgNP can influence the Na^+ and Cl^- homeostasis in fish gill cells, which could be studied in this chemically defined medium.

In toxicity tests, the AgNP elicited a particle-specific effect and seemed to particularly affect RTgill-W1 cell lysosomes. Indeed, uptake of AgNP was demonstrated to follow an endocytic pathway. However, in this thesis, cellular uptake was checked only for a few fixed times points, providing a snapshot. Yet, we know that the interaction of nanoparticles with cells is a dynamic process. Thus, time–resolved analysis of AgNP trafficking in cells will be an interesting topic in the future as well as useful to further explore the mechanism of AgNP uptake and toxicity. Visualization of particles in cells was done here by electron microscopy, which is a very time-consuming technology, and, on top, hardly allows for nanoparticle quantification. One idea to overcome the limitations of electron microscopy would be to use nanoparticles that are fluorescently labeled. With fluorescence labeling and confocal laser scanning microscopy, it possible to track nanoparticles in live cells and algorithms exist for quantification (Vercauteren et al. 2011). On the other hand, it was found that fluorescence labelling altered metal nanoparticles properties (Rodriguez-Lorenzo et al. 2014). The challenge therefore is to design probes that combine native nanoparticle properties with labelling methods that have no interference with particle properties. Application of technologies focusing on high resolution imaging of single cells are interesting in this area in future work. For example, Laser Ablation Inductively Coupled Plasma Mass Spectrometry (LA-ICP-MS) was used to study the metal distribution in zebrafish embryo (Brun et al. 2014). With the resolution increasing, LA-ICP-MS will be a probable technology to image metal nanoparticles in single cell.

Upon contact with cells, AgNP interact with intracellular proteins and form a AgNP-protein corona during trafficking in intact cells. In order to study the AgNP interaction with proteins, a method was developed to isolate the AgNP-protein corona from intact, live cells based on subcellular fractionation. This method allowed the AgNP-protein corona to be recovered from intact subcellular compartments only, thereby avoiding the background protein interference, e.g. from cytosolic proteins. Based on proteins identified in the AgNP-protein corona, an initial mechanism of AgNP uptake and toxicity was described on the cellular level, involving cell membrane functions, uptake and vesicular trafficking, as well as stress responses. This is the first study that focuses on the interaction of industrial nanoparticles with proteins in living cells. Compared with studies on nanoparticle interaction with single proteins or proteins extracted from biological liquids or cells prior to adding the nanoparticles, this system offers an *in situ* view of NP-protein interaction. Moreover, unlike the magnetic force separation with magnetic nanoparticles, this method can easily be transfer to other metal nanoparticles for studying cell-internal protein corona formation. The NP-protein corona studies are largely influenced by the subcellular fractionation. It is extremely difficult to isolate pure

endo-lysosome fractions. Endosomes and lysosomes are heterogeneous in size and density and therefore the fractions of endosomes, lysosomes, mitochondria and peroxisomes overlap in density gradient centrifugation. Moreover, another contaminant in lysosomal fractions which are non-degraded or partially degraded macromolecular substrates from other cell compartments (Schröder et al. 2010). In the future, preparation of high quality endosome and lysosome fractions by optimizing the density gradient centrifugation will be very important in NP-protein interaction studies. Affinity purification of soluble lysosomal proteins containing mannose 6-phosphate, a specific modification in lysosomes, also offers a way to avoid contamination by other cell compartments (Sleat et al. 2006).

Inasmuch as this thesis presents initial work on the NP-protein interaction in living cells, many interesting opportunities arise for future investigations. On the one hand, how the binding of intracellular proteins, as demonstrated here, impacts nanoparticle behavior remains to be explored. As discussed in chapter 1 of this thesis, the surface properties of nanoparticles are very important with regard to the particles' stability. In the NP-protein corona, the surface of the particles may be varied due to the protein adsorption. Most proteins carry different charges and can change the charge on the nanoparticle surface. If the charge shifts to zero, nanoparticles agglomerate; or if the charge rises, nanoparticles may be stabilized and thus to staying suspended. Such phenomena have been described in studies with biological fluids or isolated proteins. It was, for example, found that bovine serum albumin and fetal bovine serum can stabilize tungsten carbide (WC) and cobalt-doped tungsten carbide (WC-Co) nanoparticles suspension in cell culture media (Bastian et al. 2009; Kühnel et al. 2009; Meißner et al. 2010). It follows that the protein coating may also influence the nanoparticle transport and fate in cells. On the other hand, the binding to AgNP may impact on the function of the proteins, which is likewise little explored to date. That nanoparticles can have an effect on protein structure and/or enzyme activity has been already mentioned in Chapter 1. Specifically, BSA structure (Ravindran et al. 2010), tryptophanase (Wigginton et al. 2010) and Na^+/K^+ ATPase activity (Schultz et al. 2012) were shown to be impacted. Another recent example is the finding that AgNP elicit a particle specific inhibition of an extracellular enzyme (leucine aminopeptidase) on short-term exposure of a freshwater biofilm (Gil-Allué et al. 2015). In my current work, a number of proteins were found to bind AgNP in cells. Yet, whether they are also affected in their structure and/or function is still lacking experimental proof. Studying such interactions would be very useful to further pin-down the mechanisms that nanoparticles have in cells. The protein list established here can serve as a guide to prioritize such kind of investigations.

119

As one means to avoid the interference by proteins in the exposure media before a particle enters a cell, the RTgill-W1-pf cell line was developed, which can proliferate in a serum-free medium. Exposure of these cells to AgNP for a period that allows for cell proliferation showed that AgNP inhibited the proliferation of the RTgill-W1-pf cell line. In fact, this is the first time that a long-term nanoparticle effect could be studied in an *in vitro* cell culture system without serum protein interference. This unique cell line therefore offers novel opportunities to study nanoparticle-cell interactions. For instance, how are AgNP distributed and transferred during cell division? What are the differences in cellular and molecular response patterns in short- and long-term exposures under identical exposure conditions? One previous study already reported different cell responses on short- or long-term exposures on the molecular level: Comfort *et al* exposed human keratinocytes, the HaCaT cell line, to AgNP in a long-term exposure system for 3 months in cell culture medium with serum. Compared to short-term exposure, they determined that long-term exposures induced significant increased p38 activation, which related to cellular stress responses, including apoptosis, immune response, migration, and gene regulation (Comfort et al. 2014). This study illustrates that studying nanoparticle exposures on short vs. long-term in the RTgill-W1-pf cells and the ensuing molecular response may provide new insights into the long-term consequences of particle exposure.

Beyond exploiting the RTgill-W1-pf cell line for further nanoparticle research, it also provides the possibility to study chemical effect over long-term exposures without serum protein interference. For example, serum has been reported to influence the cellular response of cytochrome P450 monooxygenases (Nakama et al. 1995). What is more, unlike cells of internal tissues and organs, which are surrounded by a biofluid environment, i.e. the blood or lymph, fish gills face, at least on the apical side, the fresh water. Thus, the RTgill-W1-pf cells might better represent the gill cells in the organism *in vivo*. For example, they could be cultured in a multi-compartment system where the upper side represents the water-facing side and the bottom compartment the organism-facing side. The upper side could be cultured in the serum-free medium and the bottom compartment be fed with serum-containing medium. Such experimental set-ups already exist but none so far has been applicable to long-term exposures without serum in one of the compartments. Finally, though the RTgill-W1-pf cells were able to proliferate in InVitrus medium and can be successfully frozen and thawed, it was found that the cells last for only about ten passages. This means that, unlike the "wild-type" RTgill-W1 cells, the RTgill-W1-pf cell line is not immortal. Hence, there are two ways forward to culture the fish cells continuously without a serum supplement. One way is to develop a serum-free culture medium specifically for fish cells. No such medium exists as of yet; also the InVi-

trus culture medium was designed for mammalian cells and thus may not fit the specific requirements of fish cells very well. Another way is try to immortalize RTgill-W1-pf cells, e.g. by transfection with a plasmid to artificially increase telomerase activity in these cells, as is already established for mammalian cells (Schnabl et al. 2002).

In conclusion, this thesis offers a mechanistic understanding of AgNP interactions with cells by linking and quantifying both exposures and effects. It provides fundamental information about AgNP uptake and interaction with proteins in these cells, which is useful for AgNP toxicity studies. The newly developed models or methods, including d-L15/ex exposure medium, a protocol for NP-protein corona isolation from intact cells and the serum-free culture of RTgill-W1-pf cells are useful advances and can be applied in future nanoparticle-cell interaction research.

References

Bastian S, Busch W, Kuhnel D, Springer A, Meissner T, Holke R, Scholz S, Iwe M, Pompe W, Gelinsky M and others. 2009. Toxicity of tungsten carbide and cobalt-doped tungsten carbide nanoparticles in mammalian cells in vitro. Environ Health Perspect 117(4):530-6.

Brun NR, Lenz M, Wehrli B, Fent K. 2014. Comparative effects of zinc oxide nanoparticles and dissolved zinc on zebrafish embryos and eleuthero-embryos: Importance of zinc ions. Science of The Total Environment 476–477(0):657-666.

Comfort KK, Braydich-Stolle LK, Maurer EI, Hussain SM. 2014. Less Is More: Long-Term in Vitro Exposure to Low Levels of Silver Nanoparticles Provides New Insights for Nanomaterial Evaluation. Acs Nano.

Gil-Allué C, Schirmer K, Tlili A, Gessner MO, Behra R. 2015. Silver Nanoparticle Effects on Stream Periphyton During Short-Term Exposures. Environmental Science & Technology 49(2):1165-1172.

Kühnel D, Busch W, Meißner T, Springer A, Potthoff A, Richter V, Gelinsky M, Scholz S, Schirmer K. 2009. Agglomeration of tungsten carbide nanoparticles in exposure medium does not prevent uptake and toxicity toward a rainbow trout gill cell line. Aquatic Toxicology 93(2-3):91-99.

Meißner T, Kühnel D, Busch W, Oswald S, Richter V, Michaelis A, Schirmer K, Potthoff A. 2010. Physical-chemical characterization of tungsten carbide nanoparticles as a basis for toxicological investigations. Nanotoxicology 4(2):196-206.

Nakama A, Kuroda K, Yamada A. 1995. Induction of cytochrome P450-dependent monooxygenase in serum-free cultured Hep G2 cells. Biochemical Pharmacology 50(9):1407-1412.

Ravindran A, Singh A, Raichur AM, Chandrasekaran N, Mukherjee A. 2010. Studies on interaction of colloidal Ag nanoparticles with Bovine Serum Albumin (BSA). Colloids and Surfaces B: Biointerfaces 76(1):32-37.

Rodriguez-Lorenzo L, Fytianos K, Blank F, von Garnier C, Rothen-Rutishauser B, Petri-Fink A. 2014. Fluorescence-Encoded Gold Nanoparticles: Library Design and Modulation of Cellular Uptake into Dendritic Cells. Small 10(7):1341-1350.

Schnabl B, Choi YH, Olsen JC, Hagedorn CH, Brenner DA. 2002. Immortal Activated Human Hepatic Stellate Cells Generated by Ectopic Telomerase Expression. Lab Invest 82(3):323-333.

Schröder BA, Wrocklage C, Hasilik A, Saftig P. 2010. The proteome of lysosomes. PROTEOMICS 10(22):4053-4076.

Schultz AG, Ong KJ, MacCormack T, Ma G, Veinot JGC, Goss GG. 2012. Silver Nanoparticles Inhibit Sodium Uptake in Juvenile Rainbow Trout (Oncorhynchus mykiss). Environmental Science & Technology 46(18):10295-10301.

Sleat DE, Zheng H, Qian M, Lobel P. 2006. Identification of Sites of Mannose 6-Phosphorylation on Lysosomal Proteins. Molecular & Cellular Proteomics 5(4):686-701.

Vercauteren D, Deschout H, Remaut K, Engbersen JFJ, Jones AT, Demeester J, De Smedt SC, Braeckmans K. 2011. Dynamic Colocalization Microscopy To Characterize Intracellular Trafficking of Nanomedicines. ACS Nano 5(10):7874-7884.

Wigginton NS, Titta Ad, Piccapietra F, Dobias J, Nesatyy VJ, Suter MJF, Bernier-Latmani R. 2010. Binding of Silver Nanoparticles to Bacterial Proteins Depends on Surface Modifications and Inhibits Enzymatic Activity. Environmental Science & Technology 44(6):2163-2168.

Curriculum Vitae

Yang Yue   yang.yue@eawag.ch
BU-F20, UTOX, Eawag
Überlandstrasse 133, P.O. Box 611   +41 76 392 7088
CH-8600 Dübendorf
Switzerland

EDUCATION

2011-2015	Ph.D. candidate, Environmental toxicology studies, supervised by Prof. Kristin Schirmer and Dr. Renata Behra, Eawag & EPFL, Switzerland. Project: Interaction of silver nanoparticles (AgNP) with Rainbow Trout Gill Cell Lines. (Swiss National Research Programme "Opportunities and Risks of Nanomaterials" (NRP64))
2007-2010	Master in Biochemical pharmaceutics, State Key Laboratory of Biomembrane and Membrane Biotechnology, Tsinghua University, Beijing, China Project: Novel nano drug delivery system development and evaluation. (National Natural Science Foundation of China project, Contract Number:20081107**)**
2003-2007	Bachelor in Biology Science, China Agricultural University, Beijing, China

SKILLS

Laboratory work	- Cellular biology: primary and cell line culture (derive from human, mouse and fish), subcellular fractionation, density gradient centrifugation, cellular organelles isolation, adaption of cells to serum free medium, flow cytometry. - Nanotechnology: DLS, nano track analysis, ICP-MS, EDX. - Microscopy: fluorescence microscopy, confocal microscopy, electron microcopy sample preparation and imaging. - Biochemistry: enzyme activity assay, protein quantification, proteomics, 2-D gel electrophoresis, HPLC, mass spectrometry. - Molecular biology: RNA isolation, qRT-PCR.
Animal experiment	Beijing animal experiment qualification, 2008-2010.
Bioinformatics	GO ontology, Uniprot, NCBI data base, BLAST, Scaffold
Data analysis	GraphPad, R, OriginLab, ImageJ, Biostatistics training
Scientific writing	- Scientific writing training course and preparing scientific manuscript. - Participation in scientific proposal writing.
Teaching	Teaching assistant in Eawag practical courses: Molecular Ecotoxicology.

PUBLICATIONS

- **Yang Yue**, Renata Behra, Laura Sigg, Marc J-F Suter, Smitha Pillai, Kristin Schirmer, Silver nanoparticle-protein interactions in intact rainbow trout gill cells, 2015, in preparation.
- **Yang Yue**, Renata Behra, Laura Sigg, Kristin Schirmer, Silver nanoparticles inhibit fish gill cell proliferation in protein free culture, 2015, in preparation.
- **Yang Yue**, Renata Behra, Laura Sigg, Paloma Fernández Freire, Smitha Pillai, Kristin Schirmer, Toxicity of silver nanoparticles to a fish gill cell line: Role of medium composition, *Nanotoxicology*, 2015, 9: 54–63.
- Laura Sigg, Renata Behra, Ksenia Groh, Carl Isaacson, Niksa Odzak, Flavio Piccapietra, Lena Röhder, Hannah Schug, **Yang Yue**, Kristin Schirmer, Chemical Aspects of Nanoparticle Ecotoxicology, *CHIMIA*, 2014, 68: 806-811.

- **Yang Yue**, Huafeng Zhou, Guanlan Liu, Yan Li, Zemin Yan, Mingxing Duan, The advantages of a novel CoQ10 delivering system in skin photo-protection, *International Journal of Pharmaceutics*, 2010, 392: 57-63.
- Huafeng Zhou, **Yang Yue**, Guanlan Liu, Yan Li, Jing Zhang, Mingxing Duan, Zemin Yan, Characterisation and skin targeting distribution of surfactant-free coenzyme Q10-loaded lipid nanocapsules, *Nanoscale Research Letters*, 2010, 5:1561-1569.
- Huafeng Zhou, **Yang Yue**, Guanlan Liu, Yan Li, Jing Zhang, Qiu Gong, Zemin Yan, Mingxing Duan, Preparation and Characterization of a Lecithin Nanoemulsion as a Topical Delivery System, *Nanoscale Research Letters*, 2010, 5:224-230.

CONFERENCES

2015	CH analysis 2015, Swiss Chemical Society, Beatenberg, Switzerland. Presentation: Cellular uptake of AgNP in RTgill-W1 cells.
2014	5th Anniversary Swiss Centre for Applied Human Toxicology (SCAHT), Basel, Switzerland.
2014	Society of Environmental Toxicology and Chemistry (SETAC) Europe 24th, Basel, Switzerland. Presentation: Toxicity of silver nanoparticles to a fish gill cell line: Role of medium composition.
2013	8th International Conference on the Environmental Effects of Nanoparticles and Nanomaterials, Aix-en-Provence, France. Poster: How does the medium composition impact the risk of silver nanoparticle to fish gill cells?.
2013	2nd QNano Integrating Conference, Prague, Czech Republic. Poster: Role of medium composition on silver nanoparticle toxicity to a fish gill cell line.

PROFESSIONAL SERVICE

- Reviewer for PLOS ONE, Aquatic Toxicology, Environmental Science: Nano.
- Membership: in Society of Environmental Toxicology and Chemistry (SETAC) and Swiss Chemical Society (SCS).

SCHOLARSHIPS & HONORS

2014	Chinese Government Award for Outstanding Self-Financed Students Abroad.
2009	WuSu Educational Foundation Awards, Sponsored by WuSu Foundation Hong Kong, Tsinghua Univerisity, Beijing
2008	Minsheng Social Works Award, Tsinghua University, Beijing
2006	XiZhi Educational Foundation Award, China Agricultural University, Beijing
2005	NIBS Educational Foundation Award, China Agricultural University, Beijing
2004-2006	University Scholarship for Excellent Academic Achievement, China Agricultural University, Beijing

LANGUAGES

English (professional proficiency), Chinese (mother language)

PERSONAL INFORMATION

Chinese, born in 16.10.1984